

**Vibrational characterisation of coordination and  
biologically active compounds by means of  
IR absorption, Raman and surface-enhanced  
Raman spectroscopy in combination with  
theoretical simulations**

**Dissertation**

zur Erlangung des  
naturwissenschaftlichen Doktorgrades  
der Bayerischen Julius-Maximilians Universität Würzburg

vorgelegt von

**Monica-Maria Bolboaca**

aus

Cluj-Napoca, Rumänien

Würzburg 2002

Eingereicht am:.....  
bei der Fakultät für Chemie und Pharmazie.

1. Gutachter:.....  
2. Gutachter:.....  
der Dissertation.

1. Prüfer:.....  
2. Prüfer:.....  
der mündlichen Prüfung.

Tag der mündlichen Prüfung:.....

Doktorurkunde ausgehändigt am:.....

# Content

Chapter 1. Introduction.....	1
Chapter 2. Experimental.....	5
2.1. Infrared spectroscopy.....	5
2.1.1. Basics.....	5
2.1.2. Infrared measurements.....	6
2.2. Raman spectroscopy.....	6
2.3. Fourier transform Raman spectroscopy.....	7
2.3.1. Basics.....	7
2.3.2. FT-Raman measurements.....	10
2.4. Surface enhanced Raman spectroscopy.....	11
2.4.1. Basics.....	11
2.4.2. Mechanisms of surface enhancement.....	13
2.4.3. SERS-active substrates.....	15
2.4.4. SERS measurements.....	16
2.5. UV-VIS absorption measurements .....	17
Chapter 3. Theoretical simulations.....	18
3.1. Molecular mechanics and electronic structure methods.....	18
3.2. Model chemistry.....	21
3.3. DFT methods.....	22
3.4. Basis set.....	23
3.5. Computational details.....	25
Chapter 4. Structural investigations of some coordination compounds by using infrared and FT-Raman spectroscopy in conjunction with theoretical simulations.....	26

4.1. P-N bond length alterations induced by metal coordination and monitored by infrared absorption and FT-Raman spectroscopy in combination with density functional theory calculations.....	26
4.1.1. Introduction.....	26
4.1.2. Results and discussion.....	28
4.1.3. Conclusion.....	39
4.2. Vibrational and kinetic investigations of some trisoxalato complexes of silicon(IV) and germanium(IV).....	40
4.2.1. Introduction.....	40
4.2.2. Results and discussion.....	41
4.2.3. Conclusion.....	53
4.3. Vibrational and conformational analysis of some dianionic complexes with hexacoordinated silicon(IV) and three bidentate ligands of the hydroximato(2-) type.....	54
4.3.1. Introduction.....	54
4.3.2. Results and discussion.....	56
4.3.3. Conclusion.....	65
 Chapter 5. Raman and surface-enhanced Raman spectroscopy in combination with theoretical simulations on biologically active molecules.....	 66
5.1. Raman, infrared and surface-enhanced Raman spectroscopy in combination with <i>ab initio</i> and density functional theory calculations on 10-isopropyl-10H-phenothiazine-5-oxide.....	66
5.1.1. Introduction.....	66
5.1.2. Results and discussion.....	68
5.1.3. Conclusion.....	83
5.2. Infrared, Raman and SERS studies together with theoretical investigations on furan-2-carbaldehyde derivatives.....	85
5.2.1. Introduction.....	85
5.2.2. Results and discussion.....	85
5.2.3. Conclusion.....	96

5.3. Raman and surface enhanced Raman spectroscopy as well as density functional theory calculations on some quinoline derivatives.....	97
5.3.1. Introduction.....	97
5.3.2. Results and discussion.....	97
5.3.3. Conclusion.....	107
Chapter 6. Summary/Zusammenfassung.....	108
6.1. Summary.....	108
6.2. Zusammenfassung.....	112
References.....	115

## Abbreviations

asym.	asymmetric
bend.	bending
br.	broad
CCD	<i>Charge Coupled Device</i>
Calc.	calculated
def.	deformation
DFT	Density Functional Theory
Exp.	experimental
<i>fac</i>	facial
FT	Fourier Transform
HF	Hartree-Fock
IR	infrared
M	metal
m	medium
mbr	medium-broad
<i>mer</i>	meridional
ms	medium-strong
mw	medium-weak
ox	oxalate
Ph	phenyl
R	organic radical
rock.	rocking
s	strong
sh	shoulder
str.	stretching
sym.	symmetric

## Abbreviations

---

UV	ultraviolet
VIS	visible
vs	very strong
vw	very weak
w	weak

# Chapter 1

---

## Introduction

---

Infrared and Raman spectroscopy are two of the most widely used techniques in the physical and natural sciences today. In 1800 Sir William Herschel, British Astronomer Royal, while studying the heating effect produced by various portions of the solar spectrum established that it contained some form of radiant energy which could not be seen [1]. The son of the discoverer of infrared radiation, Sir John Herschel, was able to demonstrate in 1840 the existence of infrared absorption and transmission bands by noting variations in the rate of evaporation of alcohol from blackened paper upon which the solar spectrum was projected [2]. By utilizing detectors, the science of infrared moved steadily ahead and the idea that infrared radiation was quite similar to visible light was beginning to be accepted. The utility of infrared spectroscopy as a tool for identification of molecules and functional groups was realized by chemists in the late 1920s. Modern infrared spectroscopy started in the 1940s and 1950s with the tremendous improvements in instrumentation, which put the technique at the heat of physical chemical research [2].

The Raman effect also allows the observation of vibrational spectra providing information which complements that obtained by infrared spectroscopy. This effect had been repeatedly predicted. Lommel (1878) described certain anomalies of fluorescence,



the colour of which is dependent on the nature of the sample and the frequency of the exciting radiation [3]. Smekal (1923), Kramers and Heisenberg (1925), Schrödinger (1926), and Dirac (1927) predicted the Raman effect by applying quantum mechanics to molecules [4-7]. Raman was looking for the optical analogue of the Compton effect, when, on February 7th, 1928, his co-workers Krishnan and Venkateswaran observed “modified scattering” of sunlight, which Raman identified as Kramers-Heisenberg effect. A short paper describing “A New Type of Secondary Radiation” by Raman and Krishnan was cabled to Nature on February 16th, 1928 [8]. As mentioned above, the basic theory of the Raman effect was developed before its discovery. However, at this time numerical calculations of the intensity of Raman lines were impossible, because this require information on all eigenstates of a scattering system. Placzek (1934) introduced a “semi-classical” approach in the form of his polarizability theory [9]. This provided a basis for many other theoretical and experimental studies. The most important stimulus to the development of the Raman spectroscopy has been the laser, invented by Maiman in 1960 [10]. During a short period the mercury arcs were replaced by these really monochromatic and most powerful light sources. At the same time the photographic plates were replaced by photomultipliers, and scanning grating spectrometers replaced the prism spectrographs. Also, the introduction of double and triple monochromators, an elaborate sample technique (Kiefer, 1977) [11], and later of diode arrays and charge-coupled devices (CCDs) contributed considerably to the development of Raman spectroscopy. However, until about 1950, Raman spectroscopy was applied more often than infrared spectroscopy. The reverse became true after 1950, when automatically recording infrared spectrometers were introduced to the market. Infrared spectroscopy found its place in routine analysis.

In the last few years the investigation of metal coordination complexes by means of infrared absorption and Raman spectroscopy has attached much interest [12]. These spectroscopic techniques represent one of the most useful tools for obtaining information about the structure and properties of molecules from their vibrational transitions, particularly about the strength of the bonds in a molecule despite the fact that the direct assignment of the infrared or Raman bands of relatively complex molecules is rather complicated [12, 13]. Theoretical simulations can certainly assist to

obtain a deeper understanding of the vibrational spectra of complicated molecules. Recently it was shown that density functional theory (DFT) methods are a powerful computational alternative to the conventional quantum chemical methods, since they are much less computationally demanding and take account of the effects of electron correlation [14, 15].

Due to its non-destructive character Raman spectroscopy became during time an invaluable tool in the study of the structure of biologically active molecules. However, the application of conventional Raman spectroscopy is limited by the weak intensity of the Raman scattered light and the appearance of fluorescence. One way to overcome these disadvantages is the use of surface-enhanced Raman spectroscopy (SERS) [16-18]. Although the theoretical understanding of the mechanism of surface enhancement is not definite and still evolving, the experimental data accumulated in the last years has demonstrated SERS to be a sufficiently sensitive spectroscopic method for surface science, analytical applications and biophysics [19].

In the present work, a background of the spectroscopic methods and theoretical calculations is summarized in Chapters 2 and 3. Structural characterisations of various coordination compounds by means of infrared absorption and Raman spectroscopy in combination with density functional theory calculations are presented in Chapter 4. In section 4.1 experimental (infrared and FT-Raman spectroscopy) and theoretical (density functional theory calculations) investigations are performed on the starting materials  $\text{Ph}_2\text{P-N(H)SiMe}_3$  and  $\text{Ph}_3\text{P=NSiMe}_3$  and their corresponding  $[(\text{MeSi})_2\text{NZnPh}_2\text{P-NSiMe}_3]_2$  and  $\text{Li}(o\text{-C}_6\text{H}_4\text{PPh}_2\text{NSiMe}_3)_2 \bullet \text{Et}_2\text{O}$  complexes in order to find out how the P–N bond is affected by the coordination to the metal center. In the next subsections (4.2 and 4.3) two series of hexacoordinated silicon(IV) and germanium(IV) complexes with three symmetrical bidentate oxalato(2-) and unsymmetrical bidentate hydroximato(2-) ligands, respectively, are investigated using FT-Raman and infrared absorption spectroscopy in conjunction with density functional theory calculations in order to elucidate their vibrational spectra. In section 4.2 kinetic investigations of the hydrolysis of two trisoxalato complexes, one with silicon and another one with germanium, are performed at room temperature and at different pH values, while in the

section 4.3 the conformational structures, which are taken from the dianions of the hexacoordinated compounds in the solid state, are determined.

Chapter 5 deals with experimental and theoretical investigations on several biologically active molecules. SER spectra have been recorded and are analysed in order to elucidate the adsorption behavior of the molecules on colloidal silver particles. In section 5.1 a rather detailed experimental and theoretical study of 10-isopropyl-10H-phenothiazine-5-oxide is carried out. The first part of this study presents both an experimental and theoretical vibrational analysis of the above-mentioned phenothiazine derivative. In the second part of the study SER spectra at different pH values are presented and analysed in order to elucidate the adsorption behavior of the molecules on colloidal silver particles and to establish whether or not the molecule-substrate interaction and consequently the SERS effect may be dependent on the pH value of the solution. In the following section the rotational isomers of 5-(4-fluor-phenyl)-furan-2-carbaldehyde are investigated using infrared and FT-Raman spectroscopy in combination with density functional theory calculations. The SER spectra at low pH values have been recorded and are discussed in order to determine the adsorption behavior of these molecules on colloidal silver particles. In section 5.3 experimental and theoretical investigations of quinoline derivatives, isoquinoline and lepidine, by means of FT-Raman spectroscopy and density functional theory calculations are performed. SER spectra in acidic and alkaline environments have been also recorded and are analyzed in order to understand the adsorption behavior of these molecules on colloidal silver particles and to find out the influence of the pH value on the molecule-substrate interaction.

The conclusions drawn from all presented studies are summarized in Chapter 6.

# Chapter 2

---

## Experimental

---

Infrared and Raman spectroscopy are two important vibrational spectroscopy methods. These methods provide complementary images of molecular vibrations, because the mechanisms of the interaction of light quanta with molecules are quite different in those two spectroscopic techniques.

### 2.1. Infrared spectroscopy

#### 2.1.1. Basics

Interaction of infrared radiation with a vibrating molecule is only possible if the electric vector of the radiation field oscillates with the same frequency as does the molecular dipole moment. A vibration is infrared active only if the molecular dipole moment  $\mu$  is modulated by the normal vibration

$$\left(\frac{\partial\mu}{\partial q}\right)_0 \neq 0, \quad (2.1)$$

where  $q$  describes the motion of the atoms during a normal vibration and the subscript 0 refers to the derivative taken at the equilibrium configuration.

Infrared spectra are usually recorded by measuring the transmittance of infrared light quanta with a continuous distribution of the sample. The frequencies of the absorption bands  $\nu_s$  are proportional to the energy difference between the vibrational ground and excited states [20].

### 2.1.2. Infrared measurements

The infrared spectra presented in this work were recorded in the range from 400 to 4000  $\text{cm}^{-1}$  with a BRUKER IFS 25 spectrometer. For infrared measurements the samples were mixed with KBr and pressed by 9.8 Kbar in order to obtain thin pellets with a thickness of about 0.3 mm. The spectra were obtained with a spectral resolution of 2  $\text{cm}^{-1}$ .

## 2.2. Raman spectroscopy

When a molecule is exposed to an electric field, electrons and nuclei are forced to move in opposite directions, a dipole moment proportional to the electric field strength and to the molecular polarizability  $\alpha$  is being induced. A molecular vibration can be only observed in the Raman spectrum if there is a modulation of the molecular polarizability by the vibration

$$\left(\frac{\partial\alpha}{\partial q}\right)_0 \neq 0, \quad (2.2)$$

where  $q$  stands for the normal coordinates describing the motion of the atoms during a normal vibration and the subscript 0 indicates that the derivative is taken at the equilibrium configuration.

The origin of Raman spectroscopy is an inelastic scattering effect, but in a Raman experiment the elastic as well as the inelastic scattering of radiation by the sample is observed. The elastic scattering, which is also called Rayleigh scattering, corresponds to the light scattered at the frequency of the incident radiation  $\nu_0$ . The molecule “absorbs” no energy from the incident radiation in this case. The inelastic scattered light, which is

known as the Raman radiation, is shifted in frequency, and hence energy, from the frequency of the incident radiation by the vibrational energy that is gained or lost in the molecule ( $h\nu_0 \mp h\nu_s$ ). According to Boltzmann's law, most molecules are in their vibrational ground state at ambient temperature, a much smaller number being in the vibrationally excited state. Therefore, the Raman process, which transfers vibrational energy to the molecule and leaves a quantum of lower energy ( $h\nu_0 - h\nu_s$ ) has a higher probability than the reverse process, and the corresponding Raman lines are referred to as Stokes and anti-Stokes lines, respectively. The intensities of Stokes lines, caused by quanta of lower energy, are higher than those of anti-Stokes lines. Therefore usually only Stokes radiation is recorded as a Raman spectrum [20].

## **2.3. Fourier transform Raman spectroscopy**

### **2.3.1 Basics**

In 1986 Hirschfeld and Chase [21] demonstrated that Raman spectra, excited with lasers in the near-infrared region, may be recorded with the FT-IR instruments originally designed for absorption spectroscopy in the near-infrared region. They demonstrated that the excitation of fluorescence, very often associated with Raman spectroscopy excited in the UV-VIS region, can be avoided. Raman spectra of fluorescing dyes and even of explosives were obtained, demonstrating that the thermal load by the illumination with the laser was not too large. They proved that the prejudice of many scientists against this technique [22, 23] was apparently not justified. Immediately after this publication, several groups started to apply this technique and instrument manufacturers began designing FT-Raman spectrometers. The central component of a FT spectrometer is a Michelson interferometer (Fig. 2.1).

Fourier transform spectrometers operate by dividing the incoming radiation into two beams, subjecting each beam to a different time delay, and recombining the beams so that interference occurs [24].

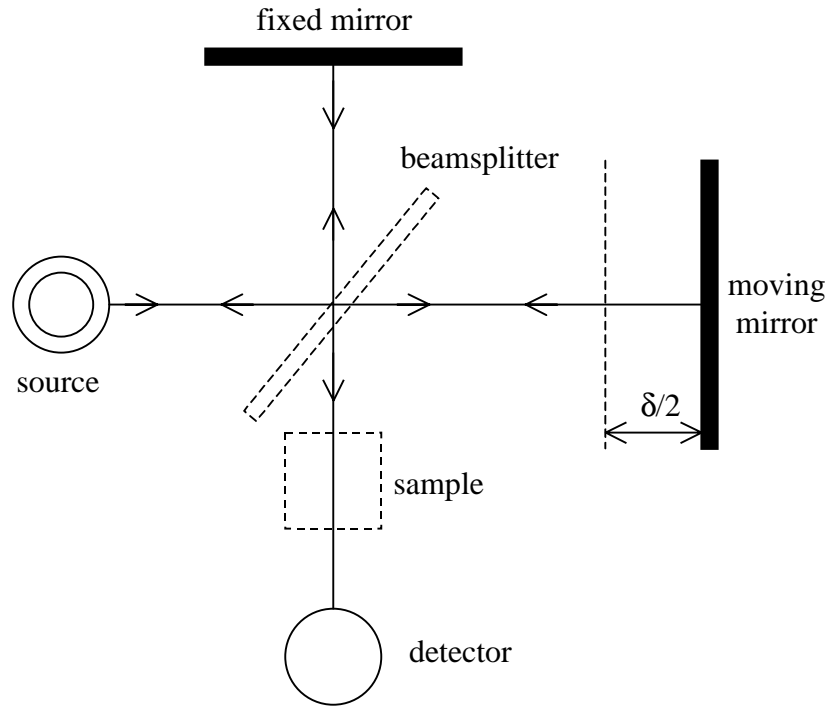


Fig. 2.1. The Michelson interferometer.

The intensity  $I$  falling on the detector is a function of the optical path difference  $\delta$  between the two beams [25], which is produced by translating a mirror along the beams:

$$I(\delta) = \int_0^{\infty} B(\bar{\nu}) [1/2 + \cos(2\pi\bar{\nu}\delta)] d\bar{\nu}. \quad (2.3)$$

where  $B(\bar{\nu})$  is the spectral power density at the wavenumber  $\bar{\nu}$ . Subtracting the first term in the integral, which represents the total power, results in:

$$I'(\delta) = I(\delta) - 1/2 \int_0^{\infty} B(\bar{\nu}) d\bar{\nu} = \int_0^{\infty} B\bar{\nu} \cos(2\pi\bar{\nu}\delta) d\bar{\nu}. \quad (2.4)$$

A plot of  $I(\delta)$ , or  $I'(\delta)$  against  $\delta$  is known as an interferogram. The interferogram contains all the spectral information, but in a form, which is not directly accessible. In order to obtain a spectrum it is necessary to calculate the Fourier transform of equation 2.4.

$$B(\bar{\nu}) \propto \int_{-\infty}^{+\infty} I'(\delta) \cos(2\pi\bar{\nu}\delta) d\delta. \quad (2.5)$$

In practice, it is of course only possible to record the interferogram over a restricted range of the path difference. If  $\delta_{\max}$  is the greatest path difference employed, the transform becomes:

$$B(\bar{\nu}) \propto \int_{-\delta_{\max}}^{+\delta_{\max}} I'(\delta) \cos(2\pi\bar{\nu}\delta) d\delta . \quad (2.6)$$

The suppression of the subsidiary maxima introduced by the finite integral is achieved by a mathematical procedure known as apodisation. Apodisation unfortunately has the effect of broadening the band, leading to a lower resolution in the apodised spectrum than in the unapodised spectrum.

A practical spectrometer has to record data at finite sampling intervals. This may be conveniently achieved by moving the mirror over successive fixed distances, giving an optical path increment  $\Delta\delta$ . The effect of the finite sampling interval is to reduce the range of wavenumbers for which meaningful spectral information is obtained. This phenomenon is known as aliasing and determines the maximum stepping interval that can be used in a particular wavenumber range. An alternative to stepping the moving mirror is to scan it rapidly at constant velocity  $v$ . Equation 2.4 becomes now:

$$I'(t) = \int_0^{\infty} B(\bar{\nu}) \cos(4\pi\bar{\nu}vt) d\bar{\nu} \quad (2.7)$$

since the optical path difference is given by  $\delta = 2vt$ . The total time for a given scan is determined by the maximum optical path difference  $D$ . The Fourier transform for a single-sided operation is then

$$B(\bar{\nu}) \propto 2 \int_0^{D/2v} I'(t) \cos(4\pi\bar{\nu}vt) dt . \quad (2.8)$$

Weak spectral signals in rapid scan Fourier transform spectroscopy require that an interferogram to be recorded repeatedly and the results (either in interferograms or the computed spectra) averaged to achieve the required signal-to-noise ratio.

An interferometer, or Fourier transform spectrometer, gives certain inherent advantages over a conventional dispersive spectrometer:

1. Multiplex advantage ( Fellgett's advantage): An interferometer provides information about the entire spectral range during the entire period of the measurement, whereas a dispersive spectrometer provides information only about the narrow wavenumber region which falls within the exit slit of the monochromator at any given time.



2. Throughput advantage (Jacquinot's advantage): The interferometer can operate with a large circular aperture, and using large solid angles at the source and at the detector, whereas a dispersive spectrometer requires long, narrow slits to achieve adequate resolution.

Several additional advantages follow from the multiplex and throughput advantages:

- (a) Large resolution power: since the resolving power mainly depends on the maximum optical path difference introduced ( $D$ ), high resolving power can be achieved by using large mirror movements. Also, unlike dispersive spectrometers, the wavenumber resolution is constant over the spectral range scanned.
- (b) High wavenumber accuracy: the wavenumber accuracy is determined by the precision with which the position of the moving mirror can be measured.
- (c) Fast scan time and a large wavenumber range are possible.

There are also some disadvantages of Fourier transform spectrometer over conventional dispersive spectrometer. There is a multiplex disadvantage, since the statistical noise of the exiting radiation scattered onto the detector is transformed to noise at all frequencies in the Raman spectrum. Another disadvantage is that FT-Raman spectroscopy is normally a single beam technique, thus comparison of sample and reference has always to be performed by computer subtraction.

### **2.3.2. FT-Raman measurements**

All FT-Raman spectra discussed in the present work were recorded at room temperature using a BRUKER IFS 120HR spectrometer equipped with a FRA 106 Raman module. The spectral resolution was  $2\text{ cm}^{-1}$ . Radiation of 1064 nm from a Nd-YAG laser with an output power of 800 mW was employed for excitation. A Ge detector cooled with liquid nitrogen was used.

For the kinetic investigations a temperature controlled sample chamber equipped with a magnetic stirrer was attached to the spectrometer (see Fig. 2.2). The stirring rate was kept constant during the measurements. The spectra were recorded at room temperature with an acquisition time of 20 min and a resolution of  $4\text{ cm}^{-1}$ .

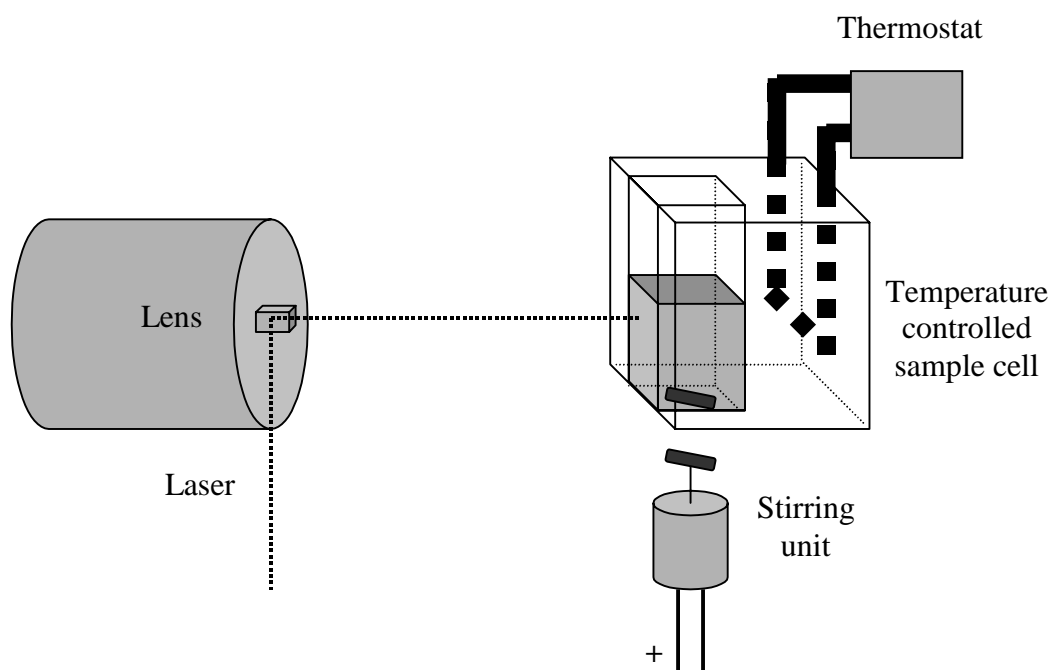


Fig. 2.2. Schematic drawing of the temperature controlled sample chamber attached to the Bruker IFS 120HR spectrometer equipped with a FRA 106 Raman module.

## 2.4. Surface enhanced Raman spectroscopy

### 2.4.1. Basics

Surface enhanced Raman spectroscopy (SERS) was first discovered by Fleischmann and co-workers in 1974, when they observed the strong Raman scattering of the pyridine molecules adsorbed on silver electrodes that had been electrochemically roughened [26]. The scientific groups of Jeanmaire and Van Duyne [27] and Albrecht and Creighton [28] confirmed this enhancement phenomenon (up to  $10^6$ ) and attributed the effect to complex surface enhancement processes. Many of the advantages of nor-

mal Raman scattering like molecularly specific vibrational spectra, simple versatile sampling and ready determination of analytes in air, under vacuum and in water are applicable to this technique. However, with SERS, increased sensitivity is obtained and much lower concentrations can be studied. Detection limits are considerably lower (down to  $10^{-9}$  M) than those for resonance Raman scattering [29]. In practice the sensitivity of these experiments to interference and the requirement for adsorption to specific metal surfaces has limited the development of the technique [30, 31]. Surface photolysis and fluorescence have proven to be a problem in some experiments. Surface selection rules are also available. In their simplest form, and assuming no specific symmetry selection rules, the most intense bands are predicted as those from vibrations, which induce a polarization of the adsorbate electron cloud perpendicular to the metal surface [32, 33]. This information can be applied qualitatively to give an approximate indication of the angle a molecule subtends to the surface.

These advantages enable scientists to gain unique insights into a number of surface problems. However, the technique does have significant limitations:

1. The analyte requires to be in close proximity to a suitable roughened surface, which can result in the involvement of complex surface chemistry.
2. The quantitative reproducibility is rather disappointing, since the signal is extremely sensitive to a number of factors including any change in adsorbate orientation at the metal surface, the extent of adsorption and the nature of the surface roughness.
3. Because of enhancement factors of up to  $10^{15}$  (single molecule detection) and specific selection rules, it might be difficult to relate the SER spectra to the Raman scattering from the parent species before adsorption. It is possible that an impurity within a sample or a species formed by surface photochemistry may be preferentially enhanced. In these cases, the spectrum becomes complex and difficult to interpret.

Despite these difficulties, SERS has become an increasingly popular analytical tool, which has been applied in numerous fields.

### 2.4.2. Mechanisms of surface enhancement

The SERS phenomenon arises from an interaction between the adsorbate and the surface plasmons, which can be considered to be a wave of electrons present on the surface of the metal substrate, if excited with the appropriate wavelength. The nature of the mechanisms, which produce the surface enhancement effect, is still unclear and remains the focus of debate [34, 35]. Most researchers believe that much of the enhancement is due to an electromagnetic (EM) mechanism [34, 35]. However a second mechanism, charge transfer (CT) mechanism, has been also proposed and there is significant evidence that this also contributes to the overall SERS enhancement [36, 37]. Discussions over the relative contribution to the total enhancement of both these mechanisms are ongoing.

#### 1. *Electromagnetic enhancement*

Surface roughness is an essential requirement of SERS. On a smooth metal surface, surface plasmons exist as waves of electrons bound to the metal surface and are capable of moving only in a direction parallel to that surface. On a roughened metal surface the plasmons are no longer confined and the resulting electric field can radiate both in parallel and perpendicular direction to the surface. When an incident photon falls on the roughened surface, excitation of the plasmon resonance of the metal may occur and on the roughened surface this permits scattering. Additionally, due to the difference in dielectric constants between the roughened surface and the surrounding media, a concentration of electric field density occurs at sharp points on the surface [34, 35]. Experimental data indicated that this enhancement may be as large as  $10^6$  [27, 28].

#### 2. *Charge transfer mechanism*

Numerous studies have been carried out in order to establish or disqualify the existence of the charge transfer (CT) mechanism [36, 37]. Its supporters use it to explain why the enhancement factor of the first adsorbate layer is much greater than subsequent layers. Basically, the enhancement experienced from charge transfer results when molecules

physisorb or chemisorb directly on the roughened surface, forming an adsorbate-metal complex. If chemisorption occurs, the molecular orbitals of the adsorbate are broadened by an interaction with the conduction bands of the metal surface. This results in a ready transfer of electrons and excitation from the metal to the adsorbate and vice versa. As the mechanism depends on a metal-adsorbate bond, the observed enhancement dramatically reduces as the distance of the adsorbate from the metal surface is increased (it is expected to occur with distances up to approximately 20 Å). Thus, it effectively operates only on the first layer of adsorbates.

Campion and co-workers reported the first direct experimental evidence of the charge transfer mechanism linking new features in the electronic spectrum of an adsorbate to SERS, under conditions where electromagnetic enhancements are unimportant [38]. They noted that it was difficult to observe charge transfer only because electromagnetic effects had to be accounted for and removed. They overcame this problem by measuring SERS enhancement on a flat, smooth single crystal surface where electromagnetic effects were small and well understood. Hildebrandt and Stockburger carried out an extensive study of surface enhanced resonance Raman scattering (SERRS) of rhodamine 6G on colloids, to explore the enhancement mechanisms involved in this technique [39]. They reported that two different types of adsorption sites on the colloid surface were responsible for the enhancement experienced: a non-specific adsorption site that had a high surface coverage on the colloid surface, which resulted in an enhancement factor of 3000 and could be explained by a classical electromagnetic mechanism; and a specific adsorption site that was only activated in the presence of certain anions ( $\text{Cl}^-$ ,  $\text{I}^-$ ,  $\text{F}^-$ ,  $\text{Br}^-$  and  $\text{SO}_4^{2-}$ ). This specific site had a low surface coverage (approximately three per colloidal particle); however, the authors claimed an enhancement of  $10^6$ . This enhancement was believed to be due to a charge transfer mechanism. In a further study, they concluded that charge transfer enhancement is strongly dependent upon the structural and electronic properties of the analyte [40].

The understanding and experimental proof supporting this enhancement mechanism is limited. The problem is even more complex due to the fact that electromagnetic enhancement increases as the adsorbate-surface distance decreases and only additional

enhancement can be classified as charge transfer. However, the degree of enhancement of the first layer is very large. Thus, many questions remain unanswered, and therefore, the charge transfer mechanism is not yet completely accepted.

### **2.4.3. SERS-active substrates**

Surface enhancement is observed from a limited number of roughened metals, i.e. silver, gold, copper, aluminium, lithium and sodium. The intensity of scattering from adsorbed analytes is no longer proportional to the frequency to the fourth power ( $\nu^4$ ), in fact, the intensity of the bands is related to the frequency of the surface plasmon resonance and the laser excitation frequency [26-28]. The exact dependence is related to the nature of the metal substrate, in particular to the identity of the metal and its roughness. Since SERS was first observed numerous SERS active substrates have been developed. Several different metal electrodes have been employed for SERS, but the largest surface enhancement was observed from those made of silver [26]. When using an electrode as a SERS substrate, the surface roughness can be controlled by the right choice of electrolytes and electrochemical cycle. The degree of adsorption is also affected by the applied electrode potential during the Raman measurement [41]. The main disadvantage of this technique is the reproducibility of the electrode surface; it is incredibly difficult to ensure that the same degree of surface roughness and potential is achieved for each experiment.

Colloidal suspensions are attractive as SERS substrates, since they can be prepared with a high reproducibility. Furthermore they are relatively inexpensive. Because a fresh reproducible colloidal surface is available for each analysis reliable SERS analysis is possible. Numerous metal colloidal suspensions have been used including gold and copper; however, silver is the most popular one. Several methods are suggested for the preparation of various silver colloids [42, 43], producing silver particles of different diameters and uniformity. The Lee-Meisel [43] preparation method produces particles with diameters in the range of 24-30 nm with an UV-visible absorption maximum around 400 nm. The SERS enhancement is further increased by aggregating of colloidal particles [44]. The act of aggregation forms clusters of colloid, within which are intersti-

ces. The electric field established in these regions is predicted to be very large, resulting in a very intensive surface enhancement.

There are many other SERS-active substrates, e.g. chemical or mechanical roughened metal island films and metal films [45, 46]. However, the production of these films is difficult to control, and hence, it is difficult to obtain reproducible results [47]. Metal colloidal particles formed upon porous membranes such as filter papers, gels, beads, polymers etc. have been also developed [48, 49]. These adsorbed substrates are not very popular because they are expensive and in some cases irreproducible. Furthermore, their preparation is rather complicated and they are more susceptible to contamination.

#### **2.4.4. SERS measurements**

In all SERS studies presented here, a sodium citrate silver colloid, prepared according to the standard procedure of Lee and Meisel [43], was employed as SERS substrate.  $\text{AgNO}_3$  (90 mg) was dissolved in 500 ml of water and heated to boiling with continuous stirring. A 10 ml portion of 1% aqueous trisodium citrate was added drop wise, and the reaction mixture was boiled for another 60 min. The resultant colloid was yellowish gray with an absorption maximum at 407 nm. Small amounts of a  $10^{-1}$  M ethanol solution were added to 3 ml of the silver colloid. NaCl solution ( $10^{-2}$  M) was also added (10:1) for producing a stabilisation of the colloidal dispersion that yields to a considerable enhancement of the SER signal [50]. The final concentration of the samples was approximately  $3 \cdot 10^{-4}$  M. NaOH, HCl and  $\text{H}_2\text{SO}_4$  were used in order to adjust the pH values. All starting materials involved in substrate and sample preparation were purchased from commercial sources as analytical pure reagents.

The SER spectra of the samples in silver colloid were collected in a  $180^\circ$  back-scattering arrangement. For excitation the 514.5-nm line (300 mW) of a Spectra Physics argon ion laser has been used. The scattered Raman light was analyzed with a Spex 1404 double monochromator and the dispersed Raman stray light was detected with a Photometrics model 9000 CCD camera. The spectral resolution was  $2 \text{ cm}^{-1}$ .

## **2.5. UV-VIS absorption measurements**

All UV-visible absorption spectra of silver colloids and their mixtures with different samples presented in the next sections have been recorded with a Perkin Elmer Lambda 19 UV-VIS-NIR spectrometer with a scan speed of 240 nm/min.



# Chapter 3

---

## Theoretical simulations

---

Computational chemistry simulates chemical structures and reactions numerically, based in full or in part on the fundamental laws of physics. It allows chemists to study chemical phenomena by running calculations on computers rather than by examining reactions and compounds experimentally. Some methods can be used to model not only stable molecules, but also short-lived, unstable intermediates and even transition states. In this way, they can provide information about molecules and reactions, which is extremely difficult to be obtained experimentally. Computational chemistry is therefore both an independent research area and a vital adjunct to experimental studies [51].

### 3.1. Molecular mechanics and electronic structure methods

There are two broad areas within computational chemistry [52] devoted to the structure of molecules and their reactivity: (i) molecular mechanics and (ii) electronic structure theory.

(i) Molecular mechanics simulations use the laws of classical physics to predict the structures and the properties of the molecules. There are many different molecular mechanics methods, each one being characterized by its particular force field.

Molecular mechanics calculations do not explicitly treat the electron in a molecular system; they perform calculations based upon the interactions among the nuclei. Electronic effects are implicitly included in force fields through parametrization. Therefore, molecular mechanics computations are quite inexpensive computationally and can be used for very large systems containing thousands of atoms. However, they also carries limitations: no force field can be usually used for all molecular systems of interest and they cannot describe molecular properties, which depend on subtle electronic details.

(ii) Electronic structure methods use the laws of quantum mechanics rather than of classical physics as the basis for their computations. Quantum mechanic states that the energy and other related properties of a particle might be obtained by solving the Schrödinger equation:

$$\left\{ \frac{-h^2}{8\pi^2 m} \nabla^2 + V \right\} \Psi(\vec{r}, t) = \frac{ih}{2\pi} \frac{\partial \Psi(\vec{r}, t)}{\partial t}. \quad (3.1)$$

In this equation  $\Psi$  is the wavefunction and depends on the coordinates  $\vec{r}$  and time  $t$ ,  $m$  is the mass of the particle,  $h$  is Planck's constant, and  $V$  is the potential field in which the particle is moving. The Schrödinger equation for a collection of particles like a molecule is very similar. In this case,  $\Psi$  would be a function of the coordinates of all particles in the system as well as of the time  $t$ . However, exact solutions of the Schrödinger equation are not computationally practical.

Electronic structure methods are characterized by their various mathematical approximations to solve the Schrödinger equation. There are two major classes of electronic structure methods:

- *Semi-empirical* methods (AM1, PM3) use parameters derived from experimental data to simplify the computation [53, 54]. They solve an approximate form of the Schrödinger equation that depends on having appropriate parameters available for the type of chemical system under investigation. Different *semi-empirical* methods are largely characterised by their different parameter sets.

- *Ab initio* methods [55], unlike either molecular mechanics or *semi-empirical* methods, use no experimental parameters. Instead, their computations are based solely on the laws of quantum mechanics and on the values of a small number of physical constants: the speed of light, the masses and charges of electrons and nuclei and Planck's constant. *Ab initio* methods use a series of rigorous mathematical approximations to solve the Schrödinger equation.

*Semi-empirical* and *ab initio* methods differ in the trade-off made between computational cost and accuracy of results. *Semi-empirical* methods are relatively inexpensive and provide reasonably qualitative descriptions of molecular systems and fairly accurate quantitative predictions of energies and structures for systems where good parameter sets exist. In contrast, *ab initio* computations provide high quality quantitative predictions for a broad range of systems. They are not limited to any specific class or size of a system [55].

Recently, a third class of electronic structure methods has gained steadily in popularity: *density functional* methods [56]. These density functional theory (DFT) methods are similar to *ab initio* methods in many ways. DFT calculations require about the same amount of computation resources as Hartree-Fock (HF) theory, the least expensive *ab initio* method. DFT methods are attractive because they include in their model the effects of electron correlation, the fact that electrons in a molecular system react to one another's motion and attempt to keep out of one another's way. Hartree-Fock calculations consider this effect only in an average sense - each electron sees and reacts to an averaged electron density - while methods including electron correlation account for the instantaneous interactions of pairs of electrons with opposite spin. This approximation causes Hartree-Fock results to be less accurate for some types of systems. Thus, DFT methods can provide the benefits of some more expensive *ab initio* methods at essentially Hartree-Fock cost.

### 3.2. Model chemistry

A model chemistry has been defined as an unbiased, uniquely defined, and uniformly applicable theoretical model for predicting the properties of chemical systems [51].

Other desirable features of a model chemistry include:

- *Size consistency*: the results given for a system of molecules infinitely separated from one another ought to equal the sum of the results obtained for each individual molecule calculated separately. Another way of describing this requirement is that the error in the predictions of any method should scale roughly in proportion to the size of the molecule. When size consistency does not hold, comparing the properties of molecules of different sizes will not result in qualitatively meaningful differences.
- Reproducing the *exact solution for the relevant  $n$ -electron problem*: a method ought to yield the same results as the exact solution of the Schrödinger equation to the greatest possible extent. What this means specifically depends on the theory underlying the method.
- *Variational*: the energies predicted by a method ought to be an upper bound to the real energy resulting from the exact solution of the Schrödinger equation.
- *Efficient*: calculations with a method ought to be practical with the existing computer technology.
- *Accurate*: ideally, a method ought to produce highly accurate quantitative results. A method should at least predict qualitative trends for molecular properties for groups of molecular systems.

A model chemistry generally consists of the combination of a theoretical method with a basis set. Each such a unique pairing of a method with a basis set represents a different approximation of the Schrödinger equation. Results for different systems generally may only be compared when they have been predicted via the same model chemistry. Different model chemistry may be compared and tested by comparing their results for the same systems and with the results of experiments.

### 3.3. DFT methods

DFT methods compute electron correlation via general *functionals* of the electron density. Such methods owe their modern origin to the Hohenberg-Kohn theorem [57], published in 1964, which demonstrates the existence of a unique functional, which determines exactly the ground state energy and density. However, the theorem does not provide the form of this functional. The approximate functionals employed by current DFT methods divide the electronic energy into several terms:

$$E = E^T + E^V + E^J + E^{xc} \quad (3.2)$$

where  $E^T$  is the kinetic energy term (arising from the motion of the electrons),  $E^V$  includes terms describing the potential energy of the nuclear-electron attraction and of the repulsion between pairs of nuclei,  $E^J$  is the electron-electron repulsion term (it is also described as the Coulomb self-interaction of the electron density), and  $E^{xc}$  is the exchange-correlation term and includes the remaining part of the electron-electron interactions. All terms except the nuclear-nuclear repulsion are functions of the electron density  $\rho$ .  $E^T + E^V + E^J$  corresponds to the classical energy of the charge distribution. The  $E^{xc}$  term in equation 3.2 accounts for the remaining terms in the energy: the exchange energy arising from the antisymmetry of the quantum mechanical wavefunction and the dynamic correlation in the motions of the individual electrons. Hohenberg and Kohn [57] demonstrated that  $E^{xc}$  is determined entirely by the electron density and is usually divided into separate parts, referred to as the *exchange* and *correlation* parts, but corresponds to the same-spin and mixed-spin interactions, respectively:

$$E^{xc}(\rho) = E^x(\rho) + E^c(\rho) \quad (3.3)$$

All three terms are again functionals of the electron density, and the functional defining the two components on the right side of equation 3.3 are termed *exchange functionals*  $E^x$  and *correlation functionals*  $E^c$ , respectively. Both components can be of two distinct types: *local* functionals depend only on the electron density  $\rho$ , while *gradient-corrected* functionals depend on both  $\rho$  and its gradient,  $\nabla\rho$ .

*Local exchange* and *correlation* functionals only involve the value of the electron spin densities. Slater and  $X\alpha$  are well-known local exchange functionals [58], and the local spin density treatment of Vosko, Wilk and Nusair (VWN) is a widely used local correlation functional [59].

*Gradient-corrected* functionals involve both the values of the electron spin densities  $\rho$  and their gradients. Such functionals are also sometimes referred to as *non-local* in the literature. A popular gradient-corrected exchange functional is the one proposed by Becke in 1988 [60]; a widely-used gradient-corrected correlation functional is the LYP functional of Lee, Yang and Parr [61]. The combination of the two forms is referred as the B-LYP method. Perdew has also proposed some important gradient-corrected correlation functionals, known as Perdew 86 and Perdew-Wang 91 [62].

There are also several *hybrid* functionals, which define the exchange functional as a linear combination of Hartree-Fock, local, and gradient-corrected exchange terms; this exchange functional is then combined with a local and/or gradient-corrected correlation functional. The best known of these hybrid functionals is Becke's three-parameter formulation [61-63]; hybrid functionals based on it are available in *Gaussian* [56] via the B3LYP and B3PW91 keywords. Becke-style hybrid functionals have proven to be superior to the traditional functionals defined so far.

### 3.4. Basis set

A *basis set* is a mathematical description of the orbitals within a system used to perform the theoretical calculation [52]. The basis set can be interpreted as restricting each electron to a particular region of space. Larger basis sets impose fewer constraints on electrons and approximate each orbital more accurately but require more computational resources. Standard basis sets for electronic structure calculations use linear combinations of basis functions (one-electron functions) to form the orbitals. An individual molecular orbital is defined as:

$$\phi_i = \sum_{\mu=1}^N c_{\mu i} \chi_{\mu} \quad (3.4)$$

where the coefficients  $c_{\mu i}$  are known as the *molecular orbital expansion coefficients*.

The basis functions  $\chi_1 \dots \chi_N$  are chosen to be normalized.

*Gaussian* and other *ab initio* electronic structure programs use basis functions which are themselves composed of a linear combination of Gaussian functions; such basis functions are referred to as *contracted functions*, and the component Gaussian functions are referred to as *primitives*. A basis function consisting of a single Gaussian function is termed *uncontracted*. The *Gaussian* program package [56] offers a wide range of pre-defined basis sets, which may be classified by the number and type of basis functions that they contain.

- *Minimal basis sets* contain the minimum number of basis functions needed for each atom. They use fixed-size atomic-type orbitals. The STO-3G basis set is a minimal basis set [64].
- *Split valence basis sets*, such as 3-21G and 6-31G, have two (or more) sizes of basis function for each valence orbital and allow orbitals to change size, but not to change shape [65-67]. *Triple split valence* basis sets, like 6-311G, use three sizes of contracted functions for each orbital-type [68, 69].
- *Polarized basis sets*, by adding orbitals with angular momentum beyond what is required for the description of each atom in the ground state, allow orbitals to change the shape. The 6-31G(d) basis set also known as 6-31G\* which contains d functions added to the heavy atoms, is becoming very popular for calculations involving up to medium-sized systems [70, 71].
- *Diffuse functions* are large-size versions of s- and p-type functions (as opposed to the standard valence-size functions). They allow orbitals to occupy a larger region of space. Basis sets with diffuse functions are important for systems where electrons are relatively far from the nucleus: molecules with lone pairs, anions and other systems with significant negative charge, systems in their excited states, systems with low ionisation potentials, and so on. The 6-31+G(d) is the 6-31G(d) basis set with diffuse functions added to heavy atoms [70, 71].

### 3.5. Computational details

The theoretical calculations of the structures and vibrational wavenumbers of all compounds investigated in the present work were performed by using the Gaussian 98 program package [56]. The density functional theory (DFT) calculations were carried out with Becke's 1988 exchange functional [60] and the Perdew-Wang 91 gradient corrected correlation functional (abbreviated as BPW91) [63] and Becke's three-parameter hybrid method using the Lee-Yang-Parr correlation functional (abbreviated as B3LYP) [62]. For comparison purposes, *ab initio* calculations performed at the Hartree-Fock (HF) level of theory were also performed. The 6-31G\*, 6-31+G\* and 6-311+G\* Pople basis sets were used for the geometry optimisation and normal modes calculations at all theoretical levels. At the optimised structure of the examined species no imaginary frequency modes were obtained, proving that a local minimum on the potential energy surface was found.



# Chapter 4

---

## **Structural investigations of some coordination compounds by using infrared and FT-Raman spectroscopy in conjunction with theoretical simulations**

---

### **4.1. P-N bond length alterations induced by metal coordination and monitored by infrared absorption and FT-Raman spectroscopy in combination with DFT calculations**

#### **4.1.1. Introduction**

The P-N bond is one of the most intriguing in chemistry and many of its more subtle aspects still elude a detailed and satisfactory description [72]. Of particular interest are phosphanylaminines ( $R_2P-NR_2'$ ) and iminophosphoranes ( $R_3P=NR'$ ) and their cyclic analogues [73]. Iminophosphoranes with their formal P=N double bond exhibit comparatively short P=N bond lengths [74, 75]. However, phosphanylaminines also typically exhibit unexpectedly short P-N bond lengths as well as trigonal planar geometry around their nitrogen atoms [76, 77].

Recently it was shown that diphenylphosphanyl(trimethylsilyl)amine  $\text{Ph}_2\text{P-N(H)SiMe}_3$  (**1a**) can be readily synthesised by the reduction of the iminophosphorane  $\text{Ph}_3\text{P=NSiMe}_3$  (**1b**) with sodium, followed by a hydrolysis with  $\text{NH}_4\text{Br}$  or water. Deprotonation of the amine with  $[\text{Zn}\{\text{N}(\text{SiMe}_3)_2\}_2]$  leads to the dimeric zinc complex  $[\{(\text{MeSi})_2\text{N}\}\text{Zn}(\text{Ph}_2\text{PNSiMe}_3)]_2$  (**2a**) [78]. On the other hand, the lithiation of the iminophosphorane (**1b**) gives the *ortho*-metallated species  $\text{Li}(o\text{-C}_6\text{H}_4\text{PPh}_2\text{NSiMe}_3)_2\cdot\text{Et}_2\text{O}$  (**2b**), which exhibits all the requirements of an organometallic ligand capable of *side-arm* donation [79, 80]. The deprotonated *ortho*-phenyl carbon atom should give access to metal-carbon  $\sigma$  bonds in transmetallation reactions, while the  $\text{Ph}_3\text{P=NSiMe}_3$  moiety should be capable of donation to the same metal centre through the imine nitrogen atom. Previous studies have demonstrated that this ligand is able to even stabilise diaryl-stannylenes and plumbylenes in their monomeric forms [81] and to chelate zinc(II), copper(I), indium(III) and iron(II) metal ions [82, 83].

Vibrational spectroscopy has been proven to be a useful tool to obtain information about the strength of the bonds in a molecule despite the fact that the assignment of the infrared and Raman bands of relatively complex molecules is rather complicated. Theoretical calculations can certainly assist to obtain a deeper understanding of the vibrational spectra of complicated molecules.

In the present study, experimental (infrared and FT-Raman spectroscopy) and theoretical (DFT calculations) investigations have been performed on the starting materials  $\text{Ph}_2\text{P-N(H)SiMe}_3$  (**1a**) and  $\text{Ph}_3\text{P=NSiMe}_3$  (**1b**) and their corresponding complexes  $[(\text{MeSi})_2\text{NZnPh}_2\text{PNSiMe}_3]_2$  (**2a**) and  $\text{Li}(o\text{-C}_6\text{H}_4\text{PPh}_2\text{NSiMe}_3)_2\cdot\text{Et}_2\text{O}$  (**2b**) in order to correlate the spectroscopic changes evidenced in the spectra of the coordination compounds with the solid state structural parameters (X-ray structures). This should provide insight to what extent the P–N bond is affected by the coordination to the metal centre and whether the Lewis-basic imido nitrogen atom is involved in coordination in the gas phase.

### 4.1.2. Results and discussion

The starting materials  $\text{Ph}_2\text{P-N(H)SiMe}_3$  (**1a**) and  $\text{Ph}_3\text{P=NSiMe}_3$  (**1b**) and their corresponding metal complexes have been investigated by using infrared absorption and FT-Raman spectroscopy in combination with DFT calculations in order to elucidate both the vibrational spectra of these species as well as to provide insights into their coordination behavior. In **2a** the deprotonated anionic  $[\text{Ph}_2\text{PNSiMe}_3]^-$  moiety coordinates *via* the phosphorus and nitrogen atoms to the zinc atoms. This coordination causes a shortening of the P-N single bond length with respect to the phosphanylamine **1a**. On the other hand, *ortho* metallation of  $\text{Ph}_3\text{P=NSiMe}_3$  (**1b**) and imino group metal *side-arm* coordination is in all known cases accompanied by P-N bond lengthening. These variations of the bond lengths should be detectable in vibrational spectroscopic experiments as not all coordination compounds can be obtained as single crystals suitable for X-ray diffraction experiments.

#### *Density functional theory calculations*

The optimised geometries of the starting material  $\text{Ph}_2\text{P-N(H)SiMe}_3$  (**1a**) and the model compound  $[(\text{SiH}_3)_2\text{NZn}(\text{CH}_3)_2\text{PNSiH}_3]_2$  (**2a\***) are illustrated in Fig. 4.1 and the selected structural parameters compared with the experimental crystal structure data are summarized in Table 4.1.

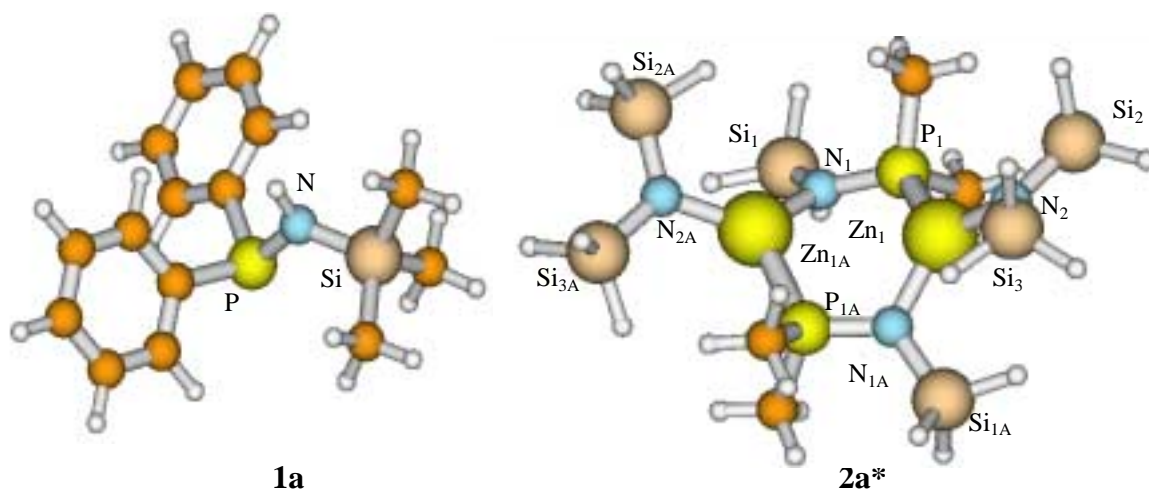


Fig. 4.1. Optimized geometries of the starting material  $\text{Ph}_2\text{P-N(H)SiMe}_3$  (**1a**) and the model compound  $[(\text{SiH}_3)_2\text{NZn}(\text{CH}_3)_2\text{PNSiH}_3]_2$  (**2a\***).

Table 4.1. Selected calculated bond lengths (pm) and angles ( $^{\circ}$ ) of the  $\text{Ph}_2\text{P-N(H)SiMe}_3$  (**1a**) and the model compound  $[(\text{SiH}_3)_2\text{NZn}(\text{CH}_3)_2\text{PNSiH}_3]_2$  (**2a\***) compared to the crystal structure data.

$\text{Ph}_2\text{P-N(H)SiMe}_3$ ( <b>1a</b> )			
	Calc. <sup>a</sup>	Calc. <sup>b</sup>	Exp. <sup>c</sup>
Bond lengths (pm)			
P-N	167.118	166.245	165.8(14)
P-C <sub>ipso</sub>	182.234	181.802	181.5(15)
Si-N	177.979	176.877	175.4(12)
Angles ( $^{\circ}$ )			
P-N-Si	127.732	128.442	128.8(9)
N-P-C <sub>ipso</sub>	104.418	102.909	103.5(6)
C <sub>ipso</sub> -P-C <sub>ipso</sub>	100.462	100.291	99.4(6)
$[(\text{SiH}_3)_2\text{NZn}(\text{CH}_3)_2\text{PNSiH}_3]_2$ ( <b>2a*</b> )			$[(\text{MeSi})_2\text{NZnPh}_2\text{PNSiMe}_3]_2$ ( <b>2a</b> )
	Calc. <sup>d</sup>	Calc. <sup>e</sup>	Exp. <sup>c</sup>
Bond lengths (pm)			
P <sub>1</sub> -Zn <sub>1</sub>	239.354	240.592	240.54(11)
P <sub>1</sub> -N <sub>1</sub>	165.062	164.245	163.5(3)
N <sub>1</sub> -Si <sub>1</sub>	175.786	174.789	175.5(3)
Zn <sub>1</sub> -N <sub>1A</sub>	197.134	196.866	195.9(3)
Zn <sub>1</sub> -N <sub>2</sub>	190.889	191.264	191.3(3)
Angles ( $^{\circ}$ )			
P <sub>1</sub> -N <sub>1</sub> -Zn <sub>1A</sub>	112.526	112.951	112.0(2)
P <sub>1</sub> -Zn <sub>1</sub> -N <sub>1A</sub>	110.414	110.160	109.92(1)
Zn <sub>1A</sub> -N <sub>1</sub> -Si <sub>1</sub>	118.300	119.890	120.5(2)
N <sub>1</sub> -P <sub>1</sub> -Zn <sub>1</sub>	119.818	120.359	120.78(12)
P <sub>1</sub> -N <sub>1</sub> -Si <sub>1</sub>	126.856	126.909	127.5(2)

<sup>a</sup>BPW91/6-31G\*, <sup>b</sup>BPW91/6-31+G\*, <sup>c</sup>ref. 78, <sup>d</sup>BPW91/6-31G\* for N, C, H, P, Si, 6-311+G\* for Zn, <sup>e</sup>BPW91/6-31+G\* for N, C, H, P, Si and 6-311+G\* for Zn.

As neutral molecule as well as deprotonated *Janus Head* ligand with the phosphorus next to the nitrogen atom  $\text{Ph}_2\text{P-N(H)SiMe}_3$  (**1a**) has two adjacent coordination sites.

Dependent on the sterical demand and the Lewis acidity of the metal, the ligand can serve as a N- and/or P-donor. The free ligand can be regarded as a phosphanamide as well as an iminophosphide [84-86]. In both cases the phosphorus atom has the oxidation state +3 (Fig. 4.2). In response to the steric requirements, the  $\text{Ph}_2\text{PNSiMe}_3^-$  anion can either coordinate as the *s-cis*- or *s-trans*-conformer. (Fig. 4.3). In its crystalline form [78], the starting material **1a** exists in the *s-trans* conformation with respect to the P-N bond (P-N-Si angle is  $128.8(9)^\circ$ , calc.  $128.442^\circ$ ), while in the dimeric zinc compound **2a** both ligands have *s-cis* conformation (P-N-Si angle is  $127.5(2)^\circ$ , calc.  $126.909^\circ$ ). The coordination of the phosphanylamide units to the metal centre is maintained through the P and N donor atoms, a six-membered  $(\text{ZnPN})_2^-$  ring in a boat-conformation being formed (Fig. 4.1). The optimised geometries of both  $\text{Ph}_2\text{P-N(H)SiMe}_3$  (**1a**) and the model compound  $[(\text{SiH}_3)_2\text{N}_2\text{Zn}(\text{CH}_3)_2\text{P-NSiH}_3]_2$  (**2a\***) agree with the experimental solid state structures, especially at the BPW91/6-31+G\* level of theory for H, C, N, Si, P and at the 6-311+G\* level for Zn. As can be observed from Table 4.1 the P-N bond length in the zinc compound (163.5(3) pm, calc. 163.245 pm) is 2 pm shorter than that of the starting material **1a** and shorter than the length corresponding to a single P-N bond (170 pm) [77], suggesting the presence of a partial P=N double bond character in the zinc complex. The agreement between the calculated and experimental values of the structural parameters suggests that the partial P=N double bond exists not only in the solid state, but also in the gas phase. A more detailed comparison between the calculated and experimental parameters is given in Table 4.1.

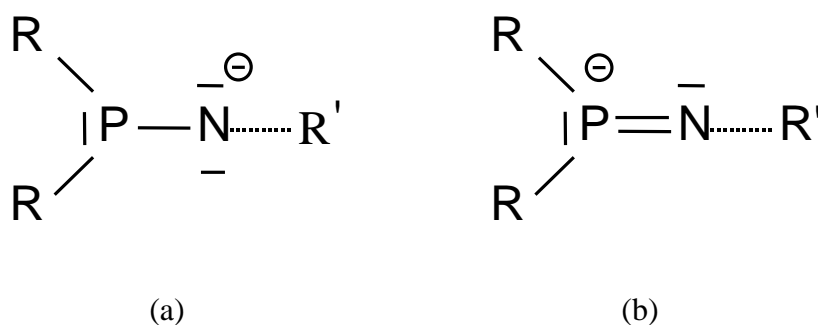


Fig. 4.2. Phosphanamide ion (a) versus iminophosphide ion (b).

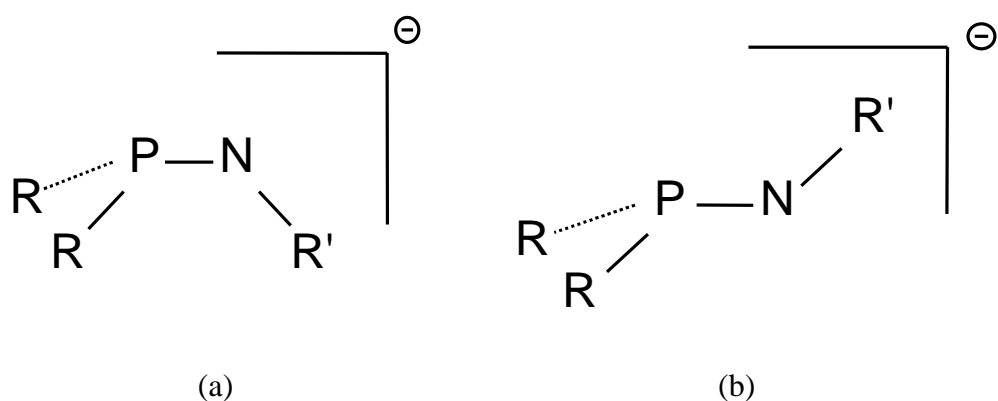


Fig. 4.3. Possible conformations of the phosphanylamide anion: *s-cis* (a), *s-trans* (b).

The optimised geometries of the starting material **1b** and the model compound  $[\text{Li}(o\text{-C}_6\text{H}_4\text{PH}_2\text{NSiH}_3)_2 \cdot \text{H}_2\text{O}]$  (**2b\***) at the BPW91/6-31+G\* level of theory are depicted in Fig. 4.4 and the selected structural parameters compared with the experimental crystal structure data are summarized in Table 4.2.

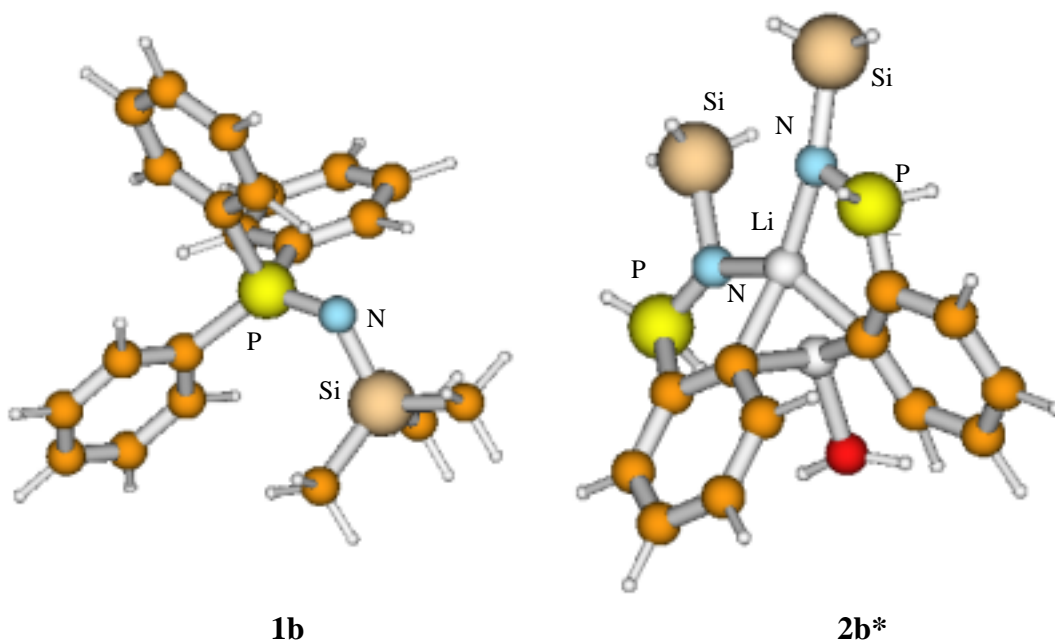


Fig. 4.4. Optimized geometries of the starting material  $\text{Ph}_3\text{P}=\text{NSiMe}_3$  (**1b**) and the model compound  $[\text{Li}(o\text{-C}_6\text{H}_4\text{PH}_2\text{NSiH}_3)_2 \cdot \text{H}_2\text{O}]$  (**2b\***).

Table 4.2. Selected calculated bond lengths (pm) and angles ( $^{\circ}$ ) of the  $\text{Ph}_3\text{P}=\text{NSiMe}_3$  (**1b**) and the model compound  $[\text{Li}(o\text{-C}_6\text{H}_4\text{PH}_2\text{NSiH}_3)]_2 \cdot \text{H}_2\text{O}$  (**2b\***) compared to the crystal structure data.

$\text{Ph}_3\text{P}=\text{NSiMe}_3$ ( <b>1b</b> )			
	Calc. <sup>a</sup>	Calc. <sup>b</sup>	Exp. <sup>c</sup>
Bond lengths (pm)			
P=N	155.0(6)	156.5(5)	154.2(2)
P-C <sub>average</sub>	182.9(2)	181.8(3)	180.2(2)
Angles ( $^{\circ}$ )			
P-N-Si	142.2(4)	139.5(2)	140.2(2)
$[\text{Li}(o\text{-C}_6\text{H}_4\text{PH}_2\text{NSiH}_3)]_2 \cdot \text{H}_2\text{O}$ ( <b>2b*</b> )		$[\text{Li}(o\text{-C}_6\text{H}_4\text{PPh}_2\text{NSiMe}_3)]_2 \cdot \text{Et}_2\text{O}$ ( <b>2b</b> )	
Bond lengths (pm)			
P <sub>1</sub> -N <sub>1</sub>	155.2(6)	157.3(4)	156.2(2)
P <sub>2</sub> -N <sub>2</sub>	153.9(3)	158.2(7)	156.2(3)
P-C <sub>average</sub>	180.9(1)	182.1(4)	181.2(3)
Li <sub>1</sub> -C <sub>2</sub>	214.5(4)	232.8(5)	233.1(5)
Li <sub>1</sub> -C <sub>2</sub> '	212.0(2)	226.4(1)	226.3(5)
Li <sub>2</sub> -C <sub>2</sub>	194.4(7)	214.0(7)	213.8(6)
Li <sub>2</sub> -C <sub>2</sub> '	195.6(5)	215.8(5)	212.0(6)
Li <sub>1</sub> -N <sub>1</sub>	192.8(4)	198.8(1)	203.7(5)
Li <sub>1</sub> -N <sub>2</sub>	191.7(9)	193.7(4)	202.7(4)
Angles ( $^{\circ}$ )			
P <sub>1</sub> -N <sub>1</sub> -Si <sub>1</sub>	124.0(3)	126.7(7)	135.18(13)
P <sub>2</sub> -N <sub>2</sub> -Si <sub>2</sub>	125.00	124.9(1)	133.47(13)
Li <sub>1</sub> -N <sub>1</sub> -P <sub>1</sub>	120.0(5)	103.0(6)	107.5(2)
Li <sub>1</sub> -N <sub>2</sub> -P <sub>2</sub>	98.5(2)	101.80	107.9(2)

<sup>a</sup>BPW91/6-31G\*, <sup>b</sup>BPW91/6-31+G\*, <sup>c</sup>ref. 80.

As one can see from Fig. 4.4 the organolithium compound **2b** consists in the solid state of two  $\text{Ph}_3\text{P}=\text{NSiMe}_3$  (**1b**) units, each deprotonated at the *ortho* position of one phenyl group [80]. The iminophosphorane units chelate through these *ortho*-carbon atoms and

the N donor centres a single lithium ion. A second lithium ion is coordinated to the two *ortho* ring carbon atoms and the oxygen atom of a diethyl ether molecule. Thus, the *ortho*-metallated species contains a tetrahedrally coordinated and a trigonal planar coordinated lithium atom. As one can notice from Table 4.2 the computed geometries of both  $\text{Ph}_3\text{P}=\text{NSiMe}_3$  (**1b**) and the model compound  $[\text{Li}(o\text{-C}_6\text{H}_4\text{PH}_2\text{NSiH}_3)]_2\cdot\text{H}_2\text{O}$  (**2b\***) match the experimental solid-state structures, especially at the BPW91/6-31+G\* level of theory. The agreement between the theoretical results calculated for the gas phase and the experimental structural parameters obtained from X-ray diffraction analysis indicates that the Lewis-basic imido nitrogen atom is involved in the coordination also in the gas phase. The P=N bond length in the lithium complex (156.2(2) pm, calc. 157.3(4) pm) is 2 pm longer than that of the iminophosphorane (**1b**) (see Table 4.2). The P-C bond lengths do not differ significantly for the lithium compound (**2b**) and the starting material (**1b**) (180.2(2)/181.2(3) pm, calc. 181.8(3)/182.1(4) pm). Table 4.2 gives a more detailed comparison between the calculated and experimental geometric features.

#### *Vibrational analysis*

FT-Raman and infrared spectroscopy have been employed to elucidate the coordination behavior of the dimeric zinc diphenylphosphanyl(trimethylsilyl)amide complex **2a** and the lithiated triphenyl(trimethylsilylimino)phosphorane compound **2b** in comparison to their parent starting materials **1a** and **2b**. In order to identify the characteristic vibrational modes of the phosphanylamines and iminophosphorane units of the zinc and lithium complexes, the spectra of the  $\text{Ph}_2\text{P-N(H)SiMe}_3$  (**1a**) and  $\text{Ph}_3\text{P}=\text{NSiMe}_3$  (**1b**) first have been measured. The assignment of the vibrational modes was performed with the help of DFT calculations. The infrared and FT-Raman spectra of the starting material  $\text{Ph}_2\text{P-N(H)SiMe}_3$  (**1a**) and the zinc compound  $[(\text{Me}_3\text{Si})_2\text{NZnPh}_2\text{PNSiMe}_3]_2$  (**2a**) in the range from 1500 to 400  $\text{cm}^{-1}$  and the FT-Raman spectra in the low wavenumber region (350-150  $\text{cm}^{-1}$ ) are presented in Fig. 4.5 and selected observed and calculated vibrational modes with their tentative assignment are summarized in Table 4.3.



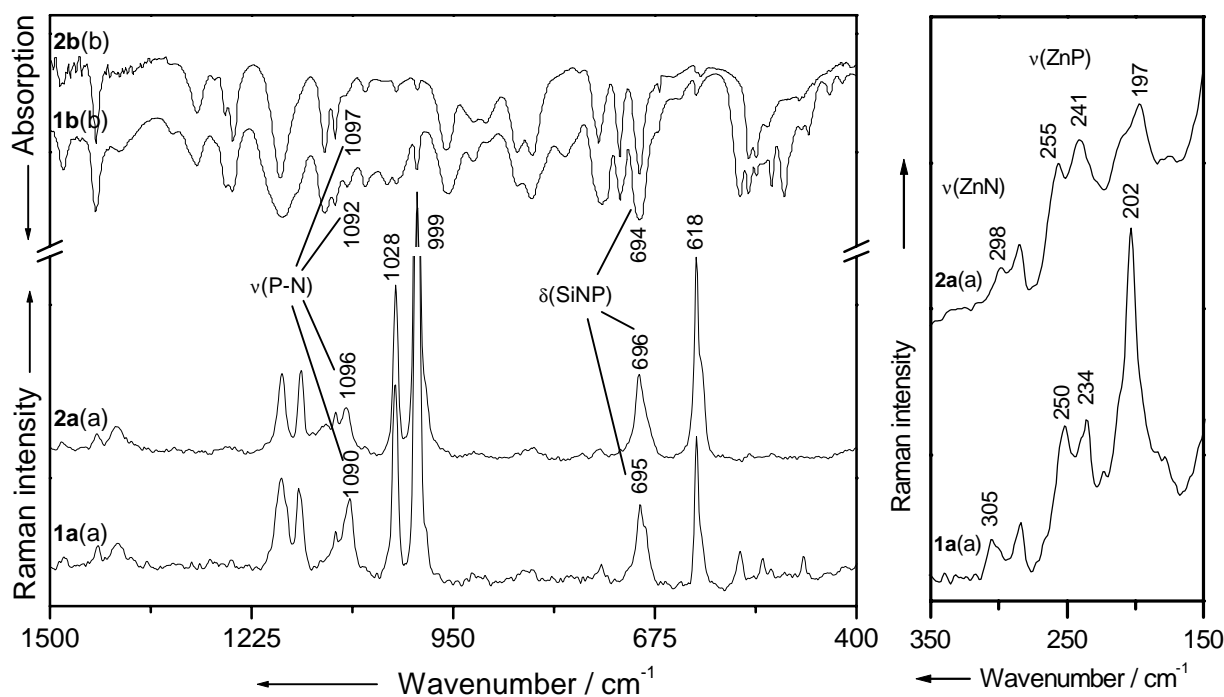


Fig. 4.5. FT-Raman (a) and infrared (b) spectra of  $\text{Ph}_2\text{P-N(H)SiMe}_3$  (**1a**) and  $[(\text{MeSi})_2\text{NZnPh}_2\text{PNSiMe}_3]_2$  (**2a**) complex.

From Fig. 4.5 and Table 4.3 one notices significant differences in the spectra of the zinc compound **2a** in comparison to the spectra of the starting material **1a**. Thus, in the low wavenumber region ( $350\text{-}150\text{ cm}^{-1}$ ) the intense band observed in the Raman spectrum of the starting material at  $202\text{ cm}^{-1}$  (calc.  $216\text{ cm}^{-1}$ ), assigned to CPC deformation vibrations is shifted to lower wavenumbers by  $5\text{ cm}^{-1}$  in the spectrum of **2a** due to the presence of the PNZn deformation vibration in the same spectral range. The medium intense band present in the Raman spectrum of **1a** at  $234\text{ cm}^{-1}$  (calc.  $242\text{ cm}^{-1}$ ) and attributed to CSiC deformation and out-of-plane ring deformation vibrations appears at  $241\text{ cm}^{-1}$  (calc.  $237\text{ cm}^{-1}$ ) in the spectrum of the zinc compound **2a** due to its convolution with a new band, the Zn-P stretching vibration appearing also in this spectral region [12, 87]. Furthermore, the shift to lower wavenumbers by  $7\text{ cm}^{-1}$  evidenced in the spectrum of the zinc complex **2a** of the weak Raman band at  $305\text{ cm}^{-1}$ , assigned to the NPC deformation vibration in the spectrum of the starting material **1a**, could be a consequence of the presence of the Zn-N stretching mode in the same spectral range [87].

Table 4.3. Selected experimental (infrared and FT-Raman) and calculated wavenumbers ( $\text{cm}^{-1}$ ) of  $\text{Ph}_2\text{P-N(H)SiMe}_3$  (**1a**) and  $[(\text{MeSi})_2\text{NZnPh}_2\text{PNSiMe}_3]_2$  (**2a**) with the tentative assignment.

$\text{Ph}_2\text{P-N(H)SiMe}_3$ ( <b>1a</b> )				$[(\text{MeSi})_2\text{NZnPh}_2\text{PNSiMe}_3]_2$ ( <b>2a</b> )				Vibrational assignment
Experimental		Theoretical		Experimental		Theoretical		
IR	Raman	Calc. <sup>a</sup>	Calc. <sup>b</sup>	IR	Raman	Calc. <sup>c</sup>	Calc. <sup>d</sup>	
	202s	212	216		197m	186	191	CPC def. + PNZn def.
	234m	248	242		241m	230	237	CSiC def. + out-of-plane ring def. + Zn-P str.
	250m	273	268		255m	277	271	CPC def. + ZnNP def.
	283w	286	300		285w	290	303	SiNP def.
	305w	301	313		298w	308	310	NPC def. + Zn-N str.
694s	695s	691	699	694ms	696s	721	717	C-H def. (ring, $\text{CH}_3$ ) + SiNP def.
862sh	852w	860	862		850w	852	851	C-H out-of-plane def.
844s	842w	849	852	842ms	839w	848	846	(ring) + PNSi str. + SiNSi str.
1092m	1090m	1082	1100	1097sh	1096w	1086	1109	P-N str.

<sup>a</sup>BPW91/6-31G\*, <sup>b</sup>BPW91/6-31+G\*, <sup>c</sup>BPW91/6-31G\* for N, C, Si, P, H and 6-311+G\* for Zn, <sup>d</sup>BPW91/6-31+G\* for N, C, Si, P, H and 6-311+G\* for Zn.

It is well known that the vibrational frequency of a molecule is proportional to the force constant  $k$  and inverse proportional to the reduced mass  $\mu$  of the molecule [20]. Having in mind that the force constants of chemical bonds are approximately proportional to the bond order, a decrease in the bond length leads to an increased force constant  $k$ . By comparing the data presented in Table 4.1 it was evidenced that the P-N bond in the zinc complex is 2 pm shorter than that of the starting material **1a**, suggesting an increased P-N stretching force constant in the zinc complex. In agreement with this observation, the band at  $1096 \text{ cm}^{-1}$  (calc.  $1109 \text{ cm}^{-1}$ ) present in the infrared and Raman

spectra of **2a** (see Table 4.3) and assigned to the P-N stretching vibration is shifted to higher wavenumbers by  $6\text{ cm}^{-1}$  in comparison to the corresponding vibration of the starting material. This shift to higher wavenumbers of the P-N stretching band further supports the assumption derived from the X-ray diffraction analysis that a partial P=N double bond is formed in the zinc compound [88]. As can be seen from Fig. 4.5 the characteristic vibrational modes of aromatic groups, which dominate the spectra of both compounds, are present in the expected spectral regions [89], and no differences can be observed in the spectra of the zinc compound in comparison to the spectra of the starting material.

The infrared and FT-Raman spectra of  $\text{Ph}_3\text{P}=\text{NSiMe}_3$  (**1b**) and the organolithium complex  $[\text{Li}(o\text{-C}_6\text{H}_4\text{PPh}_2\text{NSiMe}_3)]_2 \cdot \text{Et}_2\text{O}$  (**2b**) in the  $1800\text{-}400\text{ cm}^{-1}$  spectral region are illustrated in Fig. 4.6. Selected experimental and calculated wavenumbers together with the tentative assignment are presented in Table 4.4.

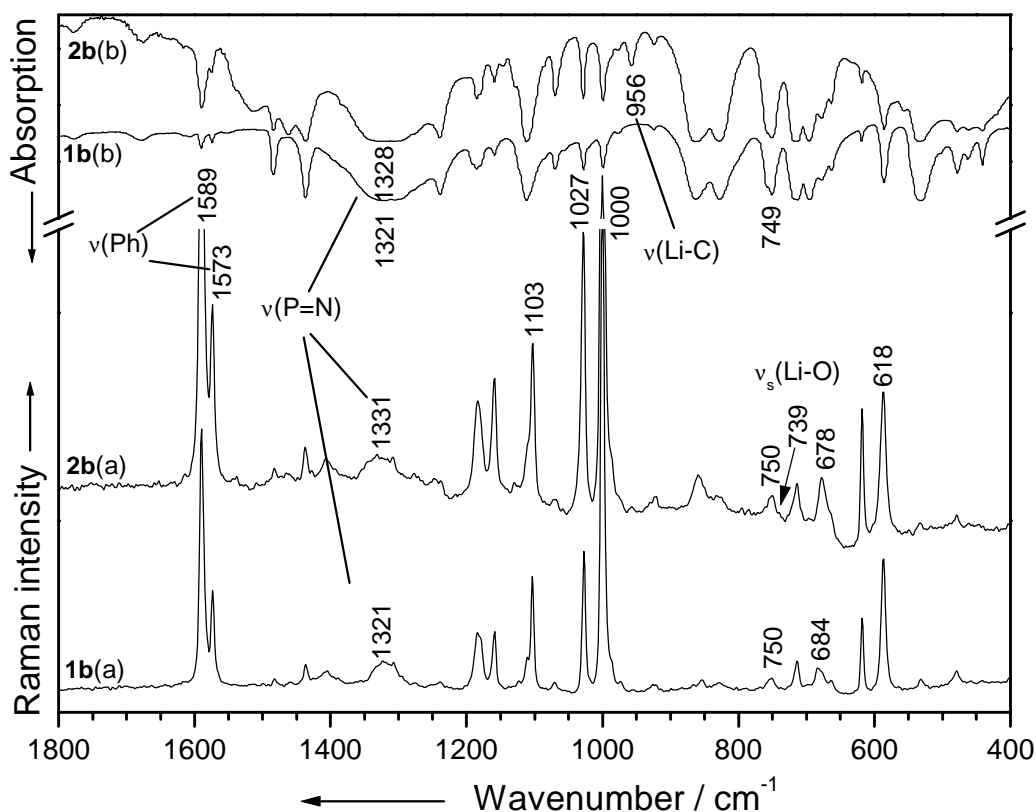


Fig. 4.6. FT-Raman (a) and infrared (b) spectra of  $\text{Ph}_3\text{P}=\text{NSiMe}_3$  (**1b**) and  $[\text{Li}(o\text{-C}_6\text{H}_4\text{PPh}_2\text{NSiMe}_3)]_2 \cdot \text{Et}_2\text{O}$  (**2b**) complex.

Table 4.4. Selected experimental (infrared and FT-Raman) and calculated wavenumbers ( $\text{cm}^{-1}$ ) of  $\text{Ph}_3\text{P}=\text{NSiMe}_3$  (**1b**) and  $[\text{Li}(o\text{-C}_6\text{H}_4\text{PPh}_2\text{NSiMe}_3)]_2\cdot\text{Et}_2\text{O}$  (**2b**) with the tentative assignment.

$\text{Ph}_3\text{P}=\text{NSiMe}_3$ ( <b>1b</b> )				$[\text{Li}(o\text{-C}_6\text{H}_4\text{PPh}_2\text{NSiMe}_3)]_2\cdot\text{Et}_2\text{O}$ ( <b>2b</b> )				Vibrational assignment
Experimental		Theoretical		Experimental		Theoretical		
IR	Raman	Calc. <sup>a</sup>	Calc. <sup>b</sup>	IR	Raman	Calc. <sup>a</sup>	Calc. <sup>b</sup>	
587s	586s	571	568	587s	587s			Si-C sym. str.
620m	618m	622	612	619m	618m	629	598	in plane ring def.
664m	663sh	662	663	663m	663sh	649	670	Si-N str.
684m	684s	671	687	677sh	678s	675	690	Si-C asym. str. + Li-N sym. str.
752s	750m	762	732	751s	749m 739sh	757	748	C-H wagging Li-O sym. str.
				956w		951	952	Li-C str.
998m	1000vs	1008	997	998m	1000vs	1012	1009	ring breathing
1113s	1104s	1126	1114	1112s	1102s	1117	1115	P-Ph str.
1185s	1184m	1191	1190	1185m	1182m	1187	1193	in plane C-H def.
1159m	1158m	1163	1165	1160m	1159m	1172	1178	
1321m	1321m	1306	1328	1328m	1331m	1326	1332	P=N str.
1436s	1437w	1457	1437	1437m	1438m	1463	1444	semicircle str.
1590w	1589vs	1623	1600	1589w	1589vs	1624	1614	C=C str. (ring)
1575w	1573s	1603	1585	1576sh	1573s	1601	1564	

<sup>a</sup>BPW91/6-31G\*, <sup>b</sup>BPW91/6-31+G\*.

One of the most remarkable features of vibrational spectra of organometallic compounds are the metal-carbon stretching vibrations, since they are directly related to the most substantial property of the molecule, that is the M-C bond strength [12]. However, the assignment of the M-C vibrational modes is often quite complicated due to the presence of other bands in the same region and due to their low intensity. In the case of the organolithium compound  $[\text{Li}(o\text{-C}_6\text{H}_4\text{PPh}_2\text{NSiMe}_3)]_2\cdot\text{Et}_2\text{O}$  (**2b**), the lithium-

carbon stretching vibration appears only in the infrared spectrum as a weak band at  $956\text{ cm}^{-1}$  (calc.  $952\text{ cm}^{-1}$ ) (Fig. 4.6). The assignment of the Li-C stretching vibration is based on the results obtained from theoretical calculations.

Significant changes in the position and relative intensities of some bands could be observed in the Raman spectrum of **2b** in comparison to the spectrum of **1b** (see Fig. 4.6 and Table 4.4). Thus, the asymmetric Si-C stretching vibration at  $684\text{ cm}^{-1}$  (calc.  $687\text{ cm}^{-1}$ ) in the spectrum of **1b** is shifted to lower wavenumbers by  $6\text{ cm}^{-1}$  and its intensity is increased due to the convolution of the above mentioned band with that of Li-N stretching vibration, which appears in the same spectral range [90]. The band around  $1100\text{ cm}^{-1}$  assigned to the P-Ph stretching vibration [91] is more intense in the spectrum of the lithiated compound **2b**. The new shoulder that arises in the spectrum of **2b** at  $739\text{ cm}^{-1}$  was attributed to the Li-O stretching mode [12].

In the Raman spectrum of  $[\text{Li}(o\text{-C}_6\text{H}_4\text{PPh}_2\text{NSiMe}_3)]_2\cdot\text{Et}_2\text{O}$  (**2b**) the broad band at about  $1321\text{ cm}^{-1}$  (calc.  $1328\text{ cm}^{-1}$ ) was assigned to the P=N stretching vibration [92]. Inspection of the selected structural parameters presented in Table 4.2 reveals a lengthening of the P-N bond in the lithium compound compared to the starting material. This leads to a decreasing of the P=N stretching force constant. Thus, a shift of the P=N stretching band to lower wavenumbers would be expected in the spectra of the organolithium compound **2b**. However, in comparison to the corresponding vibration of  $\text{Ph}_3\text{P}=\text{NSiMe}_3$  (**1b**) this band is shifted to higher wavenumbers by  $10\text{ cm}^{-1}$  in the Raman spectrum of **2b**, while in the infrared spectrum a shift of approximately  $7\text{ cm}^{-1}$  is observed. This shift to higher wavenumbers clearly indicates that the iminophosphorane units coordinate to the metal centre through the nitrogen donor atom, the coordination involving a decrease of the reduced mass. Having in view that both the force constant and the reduced mass, which are decisive for any changes in the spectra, are influenced by the coordination to the lithium atom, the shift of the P=N stretching band towards higher wavenumbers demonstrates that the reduced mass plays the dominant role [88].

As one remarks from Fig. 4.6 and Table 4.4, the bands that dominate the Raman spectra of both compounds are due to the phenyl vibrations, the most representative being assi-

gned to the ring stretching ( $1573$  and  $1589\text{ cm}^{-1}$ , calc.  $1585$  and  $1600\text{ cm}^{-1}$ ) and ring breathing ( $1000\text{ cm}^{-1}$ , calc.  $997\text{ cm}^{-1}$ ) modes. The other characteristic vibrational modes of aromatic groups were observed in the expected spectral regions [89, 92], no differences appearing in the spectrum of  $[\text{Li}(o\text{-C}_6\text{H}_4\text{PPh}_2\text{NSiMe}_3)]_2\cdot\text{Et}_2\text{O}$  (**2b**) compared to that of the starting material  $\text{Ph}_3\text{P}=\text{NSiMe}_3$  (**1b**).

#### 4.1.3. Conclusion

Infrared and FT-Raman investigations combined with density functional theory calculations have been performed on  $\text{Ph}_2\text{P-N(H)SiMe}_3$  (**1a**) and  $\text{Ph}_3\text{P}=\text{NSiMe}_3$  (**1b**), and their corresponding metal complexes  $[\{(\text{Me}_3\text{Si})_2\text{N}\}\text{Zn}(\text{Ph}_2\text{P-NSiMe}_3)]_2$  (**2a**) and  $[\text{Li}(o\text{-C}_6\text{H}_4\text{PPh}_2\text{NSiMe}_3)]_2\cdot\text{Et}_2\text{O}$  (**2b**) in order to determine the influence of the metal coordination on the P–N bond length. The coordination of the anionic  $[\text{Ph}_2\text{PNSiMe}_3]^-$  moiety to the zinc atoms leads to a shortening of the P–N bond length, while the *ortho*-metallation of the iminophosphorane and imino group metal side-arm donation cause a P–N bond lengthening. Shifts to higher wavenumbers of the P–N stretching bands have been observed in the infrared and Raman spectra of both compounds. The shift towards higher wavenumbers of the P–N stretching band evidenced in the infrared and Raman spectra of the zinc compound further supports the assumption derived from the X-ray diffraction analysis that a partial P=N double bond is formed in the coordination compound. In the spectra of the organolithium compound the shift to higher wavenumbers of the P=N stretching band clearly proves the coordination of the iminophosphorane units to the metal centre through the nitrogen donor atom, and demonstrates that the decrease of the reduced mass is responsible for this shift. The agreement between the theoretical and experimental values of the structural parameters and the calculated and observed vibrational modes indicates that the Lewis-basic imido nitrogen atom is involved in coordination not only in the solid state, but also in the gas phase.

## 4.2. Vibrational and kinetic investigations of some dianionic trisoxalato complexes of silicon(IV) and germanium(IV)

### 4.2.1. Introduction

Recently, some new dianionic silicon(IV) and germanium(IV) complexes with three symmetrical bidentate oxalato(2-) ligands have been prepared [93] and their schematic structures are presented in Fig. 4.7.

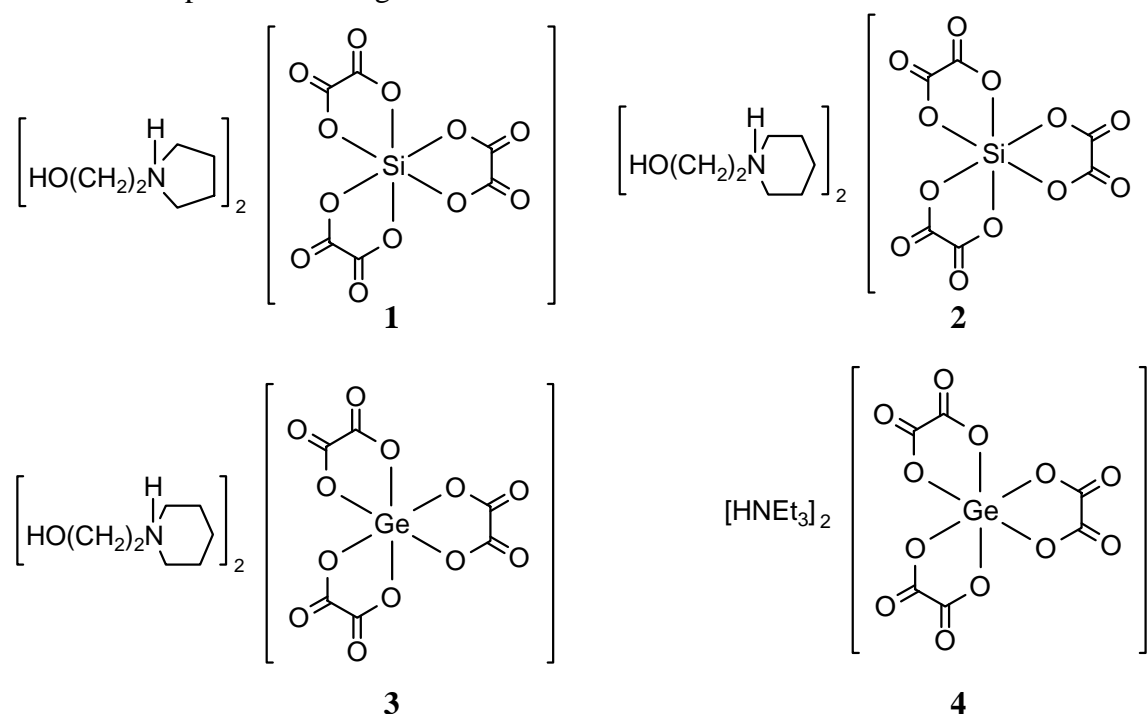


Fig. 4.7. Schematic structures of compounds 1-4.

It has been speculated that complexes with higher-coordinated silicon(IV) and chelate ligands derived from organic hydroxy compounds may play a potential role in silicon biochemistry [94]. In this context, the tris[oxalato(2-)]silicate dianion is also of interest [95].

In the present study, the hexacoordinated silicon(IV) and germanium(IV) complexes with three symmetrical bidentate oxalato(2-) ligands illustrated in Fig. 4.7 have been in-

investigated using FT-Raman and infrared absorption spectroscopy in combination with density functional theory calculations in order to elucidate their vibrational spectra. Kinetic investigations of the hydrolysis of two of them, one with silicon (**2**) and another one with germanium (**3**), have been performed at room temperature and at different pH values in order to determine the rate constants of the hydrolysis reaction and to find out the pH influence on the reaction rate.

#### 4.4.2. Results and discussion

##### *Vibrational analysis*

Crystallographic analysis of the compounds **1-4** shows that the Si/Ge-coordination polyhedra of all compounds are slightly distorted octahedra; the asymmetric units of all compounds containing two cations and one anion [93]. As expected from the presence of the potential NH and OH donor centres of the cations and the twelve potential oxygen acceptor atoms of the dianion, hydrogen bonds were observed in the crystal structures of all compounds. Density functional theory calculations were performed for the silicate dianion of **1** and for the germinate dianion of **3** at the BPW91/6-311+G\* level of theory and the optimised geometries of the dianions are illustrated in Fig. 4.8.

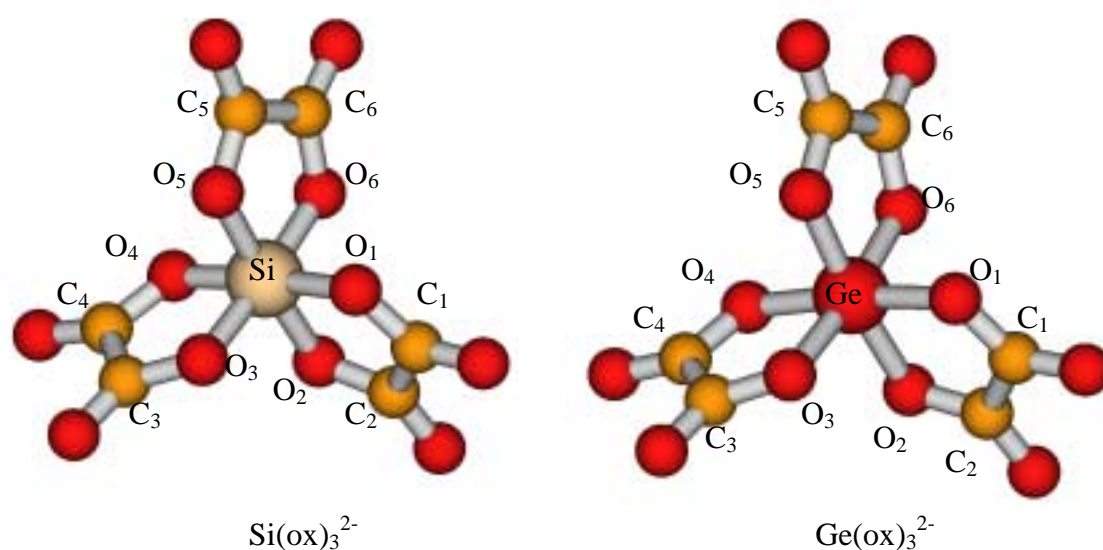


Fig. 4.8. Optimised geometries of the silicate  $\text{Si(ox)}_3^{2-}$  and germinate  $\text{Ge(ox)}_3^{2-}$  dianions at the BPW91/6-311+G\* level of theory.



The selected structural parameters compared with the experimental data are summarized in Table 4.5. For comparison purposes experimental and calculated structural parameters of the free oxalate dianion have been also included in Table 4.5.

Table 4.5. Selected calculated bond lengths (Å) and angles (°) of the silicate  $\text{Si}(\text{ox})_3^{2-}$  and germinate  $\text{Ge}(\text{ox})_3^{2-}$  dianions compared to crystal structure data of compounds **2** and **3**. The calculated and experimental parameters of the free oxalate dianion are also presented.

	$\text{Si}(\text{ox})_3^{2-}$		$\text{Ge}(\text{ox})_3^{2-}$		oxalate dianion	
	Calc. <sup>a</sup>	Exp. <sup>b</sup>	Calc. <sup>a</sup>	Exp. <sup>b</sup>	Calc. <sup>a</sup>	Exp. <sup>c</sup>
Bond lengths (Å)						
M-O	1.81896	1.78	1.93728	1.88		
O-C	1.32246	1.3113	1.3226	1.3013	1.3093	1.25
C-C	1.56612	1.5445	1.57251	1.5469	1.5396	1.56
C=O	1.22406	1.2172	1.22498	1.2050	1.2519	1.23
Angles (°)						
O-M-O	87.16	88.48	85.071	91.87		
M-O-C	115.561	114.629	114.150	113.664		
O-C-C	110.857	111.046	113.312	112.978	118.362	118.5
O-C=O	125.429	125.308	124.576	125.064	122.802	125.3
C-C=O	124.714	123.641	122.112	121.956	118.836	116.5

<sup>a</sup>BPW91/6-311+G\*, <sup>b</sup>ref. 93, <sup>c</sup>ref. 96.

In agreement with previous studies [97, 98] one remarks from Table 4.5 that the coordination to the metal center is accompanied by changes in bond lengths. Thus, after coordination the C=O bond lengths become shorter, while the C-O bonds are lengthened. The C-C bonds are slightly stronger in the metal complexes compared to the free oxalate anion. The Ge-O bond lengths are longer than the Si-O bond lengths by 10 Å (calc. 12 Å), suggesting that the Ge-O bond is slightly weaker than the Si-O bond. At the presented theoretical level the calculated and experimental values are in good agreement, the differences evidenced being most probably due to the intermolecular in-

teractions, which occur between the dianions and the neighboring cations in the crystal [93].

The infrared and FT-Raman spectra of the trisoxalato-complexes of silicon and germanium **1-4** in the range from 2000 to 400  $\text{cm}^{-1}$  are presented in Fig. 4.9 and the observed bands together with the vibrational assignment are summarized in Tables 4.6 and 4.7.

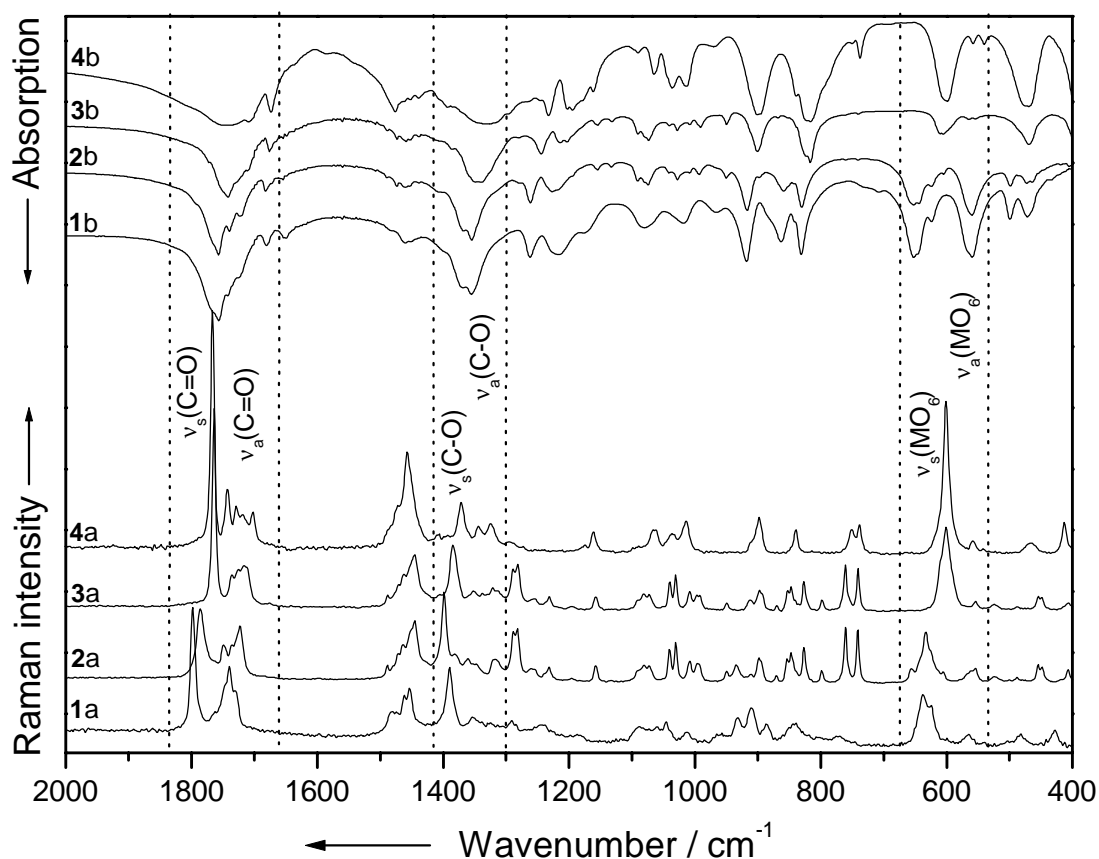


Fig. 4.9. FT-Raman (a) and infrared (b) spectra of the complexes **1-4**.

The assignment was accomplished mainly by comparison with related molecules [89, 99] and using the results obtained from DFT calculations. A perfect agreement between the experimental and calculated wavenumbers is not possible in this case because the dianions are strongly influenced by intermolecular interactions with the cations [93]. Furthermore, the theoretical calculations were performed for the gas phase, while the spectra were recorded for polycrystalline samples. However, as can be seen from Tables

4.6 and 4.7 the agreement between the experimental and theoretical data at the presented theoretical level is sufficient to be useful for the assignment of the vibrational modes.

Table 4.6. Selected experimental (infrared and FT-Raman) and theoretical wave-numbers ( $\text{cm}^{-1}$ ) of oxalic acid **0** and silicon complexes **1** and **2** with the tentative assignment.

<b>0</b>			<b>1</b>		<b>2</b>			Vibrational assignment
IR	Raman	Calc. <sup>a</sup>	IR	Raman	IR	Raman	Calc. <sup>a</sup>	
				367m		367m	325	OSiO def.
				427m		407w		C-N def.
483m	466m	493	471m	482w	462m	454m	462	CCO def.
			558m	564w	560m	554w	584	SiO <sub>6</sub> str.
			651m	637m	650m	632m	612	
						740m		skeletal str.
				768w		761m		C-N str.
	826s	814	831m	839m	829m	826m	822	O-C=O def.
	835s	826	917m	911m	917m	898m	879	C-C str.
				1045m	1028w 1041sh	1030m 1040m		CH <sub>2</sub> rock.
			1083m	1088m	1074m	1072m		C-N str.
	1174w		1179sh	1181w	1154w	1157m		CH <sub>2</sub> twist
1256m	1244w		1262m	1290w	1280sh	1281m 1288sh		CH <sub>2</sub> wagging
1443ms	1453w 1480m	1423 1463	1354s 1369sh	1353w 1389m	1354s 1368sh	1360s 1398s	1305 1322	C-O str.
			1450sh 1460w	1453m 1461sh 1480sh	1462w 1473w	1444m 1464sh 1471sh		CH <sub>2</sub> def.

(Table 4.6. continued)

<b>0</b>			<b>1</b>		<b>2</b>			Vibrational assignment
IR	Raman	Calc. <sup>a</sup>	IR	Raman	IR	Raman	Calc. <sup>a</sup>	
	1779m	1770	1724sh	1729sh	1723sh	1723s	1697	C=O str.
	1792m	1781	1742sh	1739m	1739sh	1735sh	1703	
			1757s	1762sh	1757s	1748sh	1712	
				1797s		1786s	1743	
2820sh		2982	2893sh	2891m	2875m	2876m		C-H, N-H, O-H str.
3434s		3584	2959m	2955s 2984s	2969sh	2970s		

<sup>a</sup>BPW91/6-311+G\*.

Table 4.7. Selected experimental (infrared and FT-Raman) and theoretical wave-numbers ( $\text{cm}^{-1}$ ) of oxalic acid **0** and germanium complexes **3** and **4** with the tentative assignment.

<b>0</b>			<b>3</b>		<b>4</b>			Vibrational assignment
IR	Raman	Calc. <sup>a</sup>	IR	Raman	IR	Raman	Calc. <sup>a</sup>	
				362m		361m	363	OGeO def.
				407w		412m		C-N def.
483m	466m	493	468m	454m	469s	465m	464	CCO def.
			554m	553w	558s	558w	544	GeO <sub>6</sub> str.
			604m	600m	599s	600s	579	
				740m				skeletal str.
				761m	750sh	751m		C-N str.
	826s	814	816m	826m	839sh	839m	836	O-C=O def.
	835s	826	899m	897m	899s	897m	884	C-C str.
			1028w	1030m	1034m	1035m		CH <sub>2</sub> rock.
			1040sh	1039m				
			1073m	1072m	1064m	1064m		C-N str.

(Table 4.7. continued)

0			3		4			Vibrational assignment
IR	Raman	Calc. <sup>a</sup>	IR	Raman	IR	Raman	Calc. <sup>a</sup>	
	1174w		1155m	1157m	1161sh	1161m		CH <sub>2</sub> twist
1256m	1244w		1279sh	1281m 1288sh	1296sh	1292w		CH <sub>2</sub> wagging
1443ms	1453w 1480m	1423 1463	1351s 1384sh	1352w 1384m	1345sh 1384sh	1345m 1371m	1295 1314	C-O str.
			1460w 1473sh	1444m 1462sh 1471sh	1452sh 1476s	1457m 1470sh 1483sh		CH <sub>2</sub> def.
	1779ms 1792ms	1770 1781	1710sh 1719sh 1733s	1716m 1725sh 1735sh 1764s	1708s 1737s 1748s	1703m 1728m 1743m 1766s	1686 1691 1697 1725	C=O str.
2820sh 3434s		2982 3584	2876m 2964sh	2876m 2968s	2812m 2942m 2989m	2893m 2949s 2989s		C-H, N-H, O-H str.

<sup>a</sup>BPW91/6-311+G\*.

The most important bands present in the spectra of all compounds, which proof the coordination of the symmetrical bidentate oxalato(2-) ligands to the metal center, appear around 620 cm<sup>-1</sup> and are due to metal-oxygen stretching vibrations [99]. The difference in masses of the metal atoms causes the metal-oxygen asymmetric stretching modes, where the metal moves, to be shifted more than the symmetric stretching mode, where the metal remains nearly stationary. Thus, in the Raman spectra of the germanium compounds the bands at 600 cm<sup>-1</sup> (calc. 579 cm<sup>-1</sup>) attributed to the symmetric GeO<sub>6</sub> stretching vibration are shifted to lower wavenumbers by 30 cm<sup>-1</sup> in comparison to the symmetric SiO<sub>6</sub> stretching mode, while the infrared bands around 602 cm<sup>-1</sup> assigned to the asymmetric GeO<sub>6</sub> stretching vibration are shifted to lower wavenumbers by 50 cm<sup>-1</sup> in comparison to the corresponding bands of the silicon compounds. These shifts may

be a consequence of the different metal-oxygen bond strengths, the Ge-O bond being slightly weaker than the Si-O bond.

As one can see from Fig. 4.9 and Tables 4.6 and 4.7 the infrared and Raman spectra of silicon and germanium trisoxalato-complexes resemble each other very closely, the differences observed being largely due to the different molecular weights of the metal atoms and to the different cations, which neutralize the anionic hexacoordinated compounds. Thus, in the spectra of the octahedral complexes one can distinguish between spectral regions containing a collection of bands determined by the ligand and cations vibrations.

In higher wavenumber regions ( $1800\text{-}1700\text{ cm}^{-1}$ ) the bands dominating the spectra of all compounds are due to carbonyl stretching vibrations. The strong Raman bands around  $1780\text{ cm}^{-1}$  were assigned to the symmetric stretching vibration of the carbonyl group, while the medium intense Raman bands around  $1730\text{ cm}^{-1}$  and the strong infrared bands around  $1750\text{ cm}^{-1}$  were attributed to the asymmetric stretching vibration of the carbonyl group [89, 99]. In the  $1400\text{-}1300\text{ cm}^{-1}$  spectral region the C-O stretching modes can be observed. The medium intense Raman bands around  $1380\text{ cm}^{-1}$  were assigned to the symmetric stretching vibration, while the weak Raman bands around  $1350\text{ cm}^{-1}$  and the corresponding intense infrared bands were attributed to the asymmetric stretching vibration [89, 99]. Other ligand-bands observed in the spectra of all compounds arise in the  $900\text{-}800\text{ cm}^{-1}$  spectral range, the most representative being assigned to C-C stretching and OCO deformation vibrations (around  $900$  and  $830\text{ cm}^{-1}$ , respectively). From the Tables 4.6 and 4.7 significant differences between the position of the bands given by the starting material and the bands caused by the ligand-vibrations in the coordinated compounds can be observed. Thus, the bands due to the carbonyl and C-O stretching vibrations of the trisoxalato-complexes can be seen at higher and lower wavenumbers, respectively in comparison to the corresponding bands of the free ligand. A possible explanation of the shifts could be the presence of four equivalent oxygen atoms in the free ligand, while in the hexacoordinated complexes, the two coordinated oxygen atoms are different from the two others, which are not coordinated [100]. Furthermore, the coordination to the metal center involves changes in the bond-lengths

(see Table 4.5). After coordination the C=O bond lengths become shorter, while the C-O bonds are lengthened, hence a shift of the carbonyl and C-O stretching bands to higher and lower wavenumbers, respectively is expected. Due to the coordination to the metal center the C-C and O-C=O bonds become stronger, and determine the shifts of the C-C stretching and OCO deformation vibrations to higher wavenumbers.

By comparing the spectra of the hexacoordinated compounds (Fig. 4.9) one can observe that the bands caused by the ligand-vibrations appear at lower wavenumbers in the spectra of the germanium complexes relative to their analogues bands in the silicon complexes. As it was mentioned above, the formation of the M-O bond shortens the C=O bonds and lengthens the C-O bonds. Since the Ge-O bond is weaker than the Si-O bond, smaller shifts of the carbonyl and C-O stretching bands of the germanium compounds relative to the silicon complexes to higher and lower wavenumbers, respectively in comparison to the corresponding vibrations of the free ligand, are expected.

The vibrations of the cations determine bands present only in the spectra of the metal complexes. Thus, in the 3000-2000  $\text{cm}^{-1}$  spectral region the bands attributed to the symmetric and asymmetric stretching vibrations of the C-H and N-H bonds can be observed. The intense bands around 1460  $\text{cm}^{-1}$  can be assigned to scissor vibrations of the  $\text{CH}_2$  groups [89]. Out-of-plane and in-plane deformation vibrations of these groups appear between 1300 and 1150  $\text{cm}^{-1}$  and around 1030  $\text{cm}^{-1}$  in the spectra of all compounds. Other important bands, which can be observed in all spectra, are due to C-N stretching vibrations and arise around 1080 and 765  $\text{cm}^{-1}$ , respectively [89].

#### *Kinetic investigations*

Raman spectroscopy has been recently used in a wide range of applications for process and synthesis monitoring [101]. Because the peaks in a Raman spectrum are often selective, it is possible to follow the progress of a reaction with time by monitoring the intensity changes of some representative peaks. The Raman spectra of aqueous solutions of **2** and **3** have been recorded for various times and the spectra obtained after

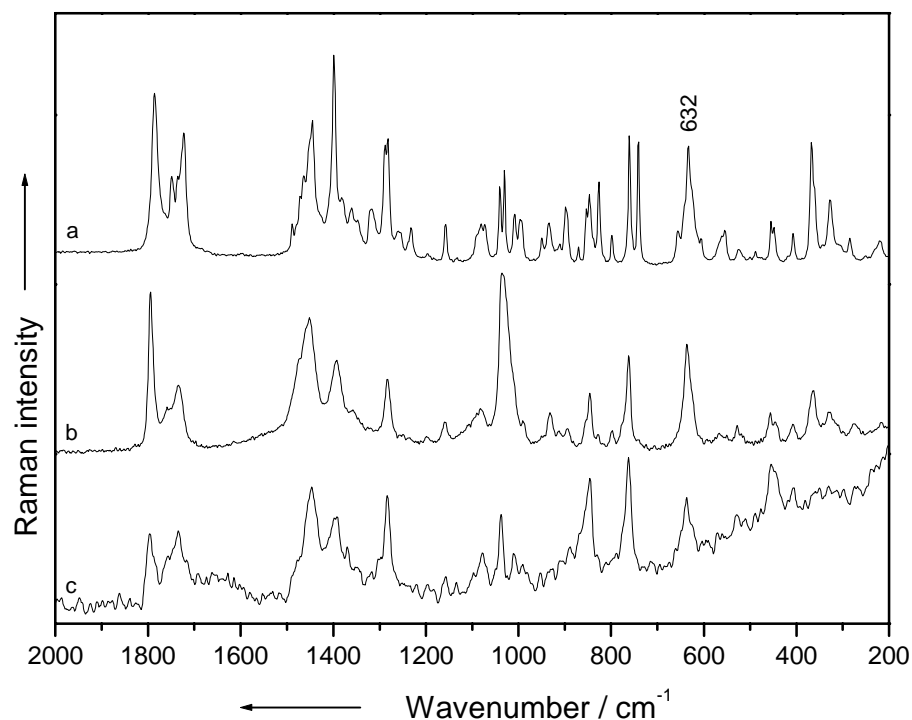


Fig. 4.10. FT-Raman spectra of polycrystalline sample (a) 1 M methanol solution after 60 min (b) and 1 M water solution after 30 min after water addition (c) of silicon compound **2**.

30 min after addition of water are illustrated in Figs. 4.10c and 4.11c. The Raman spectra of polycrystalline samples and the spectra of methanol solutions of **2** and **3** are also depicted in Figs. 4.10a, b and 4.11a, b.

If the hydrolysis reaction occurs significant changes of the Raman bands assigned to the metal-oxygen vibrations are expected. As it was already mentioned, in the Raman spectra of silicon and germanium compounds **2** and **3** the SiO<sub>6</sub> and GeO<sub>6</sub> stretching bands appear at 632 and 600 cm<sup>-1</sup>, respectively (Figs. 4.10a and 4.11a). From Figs. 4.10b and 4.11b it can be observed that the addition of methanol does not cause significant changes in the Raman spectra of both compounds recorded after 60 min. By comparing the spectra of aqueous solution of compounds **2** and **3** with the corresponding Raman spectra of the polycrystalline samples and methanol solutions a decrease of the SiO<sub>6</sub> stretching band intensity was observed even after 30 min after wa-



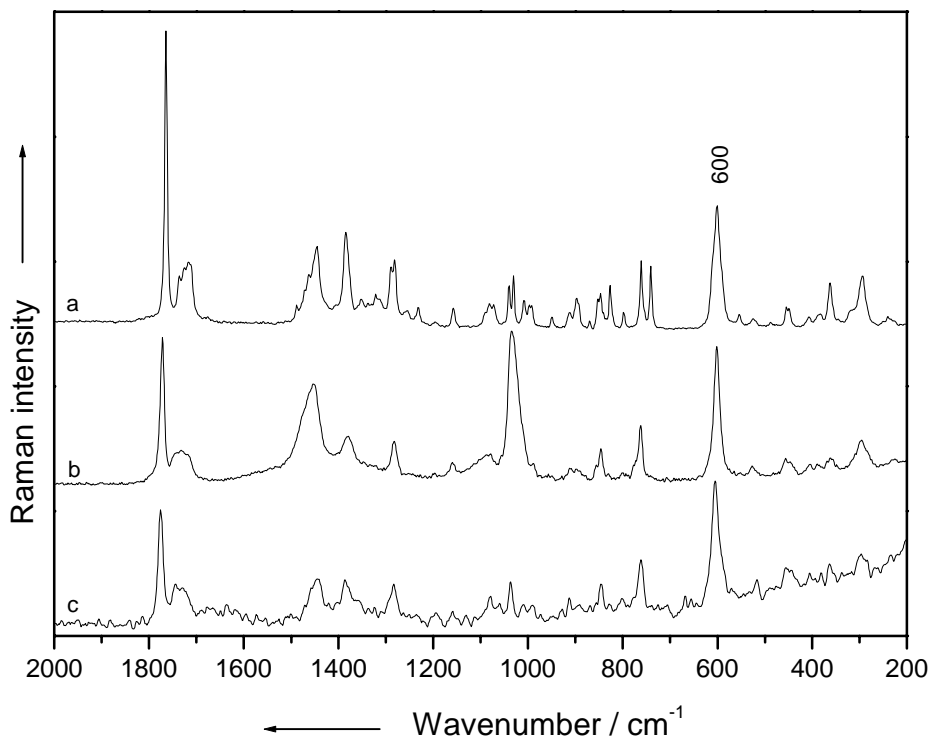


Fig. 4.11. FT-Raman spectra of polycrystalline sample (a), 1 M methanol solution after 60 min (b) and 1 M water solution after 30 min after water addition (c) of germanium compound **3**.

ter addition, while the intensity of the  $\text{GeO}_6$  stretching band remains constant (Figs. 4.10c and 4.11c). Taking into account the above observed behaviors of the metal-oxygen stretching bands, when different solvents are used, we conclude that only for the silicon compound a hydrolysis reaction occurs, while for the germanium compound water acts as a pure solvent. Furthermore, our goal was to determine the rate constant of the hydrolysis reaction of compound **2** at room temperature and to investigate the pH influence on the reaction rate. It is known [102] that the intensity of a given Raman peak for non-resonant excitation is proportional to the concentration of the scatters. Thus, a ratio method may be used to calculate the concentration  $C(t)$  at any time  $t$  after mixing given the initial intensity  $I(0)$  and concentration  $C(0)$ :

$$\frac{I(t)}{I(0)} = \frac{C(t)}{C(0)}, \quad 4.1$$

where all intensities are automatically background corrected (OPUS software) and normalized to the  $1281\text{ cm}^{-1}$  Raman peak intensity, which remains constant during the reaction. Since each spectrum represents a time average of 20 min, a linear approximation by assuming the value of intensity to be the real value at 10 min after starting the data acquisition was made. An extrapolation against  $t = 0$  min leads to the intensity at the beginning of the reaction. This intensity could be related to the starting concentration of the silicon compound (1 M).

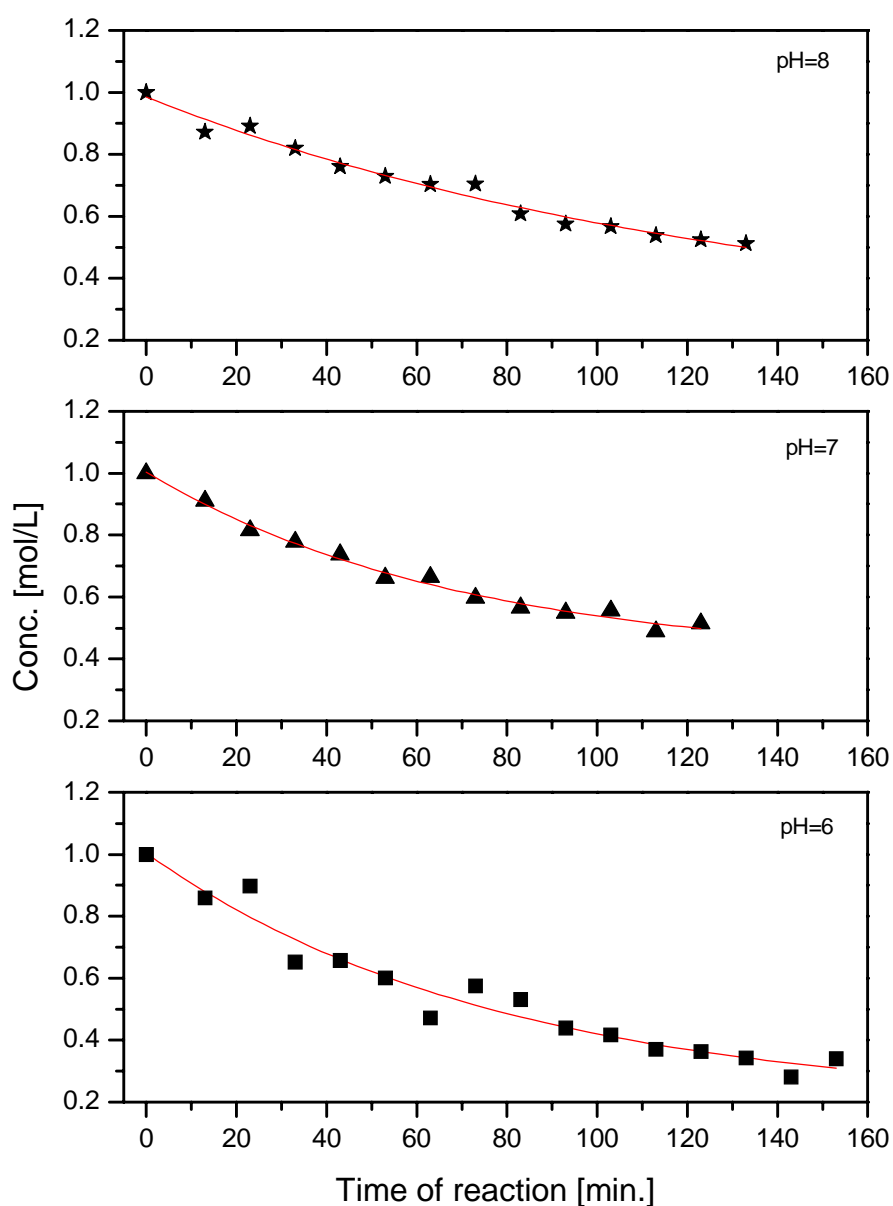


Fig. 4.12. Kinetic plots of compound **2** hydrolysis at room temperature and different pH values as indicated obtained from Raman data.

For the analysis of the hydrolysis reaction of compound **2** by means of Raman spectroscopy, the most important band is that at  $632\text{ cm}^{-1}$  assigned to the symmetric  $\text{SiO}_6$  vibrational mode. After addition of water the intensity of this band decreases and finally completely disappears in the Raman spectra. Therefore, the rate of the reaction may be followed by the decrease in the intensity of this  $632\text{ cm}^{-1}$  peak. For the kinetic curves plotted in Fig. 4.12 the concentration for different moments during the reaction have been calculated according to equation 4.1 As can be seen, for all pH values the concentration decreases exponentially in time and proves the pseudo-first order of the hydrolysis reaction.

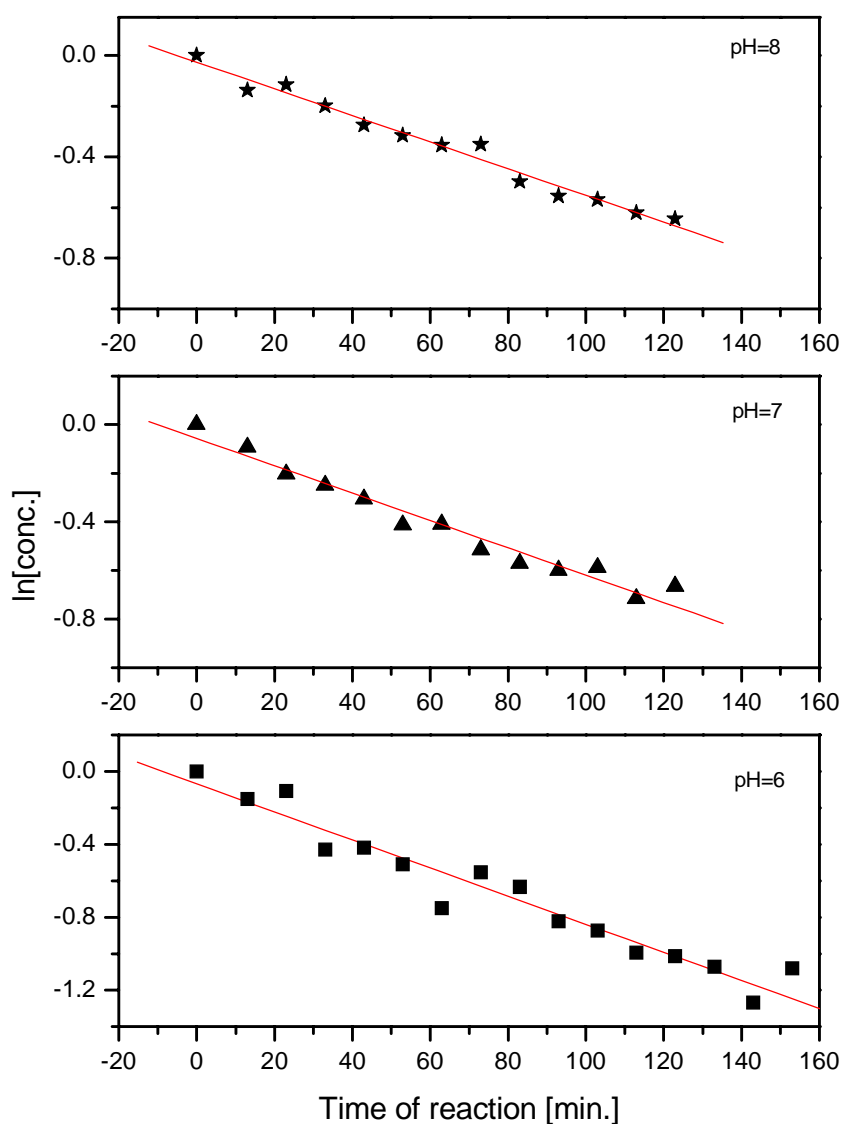


Fig. 4.13. Logarithms of the concentration of compound **2** as a function of time at room temperature and at different pH values as indicated.

Therefore, logarithmic concentrations plots (Fig. 4.13) can be used to calculate the magnitude of the rate constants  $K$  ( $12.85 \times 10^{-5} \text{ s}^{-1}$ ,  $9.36 \times 10^{-5} \text{ s}^{-1}$ , and  $8.75 \times 10^{-5} \text{ s}^{-1}$  for pH values 6, 7, and 8, respectively). Comparing the values obtained for different pH values one observes a pH dependence of the rate of hydrolysis, the fastest reaction taking place at the lowest investigated pH value.

In an acidic environment, the attack of  $\text{H}^+$  cations on the ligand oxygen atoms causes their protonation. Thus, the electron density is withdrawn from the silicon atom towards the ligands. Because the silicon atom is more stable in a tetra-coordinated state the protonated ligands dissociate. Thus, the reaction is the fastest under acidic conditions. On the other hand, in an alkaline environment the  $\text{OH}^-$  groups should directly attack the silicon atom but the probability of this behavior is very low due to the high electron density present at the metal center. Therefore, under neutral and light basic conditions the protonation of the ligand still occurs but it is hindered. Thus, the reaction kinetics become slower.

#### 4.2.3. Conclusion

FT-Raman and infrared spectroscopy together with density functional theory calculations have been applied to the vibrational characterization of some new hexacoordinate silicon(IV) and germanium(IV) complexes. Kinetic investigations of the hydrolysis of two compounds, one with silicon (**2**) and another one with germanium (**3**), have been performed and could be seen that the hydrolysis reaction occurs only for the first compound. The rate constants at room temperatures and at different pH values have been determined for the silicon compound **2**, the fastest reaction taking place at acidic pH.

### 4.3. Vibrational and conformational analysis of some dianionic complexes with hexacoordinated silicon(IV) and three bidentate ligands of the hydroximato(2-) type

#### 4.3.1. Introduction

It is known [103, 104] that coordination complexes with the coordination number six have an octahedral arrangement. The most important evidence for this structural assignment was the existence of only two geometrical isomers for octahedral complexes containing two different ligands A and B in the general formula  $MA_nB_{6-n}$ , where  $n = 2, 3$ , or 4. For  $n = 3$  ( $MA_3B_3$ ) the possible isomers are *mer* (meridional) and *fac* (facial) and are illustrated in Fig. 4.12. In the case of *mer*-isomers the ligands are arranged around the central metal atom like a circumference of a sphere, while for the *fac*-isomers the ligands occupy a face of the coordinate octahedron in such a way that they realise a triangular form.

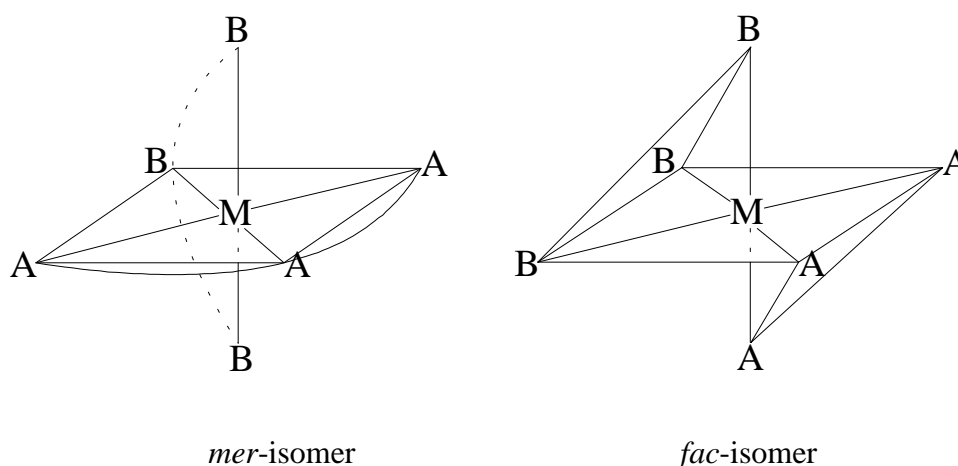


Fig. 4.12. Possible geometric isomers of octahedral compound of the  $MA_3B_3$  type.

Recently, a new series of hexacoordinated silicon(IV) complexes with three unsymmetrical bidentate ligands of the hydroximato(2-) type have been prepared [105] and their formulas are depicted in Fig. 4.13. The geometric configurations of these com-

plexes are typified by the central silicon atom which is surrounded in an octahedral environment by three hydroximato ligands. In principle, the hexacoordinated silicate dianions of compounds of this particular formula type can exist either as *mer*-isomer ( $C_1$  symmetry) or as *fac*-isomer ( $C_3$  symmetry). In both cases, the ligands form five-membered rings together with the central silicon atom, which are different for both isomers. The structures of the compounds *fac*-1•MeOH and *mer*-5•2MeOH have been established by single-crystal X-ray diffraction [106], whereas the structures of the other three compounds could not be determined by this experimental method.

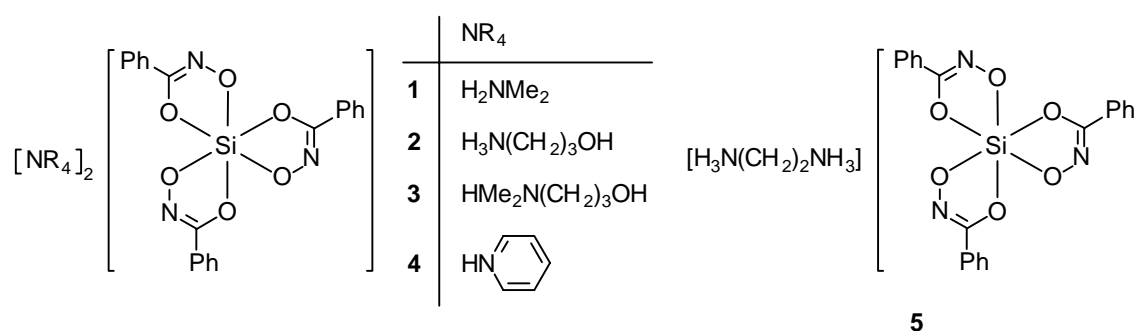


Fig. 4.13. Formulas of the compounds **1-5**.

Several other methods like infrared absorption and Raman spectroscopy, NMR and UV-VIS absorption spectroscopy along with X-ray diffraction, which give a definite proof of the structure, have been applied [103, 107] with varying degrees of success to the problem of differentiating between the *mer*- and *fac*-isomers. Infrared and Raman spectroscopy together with theoretical calculations have been successfully used for detecting and assigning the stereoisomers [108] because they are able to distinguish different ring conformations, which are conceivable for different isomers. Thus, some spectral regions of the spectra are identified as useful for determining facial and meridional isomers. In the present study, the hexacoordinated silicon(IV) complexes illustrated in Fig. 4.13 have been investigated using infrared absorption and FT-Raman spectroscopy in combination with theoretical calculations in an attempt to elucidate both the vibrational spectra of these compounds as well as to provide insights into the conformational structures that the dianions of compounds **2-4** take in solid state.

### 4.3.2. Results and discussion

Single crystal X-ray diffraction studies showed that the Si-coordination polyhedra of the hexacoordinated silicon compounds *fac-1*•MeOH and *mer-5*•2MeOH can be described as distorted octahedra [106]. As expected from the presence of the potential NH and OH donor functions of the cations and the potential nitrogen and oxygen acceptor atoms of the dianion, complex hydrogen-bonding systems were observed in the crystals of both compounds [106]. Density functional theory calculations were performed for the *fac-1*\* and *mer-5*\* model compounds (the phenyl moieties were replaced by methyl groups) at the BPW91/6-311+G\* level of theory. For the *fac*-isomer, an ideal C<sub>3</sub> symmetry has been chosen as the starting geometry, while for the *mer*-isomer the starting geometry was C<sub>1</sub>. The optimised geometries of the dianions are illustrated in Fig. 4.14 and the selected structural parameters compared with the experimental data of *fac-1*•MeOH and *mer-5*•2MeOH compounds are summarized in Table 4.8.

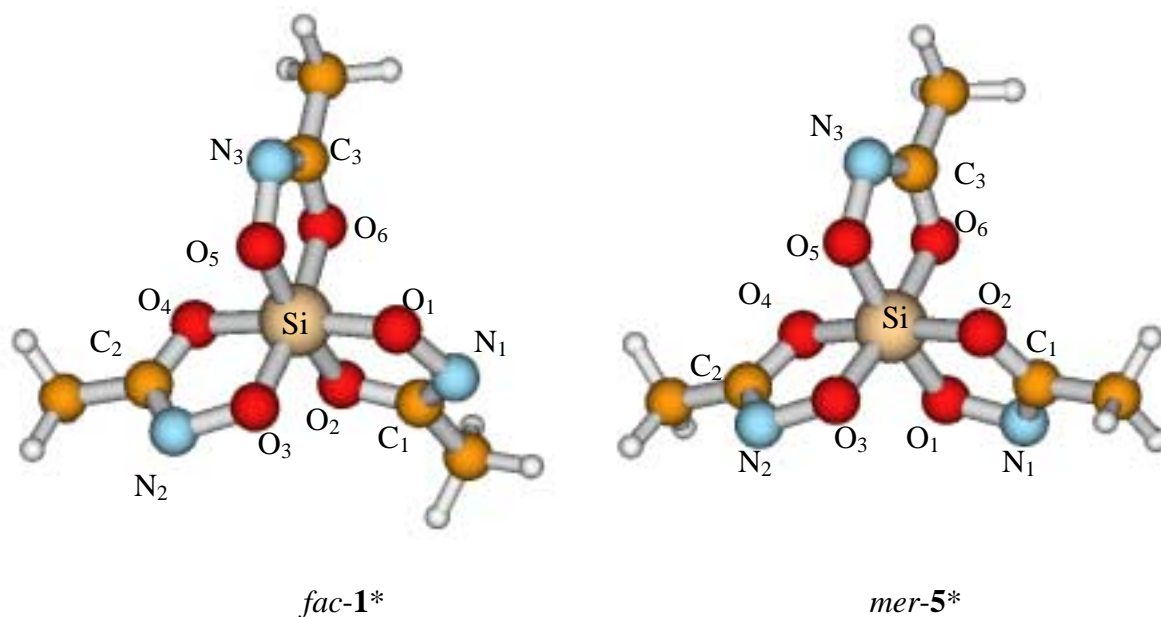


Fig. 4.14. Optimised geometries of the *fac-1*\* and *mer-5*\* dianions at the BPW91/6-311+G\* level of theory.

Theoretical calculations of the silicate dianions *fac-1*\* and *mer-5*\* revealed only a small difference in energy, the *fac-1*\* isomer being energetically more stable by 1.556 kJ/mol. This result is in accordance with the finding that the same synthetic approach can lead

to both *fac*- and *mer*-configured products, the configuration being dependent on the nature of the hydroxamic acid, amine, and solvent used for the synthesis [106].

Table 4.8. Selected calculated bond lengths (Å) and angles (°) of the *fac*-**1**\* and *mer*-**5**\* model dianions compared to crystal structure data of *fac*-**1**•MeOH and *mer*-**5**•2MeOH compounds.

	<i>fac</i> -isomer		<i>mer</i> -isomer	
	Calc. <sup>a</sup>	Exp. <sup>b</sup>	Calc. <sup>a</sup>	Exp. <sup>b</sup>
Bond lengths (Å)				
Si-O	1.8311	1.7783	1.8411	1.7809
O-N	1.4093	1.4264	1.4136	1.4289
O-C	1.3238	1.3210	1.3265	1.3248
N=C	1.3066	1.2937	1.3066	1.2925
Angles (°)				
O-Si-O	84.809	85.62	84.806	86.0
Si-O-C	109.167	111.52	109.489	111.44
Si-O-N	114.66	113.69	114.394	113.43

<sup>a</sup>BPW91/6-311+G\*, <sup>b</sup>ref. 106.

As one can notice from Table 4.8 the agreement between the calculated and experimental established structural parameters is relatively good, the differences evidenced being a consequence of the influence of the intermolecular interactions between the dianions (including hydrogen bonds) and the neighbouring cations present in the crystals [106]. Moreover, the theoretical calculations were performed for the model compounds in which the phenyl groups have been replaced by methyl moieties. From Table 4.8 it can be observed that the bond lengths belonging to the *fac*-isomer are slightly different from that of the *mer*-isomer. The differences between the Si-O, O-N, O-C and N=C bonds lengths of the *fac*- and *mer*-isomers were found to be 0.0016 Å (calc. 0.01 Å), 0.0025 Å (calc. 0.0043 Å), 0.0038 Å (calc. 0.0027 Å) and -0.0012 Å (calc. 0 Å), respectively. These variations in the bond lengths should be observable in the infrared and Raman spectra of the hexacoordinated compounds.



The infrared and Raman spectra of the compounds *fac*-**1**•MeOH, **2-4** and *mer*-**5**•2MeOH in the range from 1800-400  $\text{cm}^{-1}$  are depicted in Fig. 4.15. The observed vibrational modes together with the vibrational assignment according to the work of Brahma and Chattopadhyay [109] and the results of theoretical calculations are summarised in Tables 4.9 and 4.10. As it was mentioned above, a perfect agreement between the experimental and calculated wavenumbers is not possible in this case because the dianions are influenced by their interactions with the cations [106]. Furthermore, the theoretical calculations were performed for model compounds in the gas phase, while the spectra were recorded for polycrystalline samples. However, as can be seen from Tables 4.9 and 4.10 the agreement between the experimental and theoretical data at the presented theoretical level is sufficient to be useful for the assignment of the vibrational modes.

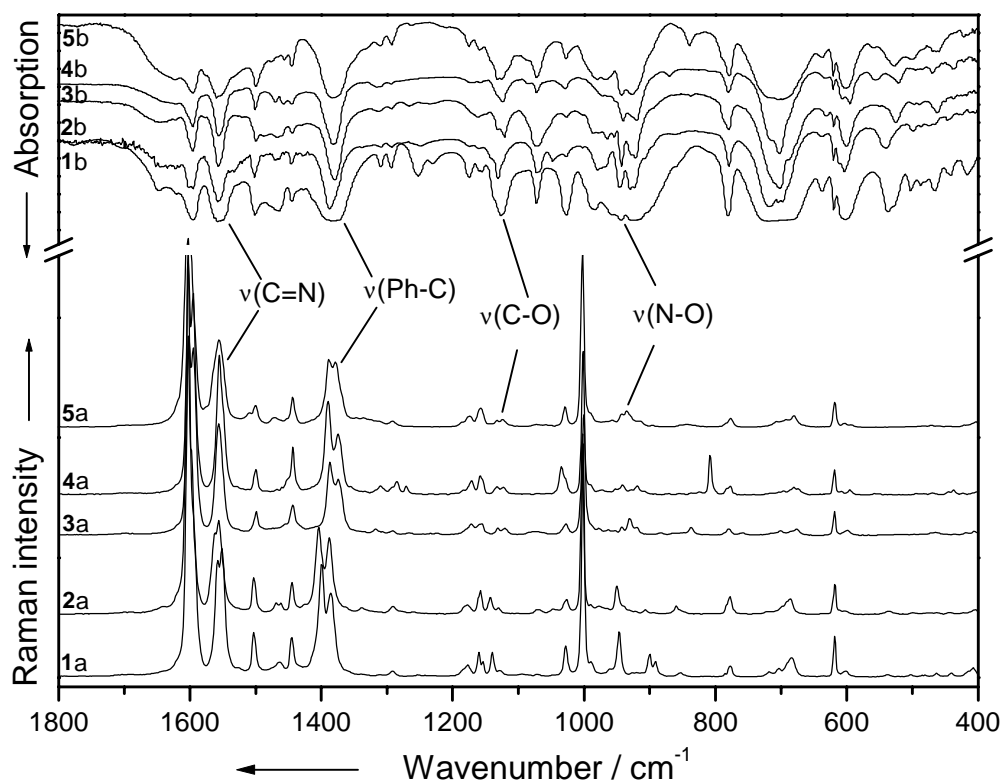


Fig. 4.15. FT-Raman (a) and infrared spectra (b) of compounds **1-5**.

From Fig. 4.15 one can see that the spectra of the different compounds resemble each other very closely, the observed differences are mainly caused by different cations, which neutralize the dianionic hexacoordinated complexes. In the spectra of the octahedral compounds **1-5** spectral regions, which contain a collection of bands given by the bidentate hydroximato(2-) ligands and bands due to cation vibrations, can be observed.

Because the existence of different conformations is a consequence of the different orientation of the ligands around the central silicon atom, it is obvious that in order to determine the conformation of these complexes, the vibrations associated with the hydroximato(2-) ligands should be considered in more detail. Thus, the bands present in the high wavenumber region of all spectra ( $3100-3000\text{ cm}^{-1}$ ) were attributed to C-H stretching vibrations belonging to the ligands and cations. The bands around  $1600\text{ cm}^{-1}$  are due to phenyl ring stretching vibrations, while the ring breathing modes give rise to the strong bands around  $1000\text{ cm}^{-1}$  in the spectra of all compounds [89]. The bands given by the C-H and ring deformation vibrations arise in all spectra at about  $1155$  and  $620\text{ cm}^{-1}$ , respectively. The medium intense infrared and Raman bands evidenced at about  $1555\text{ cm}^{-1}$  in all spectra were assigned to the C=N stretching vibration (see Fig. 4.15). In the  $1400-1380\text{ cm}^{-1}$  spectral region the bands due to the C-C (Ph-C) stretching mode can be observed. The C-O stretching vibrations give rise to the medium intense bands around  $1130\text{ cm}^{-1}$ , while the bands given by the N-O stretching vibrations are present around  $950\text{ cm}^{-1}$  in all spectra [89, 109]. Maybe the most important bands present in the spectra of all compounds, which are an evidence of the coordination to the metal centre, are due to the metal-oxygen vibrations. Thus, the weak Raman bands around  $535\text{ cm}^{-1}$  and the medium intense infrared bands observed in the spectra of all compounds at about  $530$  and  $630\text{ cm}^{-1}$  were assigned [99] to the  $\text{SiO}_6$  stretching vibration (Tables 4.9 and 4.10). The out-of-plane and in-plane deformation vibrations of the five-membered rings containing the central silicon atom give rise to the medium intense bands present in the spectra of all compounds around  $315$ ,  $600$  and  $680\text{ cm}^{-1}$ , respectively. Most of the other bands present in the spectra are due to cation vibrations.

Table 4.9. Selected experimental (infrared and FT-Raman) and calculated wave-numbers ( $\text{cm}^{-1}$ ) of compounds **1** and **2** with the tentative assignment.

<i>fac-1</i>		<b>2</b>		<i>fac-1</i> *	Vibrational assignment
IR	Raman	IR	Raman	Calc. <sup>a</sup>	
	258m		256w	266	OCC def.
	300		298	305	out-of-plane ring def.
	319		318	316	
536vw	539vw	540m	536vw	533	SiO <sub>6</sub> str.
602m	602w	604m	603w	611	out-of-plane ring def.
620s	618m	620m	618m		Ph ring def.
637m		637m		630	SiO <sub>6</sub> str.
688m	684m	697m	685m	682	in-plane ring def.
943s	947m	947vs	949m	912	N-O str.
983s	989sh 1000s		991sh 1000s		Ph ring breathing
1126s	1129w	1130m	1129w	1100	C-O str.
1137sh	1139m	1137sh	1143m	1124	
1154m	1153sh	1159w	1157m		C-H in-plane def. (Ph)
1159sh	1160m				
1385s br	1385s 1399s	1388s	1388s 1403s	1347 1355	C-C str. (Ph-C)
1549sh	1551s	1553m	1556s	1564	C=N str.
1557ms	1557sh	1557s	1562sh	1576	
1594s	1599sh 1602vs	1594s 1601sh	1602vs		C=C str. (Ph ring)
3016vw	3017sh		3021m		C-H str. (Ph)
3031vw	3029ms		3044sh		
3060vw	3062sh		3054sh		
	3068s		3064s		

<sup>a</sup>BPW91/6-311+G\*.

Table 4.10. Selected experimental (infrared and FT-Raman) and calculated wave-numbers ( $\text{cm}^{-1}$ ) of compounds **3-5** with the tentative assignment.

<b>3</b>		<b>4</b>		<i>mer-5</i>		<i>mer-5</i> *	Vibrational assignment
IR	Raman	IR	Raman	IR	Raman	Calc. <sup>a</sup>	
	256w		253w		256vw	255	OCC def.
	301 324		307 327		332	316 329	out-of-plane ring def.
525m		521w		527sh		525	SiO <sub>6</sub> str.
600m	602sh	606m	608vw	602m	602vw	607	out-of-plane ring def.
620m	618m	620m	618m	620s	618m		Ph ring def
631m		633m		637m		625	SiO <sub>6</sub> str.
	675m		680m		680m	680	in-plane ring def.
943s	942m	941s	941m	945m	943m	910	N-O str.
	990sh 1000s		990sh 1000s		991sh 1002s		Ph ring breathing
1119s 1130sh	1120m 1131m	1124m 1135sh	1122m 1133m	1126s 1132s	1124m 1133sh	1094 1119	C-O str.
1159vw	1156m		1157m	1159m	1156m		CH in-plane def. (Ph)
1379s	1374s 1387s	1383s	1374s 1389s	1385s	1378s 1388s	1345 1351	C-C str. (Ph-C)
1557s	1556s	1557s	1555s	1559m	1555s	1567	C=N str.
1597s	1594sh 1601vs	1594s	1594s 1602vs	1597m	1602vs		C=C str. (Ph ring)
	3026m 3055sh 3064s		3025m 3043sh 3054sh 3063s		3031sh 3044sh 3067s		C-H str. (Ph)

<sup>a</sup>BPW91/6-311+G\*.

Keeping in mind that the *mer*- and *fac*-isomers belong to two different point group symmetries they should be spectroscopically identifiable by means of a thorough vibrational analysis. Thus, in the spectra of the more symmetric *fac*-isomer ( $C_3$  symmetry) a different number of bands as well as different spectral band positions are expected as compared to the *mer*-isomers ( $C_1$  symmetry). Moreover, because the structures of the *fac*-**1**•MeOH and *mer*-**5**•2MeOH compounds are already known from the X-ray diffraction experiments, the conformation of the compounds **2-4** can be determined by comparing their spectra with those of the compounds **1** and **5**.

First of all, our purpose was to find out the spectral features that differentiate between the *fac*-**1**•MeOH and *mer*-**5**•2MeOH isomers. By a comparison of the spectra of *fac*-**1**•MeOH with the spectra of *mer*-**5**•2MeOH the existence of spectral regions useful for a differentiation of the stereoisomers can be observed. Furthermore, it can be noticed that, in agreement with the differences observed between the bond lengths of the *fac*- and *mer*-isomers, most of the bands, which correspond to hydroximato(2-) ligand vibrations, appear at higher wavenumbers in the spectrum of **1** in comparison to the corresponding vibrations of **5**. Thus, shifts to higher wavenumbers by 7 and 10  $\text{cm}^{-1}$  were evidenced in the Raman spectrum of **1** for the bands at 1385 and 1399  $\text{cm}^{-1}$  assigned to C-C stretching vibrations in comparison to the corresponding bands present in the spectrum of **5**, while for the infrared C-C stretching band at 1385  $\text{cm}^{-1}$  no shift could be observed (see Fig. 4.15). The C-O stretching vibrations give rise to two medium intense Raman and two strong infrared bands, all shifted to higher wavenumbers by approximately 5  $\text{cm}^{-1}$  in the spectra of the *fac*-isomer compared to the spectra of *mer*-isomer. Furthermore, the medium intense Raman and the strong infrared bands present in the spectra of **1** at 947 and 943  $\text{cm}^{-1}$ , respectively and attributed to the N-O stretching vibration appear at higher wavenumbers by approximately 4  $\text{cm}^{-1}$  in comparison to the corresponding bands observed in the spectra of **5** (Fig. 4.15 and Tables 4.9 and 4.10). In the spectra of the *fac*-isomer the bands assigned to the  $\text{SiO}_6$  vibrational modes are also shifted to higher wavenumbers by approximately 5  $\text{cm}^{-1}$  in comparison to the corresponding bands of the *mer*-isomer. In agreement with previous results [103, 104, 108], one concludes from Fig. 4.15 and Tables 4.9 and 4.10 that the facial isomer displays a larger band splitting in its spectra than the meridional one, the

infrared and Raman bands assigned to the C=N stretching and in-plane C-H deformation vibrations being splitted in the spectra of the *fac-1*•MeOH.

Taking into account the spectral characteristics differentiating the *fac-1*•MeOH and *mer-5*•2MeOH isomers we compared their spectra with the spectra of compounds **2-4** in order to determine the configuration of the last ones. The spectral regions of the Raman spectra of all compounds relevant for the differentiation of the stereoisomers are presented in Fig. 4.16. Thus, from Fig. 4.16a and Tables 4.9 and 4.10 the splitting of the bands assigned to the C=N stretching vibration can be only observed in the spectra of compound **2**. The C-C stretching Raman bands present in the spectrum of **2** at 1388 and 1403  $\text{cm}^{-1}$  show, similar to the bands belonging to the *fac-1*•MeOH, strong shifts to higher wavenumbers by 10 and 12  $\text{cm}^{-1}$  in comparison to their analogues bands present in the Raman spectra of the compounds **3-5**, while for the infrared C-C stretching band at 1388  $\text{cm}^{-1}$  only a small shift (2  $\text{cm}^{-1}$ ) can be evidenced (Fig. 4.16b). From Fig. 4.16c and Tables 4.9 and 4.10 shifts to higher wavenumbers by approximately 7 and 3  $\text{cm}^{-1}$  of the Raman and infrared bands assigned to the C-O stretching vibration of compound **2** in comparison to the corresponding vibrations of the compounds **3-5** can be observed. Both Raman and infrared bands at 949 and 947  $\text{cm}^{-1}$  due to the N-O stretching vibration appear at higher wavenumbers by 6 and 2  $\text{cm}^{-1}$ , respectively in the spectra of **2**. By comparing the bands due to the  $\text{SiO}_6$  vibrational modes present in the spectra of compound **2** with their analogues bands evidenced in the spectra of compounds **3** and **4** (Tables 4.9 and 4.10) a shift to higher wavenumbers can be observed. Taking into account that compound **2** presents the same spectral features like *fac-1*•MeOH, namely shifts to higher wavenumbers and splitting of some bands, we suppose that it is also *fac*-configured. On the other hand, the spectra of compounds **3** and **4** are similar to those of *mer-5*•2MeOH, therefore, we assume that they possess a *mer*-configuration [110].

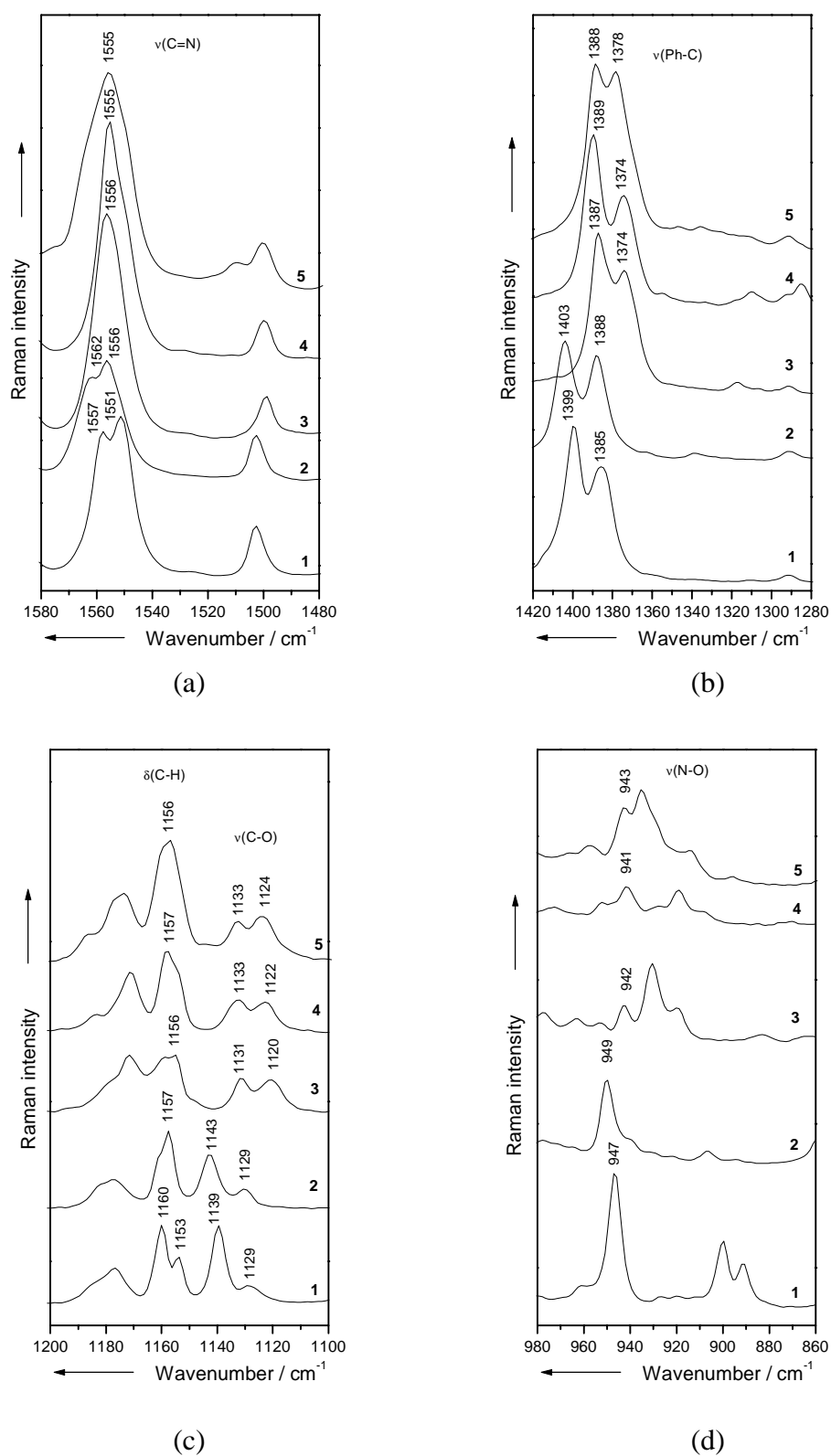


Fig. 4.16. Spectral regions of the Raman spectra relevant for differentiating the geometric isomers of compounds **2-4**: 1580–1480  $\text{cm}^{-1}$  (a), 1420–1280  $\text{cm}^{-1}$  (b), 1200–1100  $\text{cm}^{-1}$  (c), 980–860  $\text{cm}^{-1}$  (d).

### 4.3.3. Conclusion

Infrared absorption and FT-Raman spectroscopy in conjunction with DFT calculations have been successfully applied to the vibrational characterisation of the hexacoordinated silicon(IV) complexes with three unsymmetrical bidentate ligands of the hydroximato(2-) type and to the elucidation of the conformational structures that these species take in solid state. Taking into account the spectral differences evidenced by comparing the spectra of compounds **2-4** to the spectra of the *fac*-**1**•MeOH and *mer*-**5**•2MeOH, it can be concluded that compound **2** is a *fac*-isomer, while both compounds **3** and **4** are *mer*-configured. Generally, the *fac*-isomers display in their spectra a band shifting and a larger band splitting in comparison to the spectra of *mer*-isomers.



# Chapter 5

---

## Raman and surface enhanced Raman spectroscopy in combination with theoretical simulations on biologically active molecules

---

### 5.1. Raman, infrared and surface-enhanced Raman spectroscopy in combination with *ab initio* and density functional theory calculations on 10-isopropyl-10H-phenothiazine-5-oxide

#### 5.1.1. Introduction

Phenothiazine and its derivatives have been extensively investigated because of their interesting pharmacological activity [111-113]. Phenothiazine and related compounds have significant physiological activity and can be used as tranquillisers [114]. A new series of phenothiazine derivatives, which are important intermediates in the metabolism of phenothiazine drugs, have been prepared [115, 116] and the schematic structure of 10-isopropyl-10H-phenothiazine-5-oxide is illustrated in Fig. 5.1.

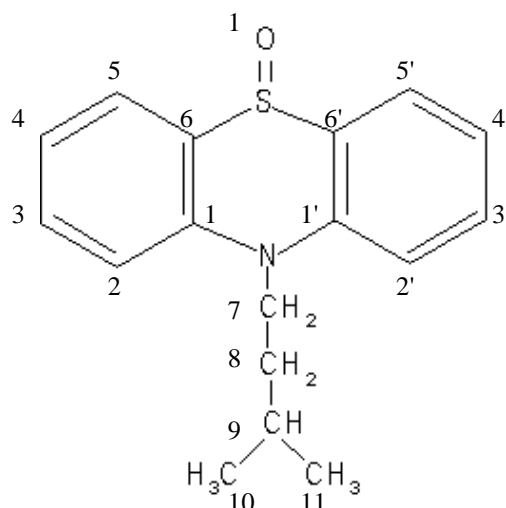


Fig. 5.1. Schematic structure of 10-isopropyl-10H-phenothiazine-5-oxide.

Raman spectroscopy is an invaluable tool to provide information about the structure and interacting mechanisms of biologically active molecules. The Raman spectra of phenothiazine and its radical cation were reported by Pan and Phillips [117], while Hester and Williams [118] have reported the resonance Raman spectra of phenothiazine, 10-methylphenothiazine and their radical cations. A number of recent studies have examined the photooxidation behavior of the phenothiazines and their radical cations using time-resolved laser flash photolysis experiments [119-121].

However, the application of the conventional Raman spectroscopy is limited by the weak intensity of the Raman scattered light and the appearance of the fluorescence. One way to overcome these disadvantages is surface-enhanced Raman spectroscopy (SERS) [16-18]. As it was already mentioned in section 2.4, the origin of the enhancement of Raman scattering cross section at rough surfaces has been an active field of research. It is now widely accepted that there are two main contributions to the overall SERS effect: an electromagnetic contribution and a chemical effect [16, 122]. The electromagnetic (EM) mechanism of the Raman enhancement is based on an increase in the electromagnetic field intensity near the metal surface due to a resonance excitation of the delocalised electrons of the metal. This effect is not dependent on specific interactions between the molecules and the metal, but is strongly related to the large-scale roughness that characterises the substrate surface [16]. In the short-range chemical or charge-transfer (CT) mechanism, a modulation of the molecule's electronic polariza-

bility arising from the interaction with the metal surface is responsible for the enhancement, and the chemical nature of the molecules becomes important [122, 123].

In this study, a rather detailed experimental and theoretical study of the 10-isopropyl-10H-phenothiazine-5-oxide compound has been carried out. The first part of the study presents vibrational analysis of the above-mentioned phenothiazine derivative from an analytical (infrared and Raman spectroscopy) and theoretical (Hartree Fock and density functional theory calculations) point of view, while in the second part of the study the SER spectra at different pH values are reported and analysed in order to elucidate the adsorption behavior of the molecules on colloidal silver particles and to establish whether or not the molecule-substrate interaction and consequently the SERS effect may be dependent on the pH of the solution.

### **5.1.2. Results and discussion**

#### *Vibrational analysis*

The crystallographic analysis of phenothiazine [124] shows that the molecule is folded about the N-S axis with the two planes containing the phenyl rings having a dihedral angle of 158.5°. The amount of folding increases for larger substituents [117], chlorpromazine having a dihedral angle of 139.4°.

Selected optimised structural parameters of 10-isopropyl-10H-phenothiazine-5-oxide calculated by various methods are given in Table 5.1 along with the available X-ray values of the ground state of the phenothiazine [124]. As can be observed the theoretical dihedral angle between the two phenyl rings of the compound has smaller values in comparison to the experimentally determined dihedral angle of the phenothiazine and is in agreement with previous results [117]. The calculated bond lengths and bond angles agree with the reported parameters [124], the B3LYP method giving the best results. At this level of calculation the differences observed between the theoretical and experimental values of the structural parameters that involve the S and N atoms are most probably due to the presence of the substituents.

Table 5.1. Selected calculated bond lengths (pm) and angles ( $^{\circ}$ ) of the 10-isopropyl-10H-phenothiazine-5-oxide compared to the experimental data of phenothiazine.

	10-isopropyl-10H-phenothiazine-5-oxide			phenothiazine
	Calc. <sup>a</sup>	Calc. <sup>b</sup>	Calc. <sup>c</sup>	Exp. <sup>d</sup>
Bond lengths (pm)				
C-S <sub>average</sub>	182.155	182.150	180.995	177
C-N <sub>average</sub>	141.925	141.927	141.717	140.6
C <sub>1</sub> -C <sub>2</sub>	141.209	141.209	140.419	138.5
C <sub>2</sub> -C <sub>3</sub>	140.209	140.208	139.584	139
C <sub>3</sub> -C <sub>4</sub>	140.258	140.258	139.565	136.7
C <sub>4</sub> -C <sub>5</sub>	140.181	140.181	139.513	136.7
C <sub>5</sub> -C <sub>6</sub>	139.620	139.619	138.976	139.1
C <sub>6</sub> -C <sub>1</sub>	141.328	141.328	140.552	139.7
C <sub>2</sub> -H <sub>2</sub>	109.187	109.187	108.450	98
C <sub>3</sub> -H <sub>3</sub>	109.367	109.367	108.670	105
C <sub>4</sub> -H <sub>4</sub>	109.282	109.282	108.584	98
C <sub>5</sub> -H <sub>5</sub>	109.365	109.365	108.633	93
S-O <sub>1</sub>	152.295	152.295	151.280	
C <sub>7</sub> -N	147.130	147.130	146.690	
Angles ( $^{\circ}$ )				
Dihedral angle	138.478	138.478	137.657	153.30
C <sub>6</sub> -S-C <sub>6'</sub>	93.068	93.068	93.676	99.60
C <sub>1</sub> -N-C <sub>1'</sub>	117.207	117.206	116.922	121.50
C <sub>1</sub> -C <sub>2</sub> -C <sub>3</sub>	120.484	120.484	120.417	119.8
C <sub>2</sub> -C <sub>3</sub> -C <sub>4</sub>	121.091	121.092	121.084	120.5
C <sub>3</sub> -C <sub>4</sub> -C <sub>5</sub>	119.165	119.165	119.192	119.4
C <sub>4</sub> -C <sub>5</sub> -C <sub>6</sub>	119.538	119.538	119.502	119.7
C <sub>5</sub> -C <sub>6</sub> -C <sub>1</sub>	122.307	122.307	122.268	119.2

(Table 5.1. continued)

	10-isopropyl-10H-phenothiazine-5-oxide			phenothiazine
	Calc. <sup>a</sup>	Calc. <sup>b</sup>	Calc. <sup>c</sup>	Exp. <sup>d</sup>
Angles (°)				
C <sub>6</sub> -C <sub>1</sub> -C <sub>2</sub>	117.377	117.377	117.501	119.5
C <sub>1</sub> -C <sub>2</sub> -H <sub>2</sub>	120.267	120.267	120.302	118.5
C <sub>2</sub> -C <sub>3</sub> -H <sub>3</sub>	118.874	118.873	118.915	115.8
C <sub>3</sub> -C <sub>4</sub> -H <sub>4</sub>	120.554	120.554	120.520	117
C <sub>4</sub> -C <sub>5</sub> -H <sub>5</sub>	121.874	121.874	121.842	122.8
C <sub>6</sub> -S-O <sub>1</sub>	110.020	110.020	109.540	
C <sub>6</sub> -S-O <sub>1</sub>	110.065	110.650	109.567	

<sup>a</sup>RHF/6-31G\*, <sup>b</sup>BPW91/6-31G\*, <sup>c</sup>B3LYP/6-31G\*, <sup>d</sup>Ref. 124.

The FT-Raman and infrared spectra of the phenothiazine derivative 10-isopropyl-10H-phenothiazine-5-oxide in the range from 3200 to 400 cm<sup>-1</sup> are presented in Fig. 5.2 and the observed bands as well as the vibrational assignment are summarized in Table 5.2.

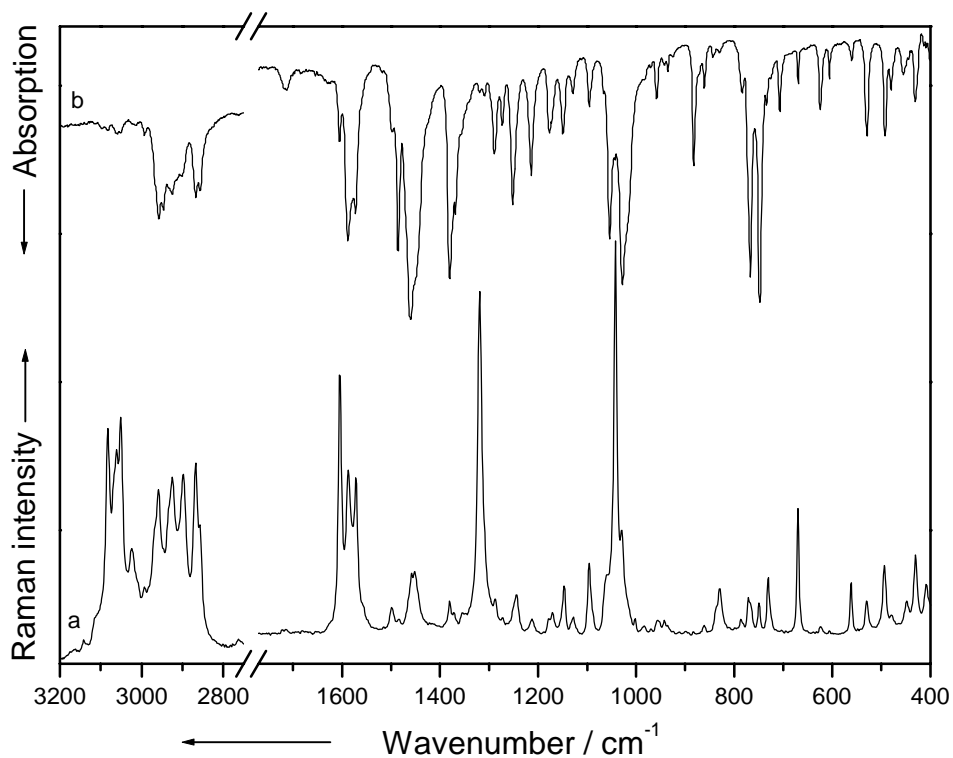


Fig. 5.2. FT-Raman (a) and infrared (b) spectra of 10-isopropyl-10H-phenothiazine-5-oxide.

Table 5.2. Assignment of the theoretical wavenumber values ( $\text{cm}^{-1}$ ) to the experimental bands of the phenothiazine 10-isopropyl-10H-phenothiazine-5-oxide.

Experimental		Theoretical			Vibrational assignment
IR	Raman	Calc. <sup>a</sup>	Calc. <sup>b</sup>	Calc. <sup>c</sup>	
	177m	193	185	196	$\text{C}_1\text{NC}_1'$ , $\text{C}_6\text{SC}_6'$ twist + S=O def.
	199m	203	202	208	CCC skeletal def.
	272m	267	275	282	C-H def. ( $\text{CH}_3$ )
	308w	320	305	320	ring chair def.
	340m	338	333	345	$\text{C}_1\text{NC}_1'$ , $\text{C}_6\text{SC}_6'$ twist
	383m	372	375	387	S=O def. + $\text{C}_{10,9,11}$ def.
402m	408m	408	403	399	out-of-plane Ph ring def.
430m	430m	438	440	436	
455sh	448sh	461	455	455	$\text{C}_{7,8,9}$ def. + C-H def. ( $\text{CH}_3$ )
479m	480sh	497	490	471	$\text{C}_1\text{NC}_1'$ , $\text{C}_6\text{SC}_6'$ wagging
492m	494m	518	508	507	
527m	530w	522	514	529	out-of-plane Ph ring def.
560w	560m	566	553	534	ring chair def.
604w	605vw	606	608	609	in-plane Ph ring def.
624m	623vw	663	658	628	
668w	670m	685	666	682	
705m	703vw	733	710	693	out-of-plane Ph ring def.
734sh	730m	752	736	754	C-H wagging (ring)
747s	749w	768	749	769	
767s	771w	776	765	778	C-H def. ( $\text{CH}_2$ )
829vw	830m	804	823	843	$\text{C}_{10,9,11}$ str. + C-H twist (ring)
844vw	835sh	859	830	874	
881m	882vw	884	871	896	$\text{C}_{3,4,5}$ , $\text{C}_{3',4',5}'$ bend.
910sh	900vw	916	904	918	C-H twist (ring)
941sh	943vw	936	939	948	

(Table 5.2. continued)

Experimental		Theoretical			Vibrational assignment
IR	Raman	Calc. <sup>a</sup>	Calc. <sup>b</sup>	Calc. <sup>c</sup>	
959vw	956vw	963	949	982	C-H def. (CH <sub>3</sub> )
983sh	984vw	970	974	1002	
1003sh	1002w	1003	1012	1042	C <sub>1,2,3</sub> + C <sub>3,4,5</sub> bend.
1027s	1030sh	1015	1031	1058	C <sub>7,8</sub> str.
1042sh	1042s	1021	1042	1067	Ph ring breathing
1053s	1059sh	1041	1059	1082	CH bend. (ring) + C <sub>6</sub> SC <sub>6</sub> ' str. + NC <sub>7</sub> str
1095m	1095m	1092	1087	1116	S=O str.
1128w	1127w	1114	1124	1154	C-H def. (CH <sub>2</sub> , CH <sub>3</sub> ) + C <sub>10,9,8</sub> str.
1150m	1142m	1146	1145	1180	
1172sh	1170w	1188	1170	1199	C-H bend. (ring) + C-H def. (CH, CH <sub>3</sub> )
1176m	1177sh	1199	1173	1206	
1214m	1212w	1211	1213	1248	C <sub>1</sub> NC <sub>1</sub> ' as. Str. + C-H bend. (ring))
1251m	1244m	1249	1247	1283	C <sub>1</sub> NC <sub>1</sub> ' s. str. + C-H rock. (ring)
1273m	1272w	1276	1272	1314	C-H def. (CH <sub>2</sub> ) + C-H rock. (ring) + NC <sub>7</sub> str.
1289m	1288sh	1281	1278	1318	
1319vw	1319s	1325	1323	1350	CCC str. (Ph ring)
1359sh	1355sh	1345	1349	1370	C-H def. (CH <sub>2</sub> , CH <sub>3</sub> )
1368sh	1372sh	1366	1365	1401	
1381s	1380w	1396	1384	1431	
1449sh	1451m	1458	1455	1499	C <sub>6,1</sub> , C <sub>6',1'</sub> str.
1460s	1457m	1467	1480	1522	
1484s	1484w	1477	1486	1529	C-H def. (CH <sub>2</sub> , CH <sub>3</sub> )
1498sh	1498w	1496	1502	1543	
1572m	1571m	1586	1573	1622	C=C str. (Ph ring)
1588s	1587m	1600	1591	1638	
1605m	1605s	1615	1612	1658	

(Table 5.2. continued)

Experimental		Theoretical			Vibrational assignment
IR	Raman	Calc. <sup>a</sup>	Calc. <sup>b</sup>	Calc. <sup>c</sup>	
2868m	2867m	2882	2935	3004	C-H str. (CH, CH <sub>2</sub> , CH <sub>3</sub> )
2901sh	2898m	2921	2997	3038	
2925m	2925m	2951	3059	3051	
2958m	2958m	3013	3069	3088	
3016vw	3025m	3030	3086	3101	C-H str. (ring)
3051vw	3050s	3042	3121	3112	
3084vw	3082s	3048	3143	3190	

<sup>a</sup>RHF/6-31G\*, <sup>b</sup>BPW91/6-31G\*, <sup>c</sup>B3LYP/6-31G\*.

The assignment of the vibrational modes was carried out with the help of the results obtained from theoretical calculations and of the study reported by Pan and Phillips [117] on phenothiazine.

*Ab initio* harmonic vibrational wavenumbers are typically larger than the fundamentals observed experimentally [55]. A major source of this disagreement is the neglect of anharmonicity effects in the theoretical treatment. Errors arise also because of incomplete incorporation of electron correlation and the use of finite basis sets. Since Hartree-Fock (HF) calculations tend to overestimate relatively uniform vibrational wavenumbers because of improper dissociation behavior, the predicted wavenumber values have to be scaled with general scaling factors to adjust the observed experimental values [125]. Thus, the restricted HF calculated vibrational wavenumbers presented in Table 5.2 have been uniformly scaled by 0.8953 according to the work of Scott and Radom [125]. Even after scaling, the RHF wavenumbers are overestimated in the high wavenumber region, but are comparable to the experimental values in the low wavenumber region.

In agreement with previous studies [125, 126] the B3LYP functional also tends to overestimate the fundamental modes in comparison to the BPW91 method. From Table 5.2 it can be seen that the calculated vibrational wavenumbers using the B3LYP method



are much larger than those calculated with the BPW91 method compared to the experimental values. Therefore, scaling factors have to be used in order to obtain a good agreement [125, 126]. The observed disagreement between the theory and experiment could be a consequence of the anharmonicity and the general tendency of the quantum chemical methods to overestimate the force constants at the exact equilibrium geometry [127]. Nevertheless, the theoretical calculations performed at the BPW91 level of theory reproduce the experimental data rather well and allow the assignment of the vibrational modes.

From Fig. 5.2 and Table 5.2 one can observe that the phenyl vibrational modes dominate the infrared and Raman spectra of the 10-isopropyl-10H-phenothiazine-5-oxide. Thus, the intense bands present in the high wavenumber region ( $3200\text{-}3000\text{ cm}^{-1}$ ) of both spectra were attributed to the C-H stretching vibrations of the aromatic groups. In the high wavenumber region between  $3000$  and  $2800\text{ cm}^{-1}$  the medium intense bands assigned to the C-H stretching vibrations of the isopropyl group can be also observed in both spectra. The strong infrared and Raman bands between  $1605$  and  $1571\text{ cm}^{-1}$  belong to C=C stretching vibrational modes. The strong Raman and the corresponding weak infrared bands at  $1319\text{ cm}^{-1}$  (calc.  $1323\text{ cm}^{-1}$ ) can be assigned to the C-C stretching vibration of the aromatic ring. The breathing vibration of the benzene shows itself as very intensive bands at  $1042\text{ cm}^{-1}$  (calc.  $1042\text{ cm}^{-1}$ ) in both spectra. The medium intense infrared and Raman bands at  $882$  (calc.  $871\text{ cm}^{-1}$ ) and  $670\text{ cm}^{-1}$  (calc.  $666\text{ cm}^{-1}$ ) can be assigned to in-plane ring deformation vibrations, while the bands attributed to out-of-plane ring deformation vibrations appear at  $703$  (calc.  $710\text{ cm}^{-1}$ ),  $530$  (calc.  $514\text{ cm}^{-1}$ ) and  $430\text{ cm}^{-1}$  (calc.  $440\text{ cm}^{-1}$ ) in the infrared and Raman spectra of the phenothiazine derivative. The bands due to in-plane and out-of-plane C-H deformation vibrations appear in both spectra around  $1200$  and  $750\text{ cm}^{-1}$ , respectively.

The S=O deformation and stretching vibrations give rise to the medium intense Raman bands at  $383$  (calc.  $375\text{ cm}^{-1}$ ) and  $1095\text{ cm}^{-1}$  (calc.  $1087\text{ cm}^{-1}$ ), respectively. The medium intense Raman band at  $1244\text{ cm}^{-1}$  and the infrared band at  $1251\text{ cm}^{-1}$  (calc.  $1247\text{ cm}^{-1}$ ) were attributed to the CNC symmetric stretching vibration, while the weak Raman band at  $1212\text{ cm}^{-1}$  and the medium intense infrared band at  $1214\text{ cm}^{-1}$  (calc.

1213  $\text{cm}^{-1}$ ) were assigned to the CNC asymmetric stretching vibration. The bands assigned to the CSC stretching vibration are present around 1055  $\text{cm}^{-1}$  (calc. 1059  $\text{cm}^{-1}$ ) both in the infrared and Raman spectrum of the compound. Ring chair deformation vibrations give rise to the medium intense infrared and Raman bands at 560  $\text{cm}^{-1}$  (calc. 553  $\text{cm}^{-1}$ ) and the weak Raman band at 308  $\text{cm}^{-1}$  (calc. 305  $\text{cm}^{-1}$ ). Other bands given by CNC and CSC out-of-plane deformation vibrations appear around 490, 340 and 177  $\text{cm}^{-1}$ , respectively.

#### *Surface enhanced Raman spectroscopy*

The SER spectra of 10-isopropyl-10H-phenothiazine-5-oxide recorded for different pH values and presented in Fig. 5.3 could be obtained only on activated silver colloids under the presence of co-adsorbed chloride anions.

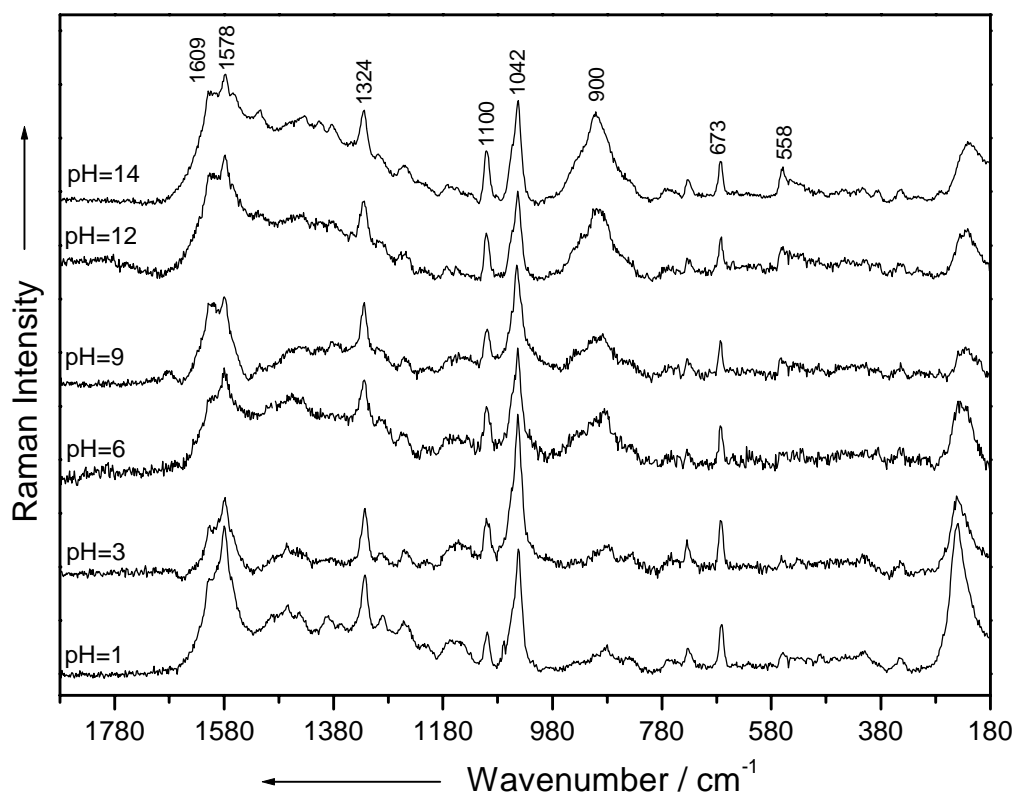


Fig. 5.3. SER spectra of 10-isopropyl-10H-phenothiazine-5-oxide on silver colloid at different pH values as indicated.

The SERS activation of the colloids in the presence of chloride anions can be explained in terms of an increased electromagnetic field or on the basis of the chemical enhancement mechanism [128]. The assignment of the vibrational modes of the phenothiazine derivative to the SERS bands at different pH values is summarized in Table 5.3. From the comparison between the Raman spectrum of the polycrystalline sample with the SER spectra (Figs. 5.2a and 5.3) we found a good correlation between the SERS and the Raman bands. The wavenumber shifts of the SERS bands relative to the corresponding Raman bands were never exceeding  $5\text{ cm}^{-1}$ .

Table 5.3. Wavenumbers ( $\text{cm}^{-1}$ ) and assignment of the normal vibrational modes of the 10-isopropyl-10H-phenothiazine-5-oxide to the SERS bands at different pH values.

Raman	SERS			Vibrational assignment
	pH 1	pH 6	pH 14	
199m	200sh	203sh	200sh	CCC skeletal def.
	217sh 238s	218sh 238s	221ms 238sh	Ag-O str. + Ag-Cl <sup>-</sup> str.
272m	266sh	264sh	269sh	C-H def. (CH <sub>3</sub> )
340m	347w	345w	342w	C <sub>1</sub> NC <sub>1'</sub> , C <sub>6</sub> SC <sub>6'</sub> twist
383m	354w	384w	388s	S=O def. + C <sub>10,9,11</sub> def.
408m	408w	408vw	413w	out-of-plane Ph ring def.
560m	558w	558m	558m	ring chair def.
670m	671m	673m	673m	in-plane Ph ring def.
730m	732m	734w	732m	C-H wagging (Ph ring)
771w	768m	763w	769w	C-H def. (CH <sub>2</sub> )
830m	839m	834m	833sh	C <sub>10,9,8</sub> str. + C-H twist (Ph ring)
882vw	880m	880m	881sh	C <sub>3,4,5</sub> , C <sub>3',4',5'</sub> bend.
900vw	905sh	899m	900s	C-H twist (Ph ring)
943w	936w	936sh	934sh	
1042s	1042s	1042s	1042s	Ph ring breathing

(Table 5.3. continued)

Raman	SERS			Vibrational assignment
	pH 1	pH 6	pH 14	
1059sh	1067m	1066sh		C-H bend. (Ph ring) + C <sub>6</sub> SC <sub>6</sub> ' str. + NC <sub>7</sub> str.
1095m	1098m	1100m	1100ms	S=O str.
1127w 1142m	1130sh 1153m	1136m 1151m	1133sh 1155m	C-H def. (CH <sub>2</sub> , CH <sub>3</sub> ) + C <sub>10,9,8</sub> str.
1170w 1177sh	1167m	1167m 1175m	1170m	C-H bend. (Ph ring) + C-H def. (CH, CH <sub>3</sub> )
1212w	1213m	1216w	1212vw	C <sub>1</sub> NC <sub>1</sub> ' as. Str. + C-H bend. (Ph ring)
1244m	1252m	1256m	1252m	C <sub>1</sub> NC <sub>1</sub> ' s. str. + C-H rock. (Ph ring)
1288sh	1290m	1296m	1298m	C-H def. (CH <sub>2</sub> ) + C-H rock. (Ph ring) + NC <sub>7</sub> str.
1319s	1322s	1324s	1324s	CCC str. (Ph ring)
1380w	1381sh	1383w	1383m	C-H def. (CH <sub>2</sub> , CH <sub>3</sub> )
1451m 1457m	1441m 1462m	1435m 1456m	1432m 1456w	C <sub>6,1</sub> , C <sub>6,1</sub> ' str.
1498w	1493sh	1501sh	1513m	C-H def. (CH <sub>2</sub> , CH <sub>3</sub> )
1571m 1587m 1605s	1566sh 1579s 1607sh	1566sh 1579s 1610sh	1563sh 1578s 1609sh	C=C str. (Ph ring)
2867m 2898m 2925m 2958m	2868ms 2890sh 2935m 2962sh	2873m 2898sh 2937ms 2959sh	2874m 2896sh 2936ms 2963sh	C-H str. (CH, CH <sub>2</sub> , CH <sub>3</sub> )
3050s 3082s	3063m 3075sh	3063m 3085sh	3068m 3081sh	C-H str. (Ph ring)

When a molecule binds to a metal surface, it can be either physisorbed or chemisorbed. In the case of physisorption [16, 17] the spectra of the physisorbed and the free molecules are similar. On the other hand, when the molecules are chemisorbed on the metal surface [122, 123] the position and the relative intensities of the SERS bands are dramatically changed, due to an overlapping of molecular and metal orbitals yielding to the formation of a new metal-molecule SERS complex. Both the electromagnetic (EM) mechanism and the charge-transfer (CT) effect contribute to the overall SERS effect, in the case of physisorbed molecules the electromagnetic mechanism being the main enhancement mechanism, while in the case of chemisorption the chemical effect is the dominant enhancement mechanism.

The phenothiazine derivative 10-isopropyl-10H-phenothiazine-5-oxide may bind to the silver surface either *via* the  $\pi$  orbitals of the aromatic rings or *via* the lone pair electrons of the nitrogen or oxygen atoms. For aromatic molecules, it is well known [129] that the bands due to the ring vibrations are red shifted by more than  $10\text{ cm}^{-1}$  and their bandwidths increase substantially, when the molecules adsorb on the metal surface *via* their  $\pi$  systems. Since our SER spectra exhibit only small shifts by  $5\text{ cm}^{-1}$  in comparison to the normal Raman spectrum and the bandwidths were hardly affected by the adsorption, it is likely that the molecules are adsorbed on the silver surface *via* the nonbonding electrons of the nitrogen or oxygen atoms. Due to the presence of the isopropyl substituent on the nitrogen atom, we assume that the interaction between molecule and surface occurs through the lone pair electrons of the oxygen atom since the interaction between nitrogen and metal is sterically hindered.

The adsorbate-metal interaction is further evidenced by the presence of some bands in the  $250\text{-}180\text{ cm}^{-1}$  region (Fig. 5.4), which are assigned to Ag-adsorbate stretching vibrations [130, 131]. By going from an acidic to alkaline pH the pair of bands present in this spectral range reverse their intensity. Thus, the intensity of the sharp band at  $238\text{ cm}^{-1}$  observed at pH 1, which is most probably due to the Ag-Cl<sup>-</sup> stretching vibration [130], is decreasing in intensity with increasing pH values, while simultaneously an increase in intensity and a small shift to higher wavenumbers of the shoulder observed at  $217\text{ cm}^{-1}$  at pH 1 that corresponds to the Ag-O stretching vibration [131] occurs.

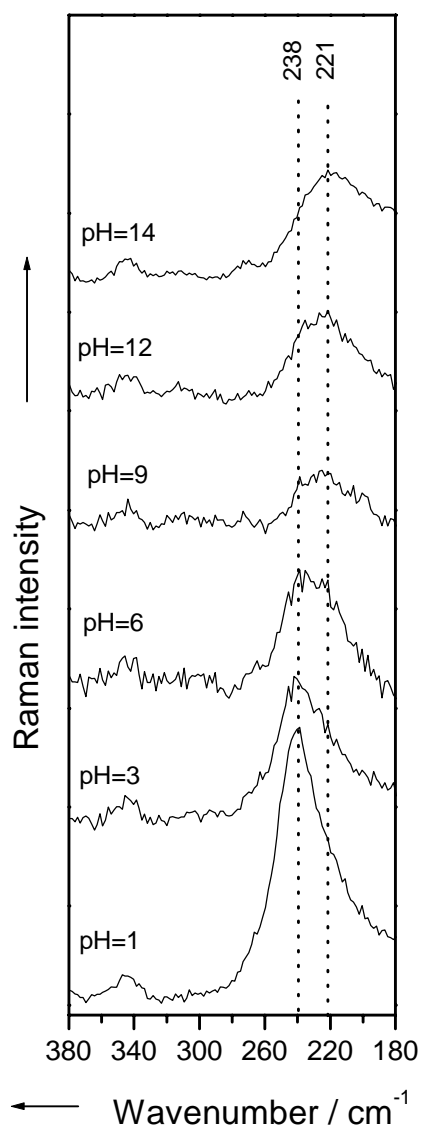


Fig. 5.4. pH dependence of the metal-adsorbate stretching mode from the SER spectra of 10-isopropyl-10H-phenothiazine-5-oxide .

The high intensity of the band at  $238\text{ cm}^{-1}$  could be explained by the increasing amount of chloride anions in an acidic environment caused by the addition of HCl for adjusting the pH values. At pH 6 the Ag-Cl<sup>-</sup> stretching band becomes broader and less intense, while the intensity of the Ag-O stretching band increases. At higher pH values (pH 14), where the concentration of the chloride ions is reduced both in the medium and also at the silver surface, the Ag-Cl<sup>-</sup> stretching vibration gives only rise to a weak shoulder at  $238\text{ cm}^{-1}$ , while the intensity of the band at  $221\text{ cm}^{-1}$ , which corresponds to the metal-oxygen interaction, further increases. The appearance of the Ag-O stretching band in the SER spectra at all pH values indicates the partial chemisorption of the molecules on the metal surface through the nonbonding electrons of the oxygen atom.

The UV-visible absorption spectra of the pure colloid and a mixture of the colloid and 10-isopropyl-10H-phenothiazine-5-oxide before and after addition of NaCl were recorded and are presented in Fig. 5.5.

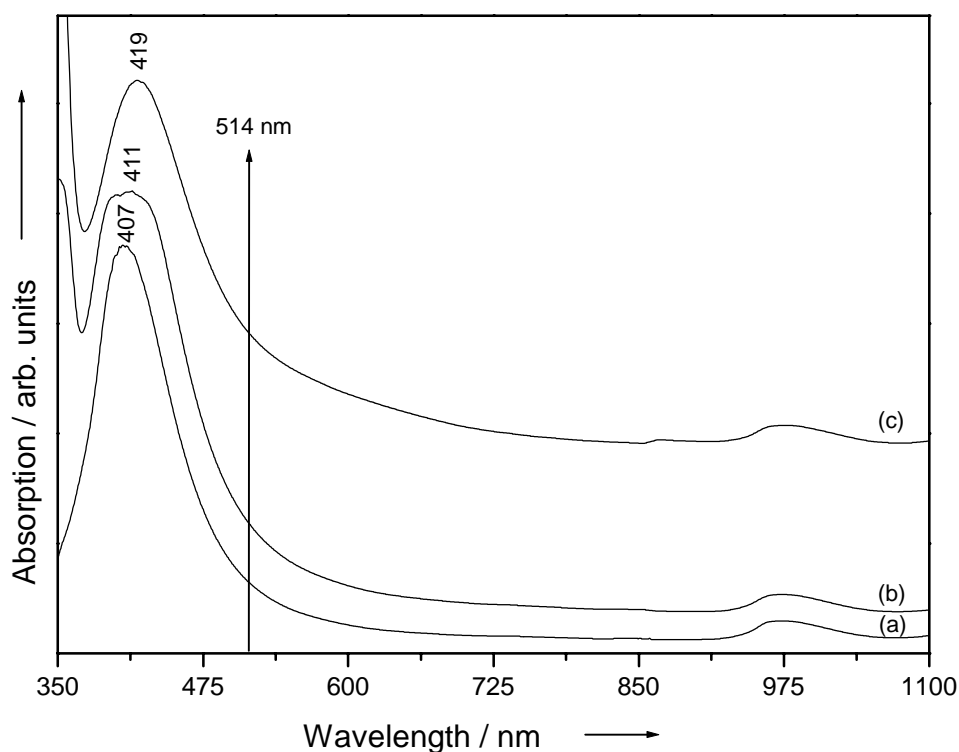


Fig. 5.5. Absorption spectra of salt-free silver colloidal dispersion (a), with  $10^{-1}$  M 10-isopropyl-10H-phenothiazine-5-oxide (b), with  $10^{-1}$  M 10-isopropyl-10H-phenothiazine-5-oxide and  $10^{-2}$  M NaCl (c).

The absorption spectrum of the silver colloid shows a single absorption maximum at 407 nm, due to the small particle plasma resonance. It is known [132] that, when two metallic spheres approach each other, this band remains at the original single sphere wavelength, while another resonance develops at longer wavelengths: hence a secondary peak occurs in the red/near infrared (500-800 nm) spectral region. The appearance of such a new broad band in the red/infrared region is generally attributed to the coagulation of silver particles in the sol in the presence of the adsorbed molecules [133, 134]. Alternatively such a band has been ascribed to a charge-transfer (CT) band due to the molecule-metal interaction [135]. As one can see from Fig. 5.5 after the addition of the sample to the silver hydrosol the band at 407 nm becomes weaker, broa-

der and is shifted to longer wavelengths by 4 nm. When NaCl is added to the colloid-sample mixture, the absorption peak is further shifted to longer wavelengths by 8 nm and its intensity decreases, while no new band due to the secondary plasmon resonance is observed. This behavior indicates the significant contribution of the electromagnetic (EM) mechanism to the overall SERS enhancement.

Variations in the SER spectra with the change of the pH value are usually attributed either to a change in the orientation of the adsorbates with respect to the metal surface [136] or to a change in the chemical nature of the adsorbates [137, 138]. Comparing the SER spectra of the phenothiazine derivative at different pH values (Fig. 5.3), since no new band appears suggesting structural changes of the molecule, the spectral changes may be attributed to orientational change of the molecule on the silver surface.

The orientation of the adsorbed molecules with respect to the metal surface can be estimated from the enhancement of the relevant Raman bands following the surface selection rules [33, 139, 140]. Briefly, these selection rules predict that if the molecular z-axis is normal to the surface, then the vibrations of the adsorbed molecules, which have a polarizability tensor component along this axis, will be enhanced. Vibrations having large x and y tensor components will result in weak Raman bands, compared to the bulk spectrum. In particular, the C-H stretching vibrations were reported to be relatively unambiguous probes for the adsorbate orientation [33].

By looking at the geometry of the 10-isopropyl-10H-phenothiazine-5-oxide it is very difficult to predict exactly the orientation of the molecule with respect to the metal surface. However, from Figs. 5.2a and 5.3 one may notice that at all pH values the ring stretching and breathing modes around 1600 and 1042  $\text{cm}^{-1}$  are enhanced, and small shifts of the bands due to the ring stretching vibrations compared to the corresponding Raman bands can be observed (Table 5.3). The enhancement of the in-plane deformation vibration of the aromatic ring at 670  $\text{cm}^{-1}$  can be observed for all pH values. At alkaline pH this band is shifted to higher wavenumbers by 3  $\text{cm}^{-1}$  in comparison to the Raman spectrum (Table 5.3). At all pH values the bands at 408, 430, 530 and 703  $\text{cm}^{-1}$ , which arise from out-of-plane deformation vibrations of the phenyl



rings, are very weakly enhanced. The behavior of the above-mentioned bands confirms the assumption made before that the molecule-metal interaction does not occur *via* the  $\pi$  orbitals of the aromatic rings. Moreover, the enhancement and the shift to higher wavenumbers by  $5\text{ cm}^{-1}$  of the band at  $1095\text{ cm}^{-1}$  due to the S=O stretching vibration (Table 5.3) gives further evidence about the existence of the molecule-surface interaction through the lone pair electrons of the oxygen atom. The enhancement of the C-H deformation and stretching vibrations of the isopropyl substituent present in all SER spectra confirm the major contribution of the electromagnetic effect to the SERS enhancement in comparison to the chemical one [141].

When comparing the SER spectra for acidic and alkaline pH values with the normal Raman spectrum (Figs. 5.2a and 5.3) changes in the relative intensities for some bands can be observed. At pH 1 some bands due to the in-plane C-H deformation vibration of the phenyl ring are enhanced. Furthermore, the enhancement of the bands at  $1441$  and  $1462\text{ cm}^{-1}$  given by the stretching vibrations of the  $C_6C_1$  and  $C_6'C_1'$  bonds, can be explained on the basis of surface selection rules [33, 139, 140]. When the molecule interacts with the silver surface and adopts an upright orientation of the phenyl groups, these bonds are exactly perpendicular to the surface. For such a case, the surface selection rules predict particularly large enhancement, which is in agreement with our results. In the high wavenumber region ( $3200\text{-}3000\text{ cm}^{-1}$ ) one can see a strong intensity of the C-H stretching bands. Therefore, we assume that for acidic pH values the molecules are oriented at the metal surface in such a way that the benzene rings are preponderant perpendicular with respect to the surface as indicated in Fig. 5.6a. According to the surface selection rules [33, 139, 140], out-of-plane vibrations are only expected to appear in a SER spectrum when the adsorbed molecules adopt a flat or at least tilted orientation on the silver surface. The increased intensity of the bands around  $900\text{ cm}^{-1}$  attributed to out-of-plane C-H deformation vibrations of the phenyl ring for alkaline pH values can be a consequence of a reorientation of the aromatic rings from an upright to a tilted orientation. In contrast to the behavior revealed for acidic pH values, the bands assigned to the  $C_6C_1$  and  $C_6'C_1'$  stretching vibrations are only weakly enhanced for alkaline pH values. Furthermore, the intensity of the C-H stretching bands

present in the high wavenumber region decreases. An enhancement of the band at  $558\text{ cm}^{-1}$  due to the ring chair deformation is also visible. Therefore, we suppose that for alkaline pH values a reorientation of the molecules occurs, the phenyl rings being tilted orientated with respect to the metal surface as suggested in Fig. 5.6b [141].

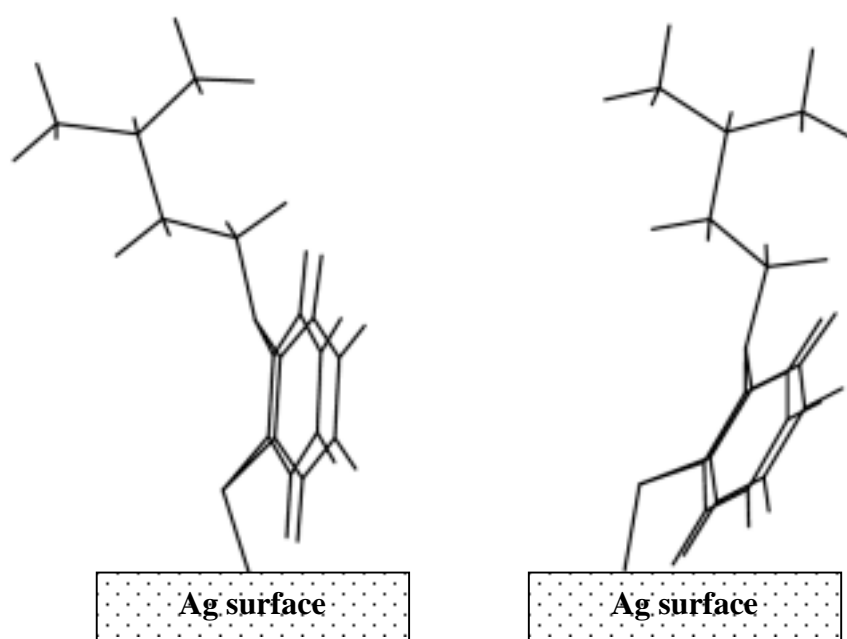


Fig. 5.6. Schematic model for the adsorption geometry of 10-isopropyl-10H-phenothiazine-5-oxide on a colloidal silver surface for acidic (a) and alkaline (b) pH values.

### 5.1.3. Conclusion

Experimental (infrared and Raman spectroscopy) and theoretical (HF and DFT calculations) investigations on 10-isopropyl-10H-phenothiazine-5-oxide have been performed. SER spectra in activated silver colloids at different pH values were recorded and compared to the normal Raman spectrum. By taking into account the shifts of the SERS bands ( $\Delta\nu \leq 5\text{ cm}^{-1}$ ) in comparison to the corresponding Raman bands and the existence of the metal-molecule stretching band at all pH values we assume the partial

chemisorption of the molecules on the silver surface *via* the nonbonding electrons of the oxygen atom. The lack of a broad band in the long-wavelength region of the absorption spectrum of the colloid with added adsorbate proves the significant contribution of the electromagnetic mechanism to the overall SERS enhancement. The changes evidenced in the SER spectra recorded for different pH values were attributed to the reorientation of the adsorbed molecules with respect to the silver surface.

## 5.2. Infrared, Raman and SERS studies together with theoretical investigations on furan-2-carbaldehyde derivatives

### 5.2.1. Introduction

Furan-2-carbaldehyde derivatives [142] are very important intermediates in organic synthesis. The bacteriostatic effects of these compounds have been checked with good results. In this study, the rotational isomers of 5-(4-fluor-phenyl)-furan-2-carbaldehyde (5-(4FP)-F-2C) have been investigated by using infrared and FT-Raman spectroscopy in combination with density functional theory calculations. In order to know the action of potentially drugs, such as the above mentioned carbaldehyde derivative, it is very important to study if the structure of the adsorbed species is the same as that of the free molecules. In these studies a silver surface serves as an artificial biological interface [143]. The SER spectra of the furan-2-carbaldehyde derivative 5-(4FP)-F-2C at low pH values have been recorded and analysed in order to elucidate the adsorption behavior of these molecules on colloidal silver particles.

### 5.2.2. Results and discussion

#### *Vibrational analysis*

By a rotation of the (CHO) group in the 5-(4-fluor-phenyl)-furan-2-carbaldehyde two rotational isomers, the *syn*-form and *anti*-form, are obtained. The optimized geometries of these isomers, calculated at the BPW91/6-311+G\* level of theory with the labels of their atoms are depicted in Fig. 5.7. The optimized structures of both isomers are planar and belong to the  $C_s$  point group. Furthermore, the analytical harmonic vibrational modes have been calculated in order to ensure that the optimized structures correspond to minima on the potential energy surface. The total energy for the *syn*- and *anti*-form, including zero-point corrections, are found to be  $-673.44774$  and  $-673.448048$  hartree,

respectively. Therefore, at this level of theory the *anti*-form isomer was found to be more stable than the *syn*-form by  $808.65 \text{ J mol}^{-1}$ .

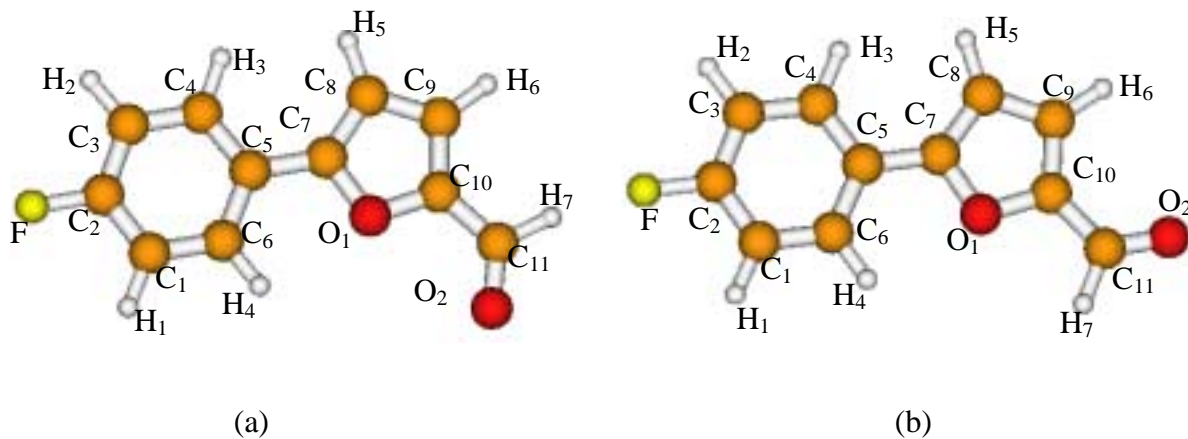


Fig. 5.7. Structural formulas of the two isomers of 5-(4-fluorophenyl)-furan-2-carbaldehyde: *syn*-form isomer (a), *anti*-form isomer (b).

From solid state sample only strong fluorescence could be observed for the visible excitation wavelength. Therefore, near IR excitation was necessary to obtain Raman spectra. FT-Raman spectra of the polycrystalline sample and 1M 5-(4FP)-F-2C ethanol solution are presented in Figs. 5.8a and 5.8b, respectively.

It is known that furfural [144] and its derivative [145] have also two rotational isomers determined by the rotation of the (CHO) group. The infrared spectrum of furfural shows two peaks at  $1675$  and  $1690 \text{ cm}^{-1}$  assigned to the C=O stretching vibration, conjugation keeping the C=O in the plane of the ring. From microwave and far infrared studies [146] it was found that, in the vapor phase, the furfural molecule is planar and both rotamers co-exist, the *anti*-form isomer being more stable than the *syn*-form isomer by  $8.36 \text{ kJ mol}^{-1}$ . A similar situation was observed for 5-substituted furfural.

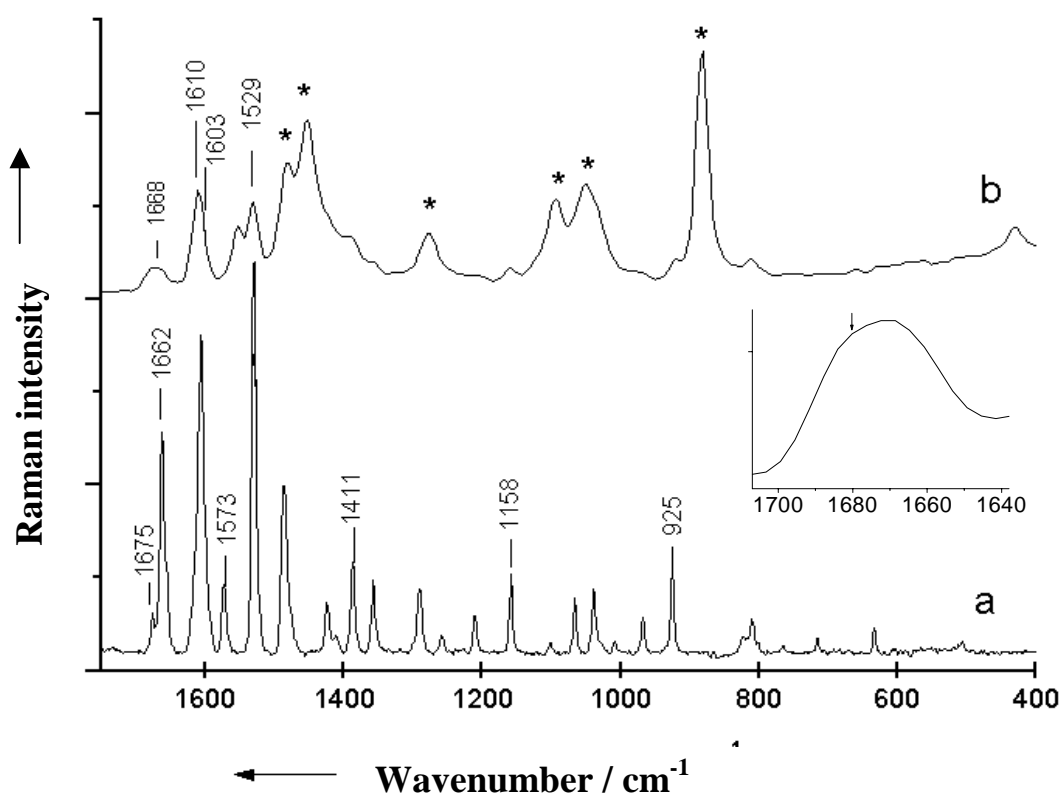


Fig. 5.8. FT-Raman spectra of polycrystalline 5-(4-fluor-phenyl)-furan-2-carbaldehyde (a), and 1M ethanol solution at pH 1 (b). \*: denotes the alcohol bands. Insert shows the band at  $1668\text{ cm}^{-1}$  from spectrum (b) enlarged.

The observed bands in infrared, FT-Raman and SER spectra of 5-(4FP)-F-2C together with the calculated wavenumbers for both rotational isomers and the tentative assignment of the vibrational modes are summarized in Table 5.4. The assignment was accomplished mainly by comparison with related molecules [89, 144, 147] and using the wavenumbers (unscaled values) and intensities as obtained by the BPW91 method. A strict comparison between the experimental and calculated wavenumbers and intensities is not possible in this case because the experimental data were obtained for a crystalline sample, whereas the theoretical calculations have been performed for the gas phase. It is well known that the calculated wavenumbers are obtained applying a harmonic approximation, whereas the experimental wavenumbers are of anharmonic nature. Nevertheless, as revealed by Fig. 5.9 and Table 5.4, the quality of the quantum chemical results at the present theoretical level is sufficient for the assignment of the experimental data.

Table 5.4. Experimental (infrared and FT-Raman) and calculated wavenumbers ( $\text{cm}^{-1}$ ) (*anti/syn* forms) of 5-(4-fluor-phenyl)-furan-2-carbaldehyde with the tentative assignment.

Experimental		Theoretical	Vibrational assignment
IR	Raman	Calc. <sup>a</sup> <i>anti/syn</i>	
	151w	124/128	C=O wagging (COH)
	199w	203/177	C <sub>10</sub> C <sub>11</sub> def.
	300vw	273/302	C <sub>4</sub> C <sub>5</sub> C <sub>7</sub> bend.
	310w	321/329	ring 1 <sup>b</sup> + ring 2 <sup>c</sup> out-of-plane def.
	386vw	365/371	C-F bend. + C <sub>5,7,8</sub> bend.
510m	507vw	501/495	ring 1 out-of-plane def.
604w	604vw	610/625	C <sub>1,2,3</sub> bend.
635vw	634w	628/653	C <sub>2,1,6</sub> bend. + C <sub>3,4,5</sub> bend.
668m	716w	700/694	ring 1 out-of-plane def.
765m	764vw	768/760	C-H wagging (ring 2)
787m	802sh	788/787	C-H wagging (ring 1)
804w	809w	807/806	C <sub>4,5,6</sub> bend.
833m	823sh	816/817	C-H wagging (ring 1)
879vw	866vw	855/838	C-H twist (ring 2)
925w	925m	910/908	C-H twist (ring 1)
967m	968w	961/951	C <sub>9,10</sub> O <sub>1</sub> bend.
1009sh	1008vw	1001/1001	C <sub>1,2,3</sub> bend. + C <sub>4,5,6</sub> bend.
1038m	1039m	1025/1032	C-H bend. (ring 2)
1066vw	1066m	1059/1058	C <sub>5,7</sub> O <sub>1</sub> str.
1102m	1102vw	1101/1100	C-H bend. (ring 1)
1159m	1158m	1153/1153	
1212sh	1211mw	1211/1214	C-H rock. (ring 2)
1227m	1220vw	1216/1239	C-F str. + C-H bend. (ring 1)
1260m	1258w	1266/1282	C <sub>7</sub> O <sub>1</sub> C <sub>10</sub> str.
1291w	1290m	1293/1294	C-H rock. (ring 1)

(Table 5.4. continued)

Experimental		Theoretical	Vibrational assignment
IR	Raman	Calc. <sup>a</sup> <i>anti/syn</i>	
1357w	1357m	1366/1352	C-H bend. (COH) + C <sub>5,7</sub> str.
1385w	1387m	1388/1388	
1410w	1411sh	1417/1417	C-H bend. (COH) + CCC str. (ring 1)
1423m	1424w	1444/1450	
1487vs	1485s	1470/1473	CCC str. (ring 2) + C <sub>5,7</sub> , C <sub>10,11</sub> str.
1528vw	1529vs	1517/1516	C=C str. (ring 2)
1575w	1573m	1559/1554	C=C str. (ring 1)
1605m	1606vs	1604/1603	
1670sh	1662s	1679/1682	C=O str. (COH) <i>anti</i> -form
1678vs	1675sh		C=O str. (COH) <i>syn</i> -form
2853w	2854m	2834/2815	C-H str. (COH)
3099w	3054sh	3120/3119	C-H str. (ring 1)
	3080m	3140/3140	
3112w	3094sh	3183/3175	C-H str. (ring 2)
	3116w	3198/3191	

<sup>a</sup>BPW91/6-311+G<sup>\*</sup>; ring 1<sup>b</sup>-phenyl ring, ring 2<sup>c</sup>-furan ring.

The crystalline 5-(4FP)-F-2C contains both isomers, identified by the presence of two bands given by the C=O stretching vibrations, at 1662 and 1675 cm<sup>-1</sup> in the Raman spectrum and at 1670 and 1678 cm<sup>-1</sup> in the infrared spectrum. The assignment of these bands to the corresponding rotamer has been made with the help of theoretical calculations. The band at 1662 cm<sup>-1</sup> (calc. 1679 cm<sup>-1</sup>) is specific to the *anti*-form isomer, while the band at 1675 cm<sup>-1</sup> (calc. 1682 cm<sup>-1</sup>) corresponds to the *syn*-form isomer. Comparing the intensities of these two bands we assume that the *anti*-form is the preponderant rotamer in the solid state sample [148].



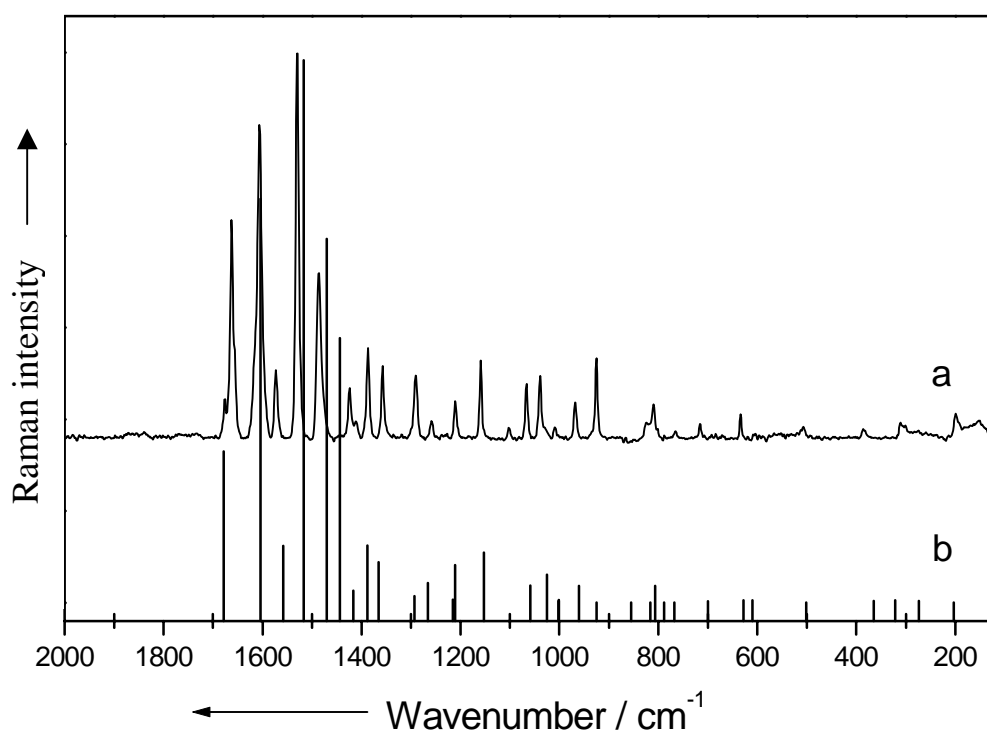


Fig. 5.9. FT-Raman spectrum (a) and the calculated Raman wavenumbers (b) of 5-(4-fluor-phenyl)-furan-2-carbaldehyde.

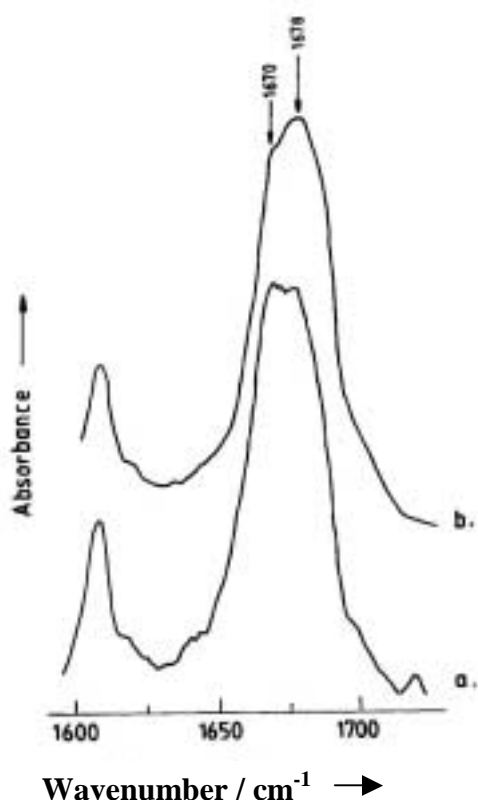


Fig. 5.10. The 1600-1700  $\text{cm}^{-1}$  spectral region of the infrared spectrum of 5-(4-fluor-phenyl)-furan-2-carbaldehyde recorded for two different temperatures: 148 K (a), 298 K (b).

Temperature dependent studies provide additional information concerning the most stable rotamer. The spectral region, corresponding to the C=O stretching vibration, in the infrared spectrum of 5-(4FP)-F-2C recorded at two different temperatures, 148 K and 298 K, respectively is shown in Figs. 5.10a and 5.10b. The intensity of the band at  $1670\text{ cm}^{-1}$ , specific to the *anti*-form isomer, decreases as the temperature increases, and confirms the results obtained from theoretical calculations that this isomer is the more stable one [148].

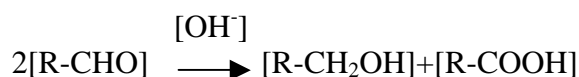
In the Raman spectrum of 1M ethanol solution of 5-(4FP)-F-2C at pH value of 1 (Fig. 5.8b) a weak broad and slightly asymmetric band at  $1668\text{ cm}^{-1}$  could be observed (see insert Fig. 5.8). Therefore, we assume that in solution both isomers are present, approximately in the same proportion. The assignment of other bands, specific to these isomers, only from the Raman spectrum of the polycrystalline sample is very difficult due to the complexity of the spectrum and the different concentration of the rotamers.

As can be observed from Fig. 5.9 and Table 5.4 the bands given by the phenyl and furan ring stretching modes are present in the  $1600\text{-}1400\text{ cm}^{-1}$  spectral region of the infrared and FT-Raman spectra of 5-(4FP)-F-2C. Most of the bands due to the in-plane C-C and C-H deformation vibrations of furan and phenyl rings can be observed in the  $1200\text{-}1000\text{ cm}^{-1}$  spectral range. The  $1000\text{-}400\text{ cm}^{-1}$  spectral region corresponds to out-of-plane ring and C-H deformation vibrations (see Table 5.4).

#### *Adsorption on the silver surface*

The FT-Raman spectrum of polycrystalline 5-(4FP)-F-2C and the SER spectrum in a silver colloid at pH value of 1 are presented in Figs. 5.11a and 5.11b. The assignment of the vibrational modes of the carbaldehyde derivative to the SERS bands at pH 1 is summarized in Table 5.5.

In an alkaline environment, according to *Cannizaro* reaction



two species can be obtained from aldehydes. Furthermore, in the presence of strong H-donor group, like a hydroxyl group, a dimer can be obtained by an interaction with the carbonyl oxygen atom. Therefore, the SER spectra of 5-(4FP)-F-2C have been analyzed only at an acidic pH values, due to the presence of many different species in an alkaline solution.

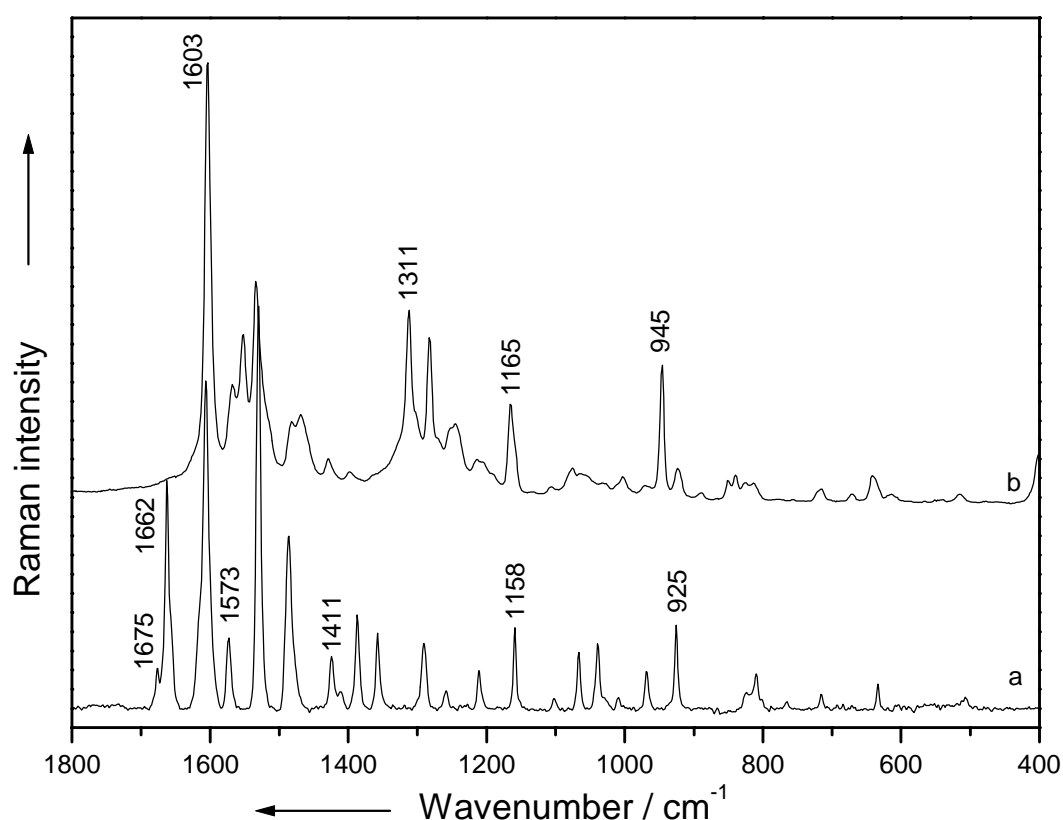


Fig. 5.11. FT-Raman spectrum of polycrystalline 5-(4-fluorophenyl)-furan-2-carbaldehyde (a), and SER spectrum of 5-(4-fluorophenyl)-furan-2-carbaldehyde in silver colloid at pH 1 (b).

The significant differences between the FT-Raman and SER spectra concerning the relative intensities, bandwidths and peak positions indicate an interaction between the metal and adsorbate, causing a quite different derivative of the molecule's polarizability tensor. The spectra of physisorbed molecules are practically the same as those of the free molecules, small differences might be observed only for the bandwidth [16, 17].

Table 5.5. Wavenumbers ( $\text{cm}^{-1}$ ) and assignment of the normal vibrational modes of 5-(4-fluor-phenyl)-furan-2-carbaldehyde to the SERS bands at pH 1.

Raman	SERS pH 1	Vibrational assignment
199w	190vw	$\text{C}_{10}\text{C}_{11}$ def. + Ag-O str.
386vw	401w	C-F bend. + $\text{C}_{5,7,8}$ bend.
507vw	515vw	ring 1 <sup>a</sup> out-of-plane def.
604vw	613w	$\text{C}_{1,2,3}$ bend.
634w	641w	$\text{C}_{2,1,6}$ bend. + $\text{C}_{3,4,5}$ bend.
716w	671vw	ring 1 out-of-plane def.
764vw	756vww	C-H wagging (ring 2 <sup>b</sup> )
802sh	779vww	C-H wagging (ring 1)
809w	813w	$\text{C}_{4,5,6}$ bend.
823sh	825w	C-H wagging (ring 1)
866vw	889vw	C-H twist (ring 2)
925m	923w	C-H twist (ring 1)
	945m	
968w	969vw	$\text{C}_{9,10}\text{O}_1$ bend.
1008vw	1002vw	$\text{C}_{1,2,3}$ bend. + $\text{C}_{4,5,6}$ bend.
1066m	1075w	$\text{C}_{5,7}\text{O}_1$ str.
1102vw	1105vw	C-H bend. (ring 1)
1158m	1165m	
1211mw	1213vw	C-H rock. (ring 2)
1220vw	1244m	C-F str. + C-H bend. (ring 1)
1258w	1252w	$\text{C}_7\text{O}_1\text{C}_{10}$ str.
1290m	1282m	C-H rock. (ring 1)
1357m	1311s	C-H bend. (COH) + $\text{C}_{5,7}$ str.
1387m	1398w	

(Table 5.5. continued)

Raman	SERS pH 1	Vibrational assignment
1411sh 1424w	1429w	C-H bend. (COH) + CCC str. (ring 1)
1485s	1468m 1482w	CCC str (ring 2) + C <sub>5,7</sub> , C <sub>10,11</sub> str.
1529vs	1533m	C=C str. (ring 2)
1573m 1606vs	1551m 1567m 1603vs	C=C str. (ring 1)
1662s 1675sh		C=O str. (COH) <i>anti</i> -form C=O str. (COH) <i>syn</i> -form

ring 1<sup>a</sup>-phenyl ring, ring 2<sup>b</sup>-furan ring.

When the molecules are chemisorbed on a silver surface an overlapping of the molecular and metal orbitals takes place causing dramatic changes in the position and relative intensities of the SERS bands [18, 122]. Comparing the SER spectrum of 5-(4FP)-F-2C to the corresponding conventional Raman spectrum (see Fig. 5.11 and Table 5.5) a shift of the peak positions can be observed. Therefore, we conclude that the 5-(4FP)-F-2C molecules are chemisorbed on the silver surface. In our case, it is difficult to differentiate between the contribution of the electromagnetic (EM) mechanism and charge-transfer (CT) effect, both contributing to the enhancement of the Raman signal. Additionally, it is possible to have some resonance Raman contribution to the total enhancement, because the excitation wavelength of 514.5 nm falls in the wing of the absorption band of the 5-(FP)-F-2C solution.

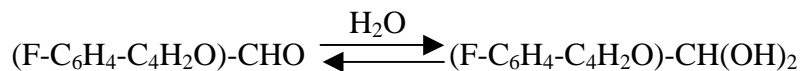
From Fig. 5.11 and Table 5.5 one clearly sees that in the SER spectrum at pH 1 the strong band due to the C=O stretching vibration of the *anti*-form isomer is absent, while in the Raman spectrum this band appears at 1662 cm<sup>-1</sup>. Mukherjee et al. [147] also observed the absence of the carbonyl stretching mode in the SER spectrum of the 2-isomer of formylpyridine, while the 3-isomer of formylpyridine showed an intense C=O stretching band. In the SER spectrum of 2-formylthiophene the band assigned to the

C=O stretching vibration is more intense than in the spectrum of 3-formylthiophene [147], determined by the dominance of the *syn*-form isomer in the surface adsorbed state. The absence or the extremely weak intensity of the carbonyl band in the SER spectra of 4- and 2-acetylpyridine isomers on a silver electrode has been explained [149] considering the hydration of the C=O bond of the adsorbed molecules in the presence of water.

According to the electromagnetic surface selection rules [33, 139, 140] a vibrational mode with its normal component mode perpendicular to the metal surface is likely to become more enhanced than the parallel one. Gao and Weaver [129] observed a significant red shift (more than  $10\text{ cm}^{-1}$ ) of the ring stretching bands of the flat adsorbed aromatic molecules relative to the bulk spectra, due to the backdonation of electron density from the metal to the  $\pi^*$  antibonding orbital of the ring system.

In the SER spectrum of 5-(FP)-F-2C at pH value of 1 (Fig. 5.11b) the bands at  $1603$  and  $1533\text{ cm}^{-1}$  attributed to the ring stretching modes and the band at  $1165\text{ cm}^{-1}$  assigned to the in-plane C-H deformation vibration are more enhanced than other modes and red shifted by approximately  $5\text{ cm}^{-1}$  in comparison to the bulk spectrum. At this pH value the bands at  $515$  and  $671\text{ cm}^{-1}$  due to out-of-plane deformation vibrations of the phenyl ring and the bands at  $825$ ,  $889$  and  $923\text{ cm}^{-1}$  given by the C-H wagging and C-H twisting modes are only weakly enhanced. Therefore, we suppose that the molecular planes of adsorbed molecules are vertical orientated or less tilted with respect to the silver surface. The strong bands at  $1311$  and  $945\text{ cm}^{-1}$  present in the SER spectrum cannot be observed in the bulk spectrum and are probably due to a surface complex formed by adsorption [150].

If both rotamers are present in the solution, as observed from the FT-Raman spectrum, and the molecular planes are orientated perpendicular or tilted on the metal surface, the C=O stretching mode of at least the *syn*-isomer should be present in the SER spectrum, since this bond is approximately perpendicular to silver surface. The absence of the bands corresponding to both isomers in the SER spectrum could be a consequence of the hydration of the C=O bond according to the following reaction:



The red shift by  $6\text{ cm}^{-1}$  and the enhancement of the band at  $1252\text{ cm}^{-1}$  that involves a vibration of the furan ring oxygen reveal that the 5-(FP)-F-2C molecules are chemisorbed on the silver surface *via* the lone pair electrons of the ring oxygen. Taking into account the weak enhancement of this band we suppose that the interaction between the oxygen atom and the metal surface is not so strong. This assumption is further supported by the very weak intensity of the band at about  $190\text{ cm}^{-1}$  assigned to the Ag-O stretching vibration [150].

### 5.2.3. Conclusion

Infrared, FT-Raman and surface-enhanced Raman spectroscopy were applied to the vibrational characterisation of 5-(4-fluor-phenyl)-furan-2-carbaldehyde. Theoretical calculations performed for both conformations of the sample revealed that the *anti*-form isomer is more stable than *syn*-form isomer by  $808.65\text{ J mol}^{-1}$ . It was found that the *anti*-form isomer is the preponderant species in solid state sample, while in solution both rotamers exist approximately in the same proportion. The changes in peak positions and relative intensities observed in the SER spectrum compared to the FT-Raman spectrum indicate the chemisorption of the 5-(4-fluor-phenyl)-furan-2-carbaldehyde molecules on the silver surface. The absence of the carbonyl band in the SER spectrum was explained by the hydration of the C=O bond in the surface adsorption state. The molecules are adsorbed on colloidal silver particles *via* the nonbonding electrons of the ring oxygen and are perpendicular orientated or at least tilted with respect to the silver surface.

### **5.3. Raman and surface-enhanced Raman spectroscopy as well as density functional theory calculations on some quinoline derivatives**

#### **5.3.1. Introduction**

The quinoline derivatives, isoquinoline and 4-methylquinoline are well known analytical reagents and biologically active compounds. Due to its broad biological activity, isoquinoline was used as a chelating, nonleaving ligand in *cis*-platinum(II) complexes [151]. Lepidine (4-methylquinoline) is known as the most mutagenic form of the quinoline derivatives examined so far [152].

The goal of this study was to perform analytical (FT-Raman spectroscopy) and theoretical (density functional theory calculations) investigations on isoquinoline and lepidine and to analyze the SER spectra in order to elucidate the adsorption behavior of these molecules on colloidal silver particles. Previous vibrational (Raman and infrared) and SERS studies of isoquinoline using Ag and Cu electrodes at different potentials have been reported in the literature [153, 154]. In the present work, the adsorption behavior of isoquinoline and lepidine on colloidal silver particles in acidic and alkaline environments has been discussed in order to establish whether or not the molecule-substrate interactions, and consequently, the SERS effect may be dependent on the pH value of the solutions.

#### **5.3.2. Results and discussion**

Isoquinoline and lepidine are colored liquid samples and present a large fluorescence for visible excitation wavelengths, therefore near IR excitation was necessary to obtain Raman spectra. The FT-Raman spectra of isoquinoline and lepidine together with the calculated unscaled Raman intensities are presented in Figs. 5.12 and 5.13, respectively.



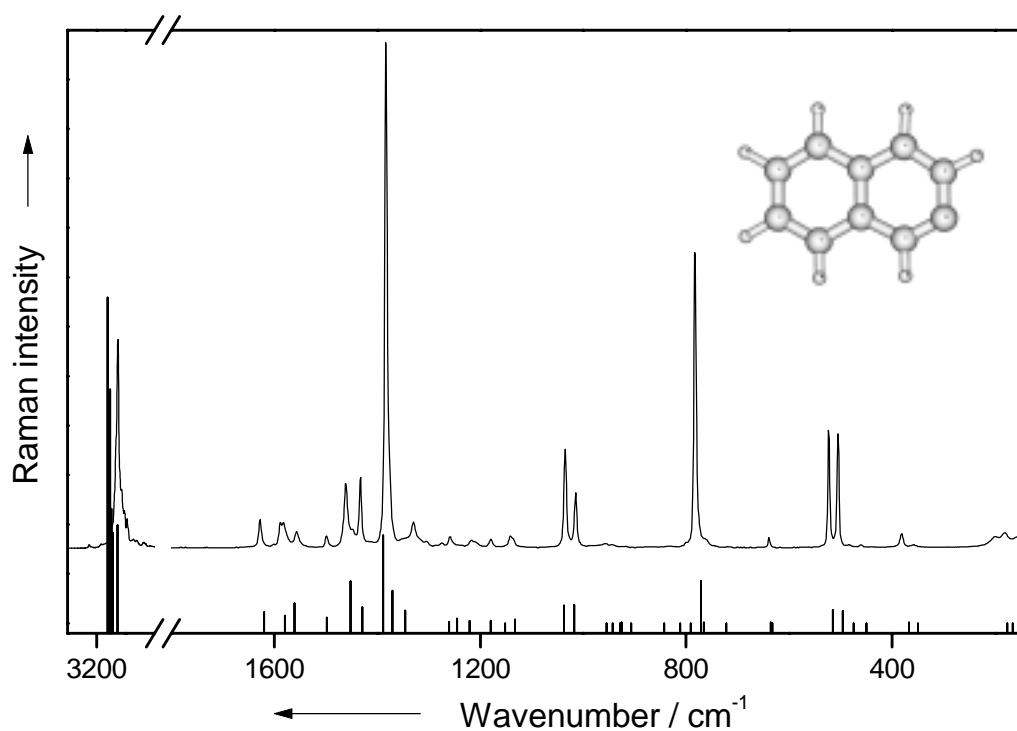


Fig. 5.12. FT-Raman spectrum (upper) and the calculated Raman wavenumbers (lower) of isoquinoline.

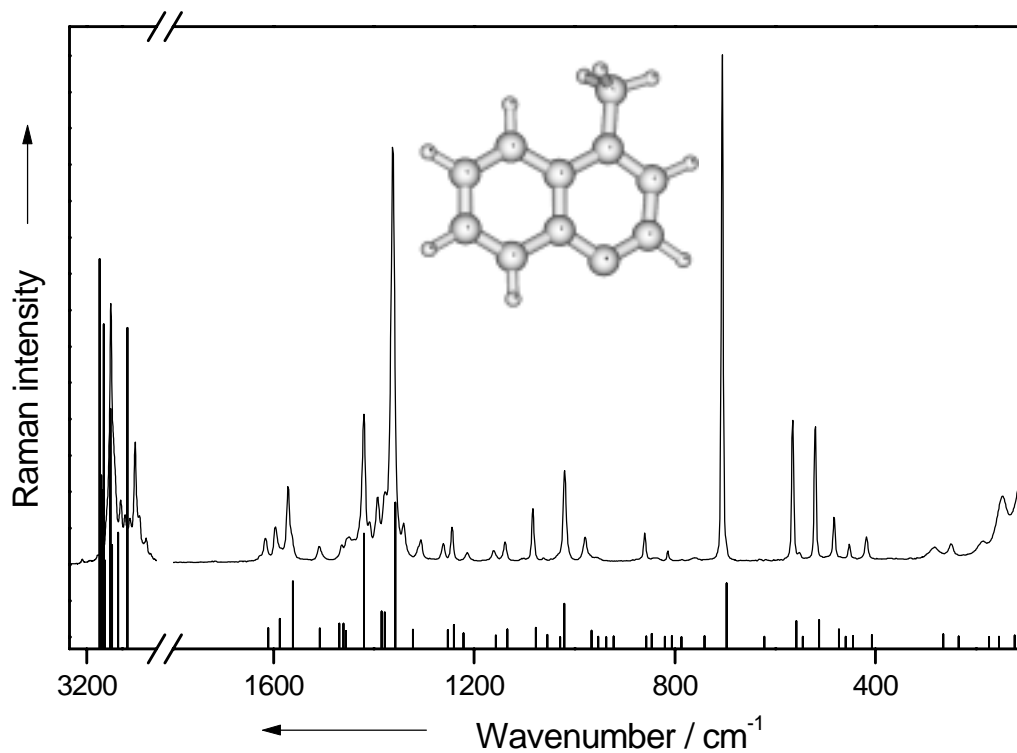


Fig. 5.13. FT-Raman spectrum (upper) and the calculated Raman wavenumbers (lower) of 4-methylquinoline.

The low concentrations ( $\sim 3.3 \cdot 10^{-4}$  M) required to obtain SER spectra are a proof of the enhancement of the Raman signal. In order to understand the enhancement we recorded the UV-visible absorption spectra of the silver colloid before and after addition of NaCl and also that of a mixture of the colloid and isoquinoline and lepidine after addition of NaCl. The results are shown in Fig. 5.14. The bands at 408 and 973 nm in Fig. 5.14a are characteristic for the plasmon resonance adsorption of silver spheres in water. After addition of NaCl these bands are shifted to 420 and 963 nm, respectively. When isoquinoline and lepidine are added to the sol the absorption peaks are weaker and broader and a new broad band around 800 nm appears, as can be seen clearly in Figs. 5.14c and 5.14d. This behavior is believed to be due to the formation of silver cluster particles [42]. The main absorption maximum located near the applied excitation wavelength (514.5 nm) shows that the colloidal aggregate state is moderate and it is consistent with the experimental fact that both samples show very good surface enhanced Raman spectra in silver sol.

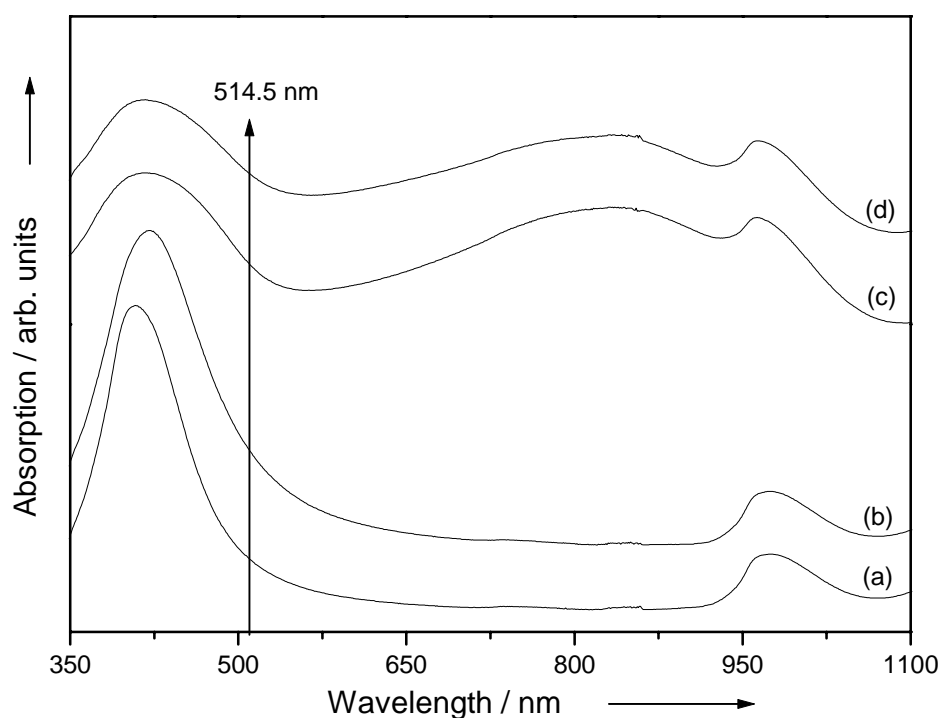


Fig. 5.14. Absorption spectra of a pure silver sol (a), with  $10^{-2}$  M NaCl added to the silver sol with a volume ratio 1:10 (b), with isoquinoline added to the activated silver sol (c), with 4-methylquinoline added to the activated silver sol (d).

The observed bands in the FT-Raman and SER spectra of isoquinoline and lepidine at pH values of 1 and 14 with the tentative assignment of the vibrational modes are summarized in Table 5.6. The assignment was made with the help of results obtained from DFT calculations and the work of Wait and McNerney [153]. Although the BPW91 method used the theoretical calculations do account for certain electronic correlation effects, the differences between the experimental and calculated results arise from the presence of systematic errors due to the anharmonicity and basis set deficiencies. Nevertheless, the degree of agreement between the experimental and calculated wavenumbers was reasonably good (see Figs. 5.12 and 5.13 and Table 5.6).

Table 5.6. FT-Raman (experimental and calculated) and SERS wavenumbers ( $\text{cm}^{-1}$ ) of isoquinoline and lepidine.

Raman				SERS				Vibrational assignment
Isoquinoline		Lepidine		Isoquinoline		Lepidine		
Exp.	Calc. <sup>a</sup>	Exp.	Calc. <sup>a</sup>	pH 1	pH 14	pH 1	pH 14	
		248w		247s	237w		245m	Ag-N str.
381w	367	418m	407	420m		417vw	416w	out-of-plane ring def.
504m	496	482m	473	509m		486w	485w	in-plane ring def.
523m	515	519m	512	525m	525m	524m	520m	
540sh		551sh	545	550m		567sh	565m	out-of-plane ring def.
639w	632	564m	558	647m	637w			
759sh	766			748w	739w	578m	579sh	in-plane ring def.
783s	771	705s	697	776m	787m	707s	708s	
800sh	791			819m	815w			
916vw	925	814w	820	919m		789w	808w	N-H bend. + C-H wagging
		860m	857			813w	866w	
956vw	928			976w	958m			in-plane ring def.

(Table 5.6. continued)

Raman				SERS				Vibrational assignment
Isoquinoline		Lepidine		Isoquinoline		Lepidine		
Exp.	Calc. <sup>a</sup>	Exp.	Calc. <sup>a</sup>	pH 1	pH 14	pH 1	pH 14	
		978m	966			982vw	984w	C-H wagging
1014m	1017	1019m	1020	1016m	1018m	1025m	1025m	ring breathing (benzene) (ring with N)
1035m	1037	1082m	1077	1036m	1039m	1101w	1108m	
1140w	1132	1137w	1134	1134w	1134m	1168m	1152w	C-H bend.
1179w	1180	1160w	1157	1172m	1180w	1183m	1175w	
1258w	1245	1244m	1240	1259m	1268sh	1250w	1242m	C-H rock. + C-C str.
1274w	1260	1261w	1253	1288w	1279w	1268w	1271m	
		1306m				1289sh	1290m	CCC str. + CNC str. + C <sub>9</sub> C <sub>10</sub> str.
1329m	1345	1340sh	1322	1359sh	1334w	1340sh	1345sh	
1383vs	1371	1362s	1357	1386s	1389s	1362s	1363s	CCC str.
1432m	1429	1391m	1385	1442m	1439m	1391sh	1389sh	C-H rock.
1461m	1452			1464sh	1465m			
		1419m	1420			1423m	1424w	C-H rock. + CCC str.
		1450sh	1455			1455sh	1440w	
		1464sh				1464w	1465sh	
1498w	1498	1507w	1508	1503m	1502vw	1509sh	1512sh	CCC str. + N-H bend.
						1530m		
1556m	1561	1565sh	1561	1552m	1557sh	1564s	1553sh	CCC str. + CNC str.
		1571m				1570sh	1578sh	
1582m	1579	1595m	1587	1585m	1579m	1595s	1599sh	CCC str. (ring with N)
1588m					1597sh			
1627m	1620	1616w	1611	1642sh	1631m	1609sh	1610s	CCC str. (benzene)
		2922m	2968			2923m	2921m	C-H str. (CH <sub>3</sub> )
3053s	3098	3063s	3068	3066m	3063s	3065mw	3068ms	C-H str.

<sup>a</sup>BPW91/6-311+G\*.

The bands that dominate the FT-Raman spectra of both samples (Figs. 5.12 and 5.13) are determined by the ring vibrations. Thus, the bands at  $504\text{ cm}^{-1}$  (calc.  $496\text{ cm}^{-1}$ ),  $523\text{ cm}^{-1}$  (calc.  $515\text{ cm}^{-1}$ ) and  $783\text{ cm}^{-1}$  (calc.  $771\text{ cm}^{-1}$ ) in the spectrum of isoquinoline and at  $519\text{ cm}^{-1}$  (calc.  $512\text{ cm}^{-1}$ ),  $564\text{ cm}^{-1}$  (calc.  $558\text{ cm}^{-1}$ ) and  $705\text{ cm}^{-1}$  (calc.  $697\text{ cm}^{-1}$ ) in the spectrum of lepidine, are due to ring deformation vibrations. The bands at  $1014\text{ cm}^{-1}$  (calc.  $1017\text{ cm}^{-1}$ ) and  $1035\text{ cm}^{-1}$  (calc.  $1037\text{ cm}^{-1}$ ) in the spectrum of isoquinoline and at  $1019\text{ cm}^{-1}$  (calc.  $1020\text{ cm}^{-1}$ ) and  $1082\text{ cm}^{-1}$  (calc.  $1077\text{ cm}^{-1}$ ) in the spectrum of lepidine can be assigned to ring breathing vibrations. The ring stretching modes give rise to the bands present in the range  $1600\text{-}1400\text{ cm}^{-1}$  in the Raman spectra of both samples. The other characteristic bands observed in both FT-Raman spectra are given by the C-H vibrations (see Table 5.6).

Comparing the FT-Raman spectra of isoquinoline and lepidine to the corresponding SER spectra differences in the position and relative intensities could be observed. The differences between the spectra indicate a strong interaction between the metal and adsorbate.

Comparing the SER spectra of isoquinoline at pH values 1 and 14 with the FT-Raman spectrum (see Figs. 5.15 and 5.12 and Table 5.6) a blue shift and an enhancement of the bands determined by the ring vibrations can be observed in both SER spectra. Thus, the bands that appear in the range  $1600\text{-}1400\text{ cm}^{-1}$  are shifted to higher wavenumbers in the SER spectra by  $3\text{-}15\text{ cm}^{-1}$ . The medium intense bands present in the FT-Raman spectrum at  $504$ ,  $523$ ,  $783$ ,  $1014$  and  $1035\text{ cm}^{-1}$  are enhanced and shifted to  $509$ ,  $525$ ,  $776$ ,  $1016$  and  $1036\text{ cm}^{-1}$  in the SER spectrum at pH 1 and to  $525$ ,  $787$ ,  $1018$  and  $1039\text{ cm}^{-1}$  in the SER spectrum at pH 14, respectively. The other bands present in the Raman spectrum of isoquinoline also show corresponding shifted bands in the SER spectra. Additionally, the appearance of a new band at about  $242\text{ cm}^{-1}$  in both SER spectra, characteristic of an Ag-N stretching mode, suggests a chemical interaction between the silver substrate and the lone-pair electrons of the nitrogen. Therefore, we assume that the isoquinoline molecules are chemisorbed on the silver surface through the nonbonding electrons of the nitrogen.

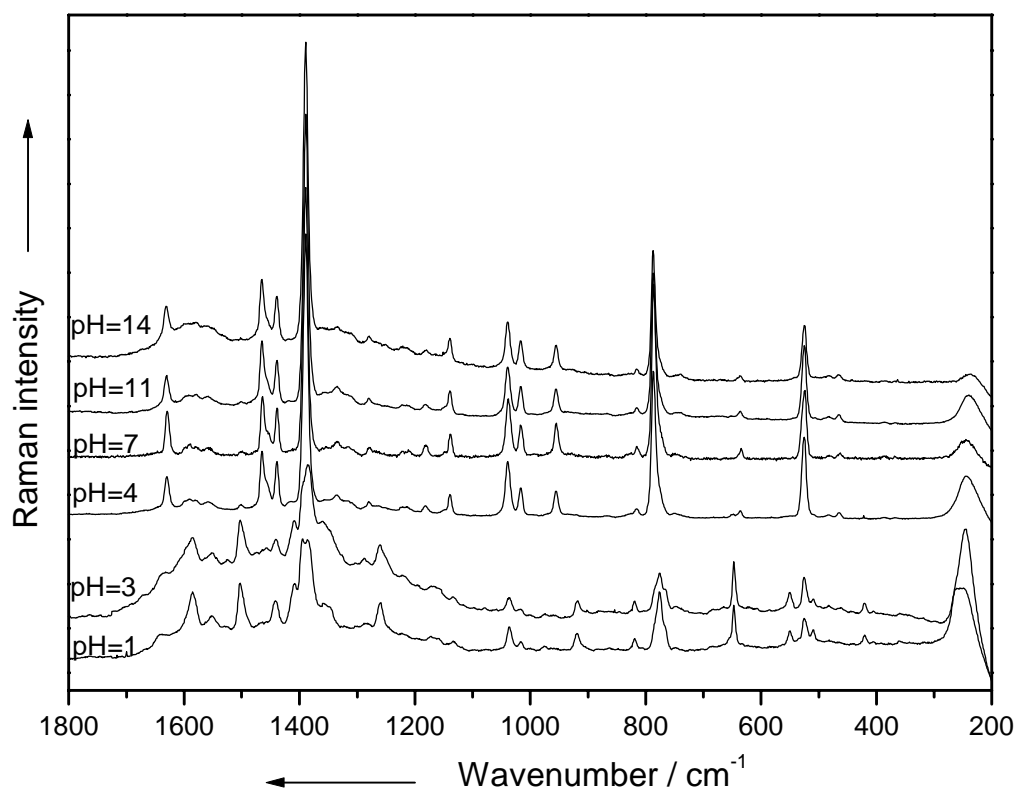


Fig. 5.15. SER spectra of isoquinoline in silver colloid recorded for different pH values as indicated.

Comparing the SER spectra of lepidine at pH 1 and 14 with the corresponding FT-Raman spectrum (see Figs. 5.16 and 5.13 and Table 5. 6) different changes can be observed. In the SER spectrum at pH 1 the bands that appear in the range between 1600 and 1400  $\text{cm}^{-1}$  are shifted to lower wavenumbers by 2-6  $\text{cm}^{-1}$ , while in the SER spectrum at pH 14 these bands are shifted to higher wavenumbers by 1-5  $\text{cm}^{-1}$ . The medium intense bands present in the FT-Raman spectrum at 519, 564, 705, 1019 and 1082  $\text{cm}^{-1}$  appear only weakly enhanced at 524, 578, 707, 1025 and 1101  $\text{cm}^{-1}$  in the SER spectrum at pH 1 and at 520, 579, 708, 1025 and 1108  $\text{cm}^{-1}$  in the SER spectrum at pH 14, respectively. In the case of lepidine, the band caused by the Ag-N stretching vibration can be only seen in the SER spectrum at pH 14, but significant changes in the relative intensities compared to the normal Raman spectrum can be observed in both SER spectra. The behavior of the adsorbed lepidine molecules denotes a partial chemisorption on the silver surface through the nonbonding electrons not only from the

nitrogen but also from the ring. In this case, it is also very difficult to separate the two mechanisms of Raman enhancement. However, it can be noted that the charge-transfer (CT) effect has a dominant contribution.

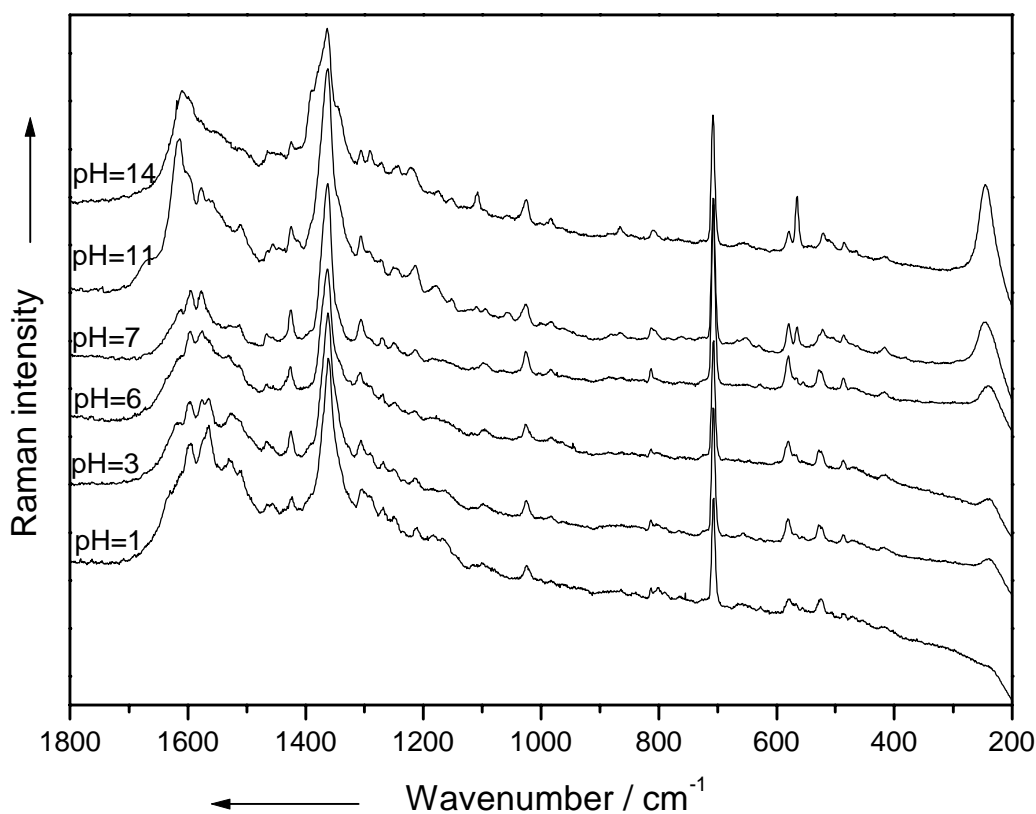


Fig. 5.16. SER spectra of 4-methylquinoline in silver colloid at different pH values as indicated.

SER spectra have been widely used to probe the orientation of adsorbed molecules with respect to the metal surface [155]. In deriving such orientational information, one makes use of the surface selection rules for roughened surface [33, 139, 140]. In particular, the surface geometry of compounds which have a planar structure can be determined from the relative magnitude of the intensity of the C-H stretching bands in their SER spectra [33]. A significant red shift ( $\sim 25 \text{ cm}^{-1}$ ) of the ring bands of the flat adsorbed substituted benzene derivatives relative to the bulk spectra was observed, due to the backdonation of the electron density from the  $\pi^*$  antibonding orbitals [129]. A similar phenomenon

was observed in the case of pyridine [156]. All these considerations can be extended to the molecules studied here.

Comparing the SER spectra of isoquinoline and lepidine at different pH values (Figs. 5.15 and 5.16) significant changes can be observed. Variations in SER spectra with a change of the pH are usually attributed either to a change in orientation of the adsorbed molecule with respect to the metal surface or to a change in its chemical nature [157].

From Fig. 5.15 one can notice the different behavior of the adsorbed isoquinoline molecules on the silver surface in acidic and alkaline environment. In the SER spectrum of isoquinoline at pH 14 a blue shift by  $4\text{ cm}^{-1}$  of the bands from  $1018$  and  $1039\text{ cm}^{-1}$ , assigned to the ring breathing modes, can be observed. The in-plane ring deformation vibrations are enhanced and shifted to higher wavenumbers from  $523$ ,  $783$ ,  $956\text{ cm}^{-1}$  to  $525$ ,  $787$  and  $958\text{ cm}^{-1}$ , respectively, while the out-of-plane ring and C-H deformation vibrations are only weakly enhanced or disappear in the SER spectrum. The weak enhancement of the bands determined by the CCC stretching vibration of the benzene ring might be a consequence of the relatively large distance between the ring and metal surface. Taking into account the characteristics of the SER spectra at pH values higher than 4 we assume that the adsorbed isoquinoline molecules are standing up on the surface. Furthermore, the presence of the enhanced band at  $3063\text{ cm}^{-1}$  due to the C-H stretching vibration confirms this assumption [158].

In spite of the differences between the SER spectra at pH 14 and 1, the bands due to the ring breathing modes are also shifted to higher wavenumbers from  $1014$  and  $1035\text{ cm}^{-1}$  to  $1016$  and  $1036\text{ cm}^{-1}$ , respectively in the SER spectrum of isoquinoline at pH 1. At this pH value out-of-plane ring and C-H deformation vibrations are enhanced and blue shifted from  $381$ ,  $540$ ,  $639$  and  $916\text{ cm}^{-1}$  to  $420$ ,  $550$ ,  $647$  and  $919\text{ cm}^{-1}$ , respectively, while the intensity of the band given by the C-H stretching vibration is very weak. In this spectrum the CCC stretching vibrations of the benzene ring are enhanced. We assume that the changes between the SER spectra at different pH values reveal a reorientation of the adsorbed molecules with respect to the metal surface, the molecules being tilted orientated on the surface at pH values lower than 4 [158].



In the SER spectra of lepidine at acidic pH ( $\text{pH} \leq 6$ ), two new bands at 789 and 1530  $\text{cm}^{-1}$  can be observed (Fig. 5.16). These bands are not present in the Raman spectrum of lepidine and we suppose that they are due to the N-H deformation vibrations [38]. Taking into account the presence of these new bands and the disappearance of the band at 245  $\text{cm}^{-1}$  given by the Ag-N stretching vibration we assume that the lepidine molecules are protonated in acidic environment ( $\text{pK}_a = 5.67$ ). The in-plane ring deformation vibrations are blue shifted from 482, 519 and 705  $\text{cm}^{-1}$  to 486, 524 and 707  $\text{cm}^{-1}$ , respectively and are enhanced, while the intensity of the band determined by the C-H stretching vibration is weak in the SER spectrum at these pH values. The bands at 1019 and 1082  $\text{cm}^{-1}$ , assigned in the Raman spectrum of the lepidine to the ring breathing modes, are shifted to higher wavenumbers to 1025 and 1101  $\text{cm}^{-1}$ , respectively. The features of the SER spectra at acidic pH values gives evidence for the partial chemisorption of the protonated lepidine molecules *via* the  $\pi^*$  electrons of the ring, and their not perfectly parallel orientation with respect to the silver surface. This assumption is confirmed by the red shift of 1-7  $\text{cm}^{-1}$  of the bands attributed to CCC ring stretching vibrations and the weak enhancement of the ring breathing modes.

Comparing the SER spectra of lepidine at alkaline pH values with the corresponding normal Raman spectrum, a blue shift by 3-20  $\text{cm}^{-1}$  and an enhancement of the bands due to the in-plane ring and C-H deformation and to the ring breathing vibrations can be observed. The bands assigned to CCC and C-H stretching vibrations are also enhanced at these pH values. The characteristics of the SER spectra at alkaline pH values reveal a partial chemisorption of lepidine molecules on the silver surface *via* the nonbonding electrons of the nitrogen, the band at 247  $\text{cm}^{-1}$  proofs this assumption. The weak enhancement of the bands assigned to the stretching vibrations of the benzene ring can be due to the relatively large distance between the ring and the metal surface. Additionally, the enhancement of the band at 565  $\text{cm}^{-1}$  due to the out-of-plane ring deformation vibration shows that the molecules are not perpendicular but more likely tilted with respect to the silver surface [158].

### 5.3.3. Conclusion

Experimental (FT-Raman and SER spectroscopy) and theoretical (DFT calculations) investigations have been performed on isoquinoline and lepidine molecules. It was found from SER spectra that the adsorbed molecules are strongly dependent on the pH conditions. The isoquinoline molecules are adsorbed *via* the nonbonding electrons of the nitrogen as neutral molecules, the variation in the SER spectra at different pH values being attributed to a change in orientation of the adsorbed molecules. In contrast, the lepidine molecules at acidic pH values are preferentially adsorbed on the silver surface in the protonated form, *via* the  $\pi^*$  electrons of the ring. At alkaline pH values the adsorbed molecules are tilted orientated to the metal surface and bonded to it *via* the lone-pair of the nitrogen.

# Chapter 6

---

## Summary/Zusammenfassung

---

### 6.1. Summary

In the present work, structural investigations on several coordination compounds have been performed by using infrared absorption and FT-Raman spectroscopy together with density functional theory calculations. Furthermore, Raman and surface-enhanced Raman spectroscopy in combination with theoretical calculations have been applied to the vibrational characterization of some biologically active molecules. The experimental results have been discussed in Chapters 4 and 5 and the conclusions drawn from these studies are presented in the next paragraphs.

In section 4.1 infrared and FT-Raman investigations combined with density functional theory calculations have been performed on  $\text{Ph}_2\text{P-N(H)SiMe}_3$  (**1a**) and  $\text{Ph}_3\text{P=NSiMe}_3$  (**1b**) and their corresponding metal complexes  $[(\text{Me}_3\text{Si})_2\text{N}\{\text{Zn}(\text{Ph}_2\text{P-NSiMe}_3)_2\}]_2$  (**2a**) and  $[\text{Li}(o\text{-C}_6\text{H}_4\text{PPh}_2\text{NSiMe}_3)]_2\cdot\text{Et}_2\text{O}$  (**2b**) in order to determine how the P–N bond length is influenced by the metal coordination. The coordination of the anionic  $[\text{Ph}_2\text{PNSiMe}_3]^-$  moiety to the zinc atoms results in a shortening of the P–N bond length,

while the *ortho*-metallation of the iminophosphorane and the imino group metal side-arm donation causes a P–N bond lengthening. In the infrared and Raman spectra of both compounds shifts to higher wavenumbers of the P–N stretching bands were observed. The shift towards higher wavenumbers of the P–N stretching band observed in both infrared and Raman spectra of the zinc compound further supports the assumption derived from X-ray diffraction analysis that a partial P=N double bond is formed in the coordination compound. On the other hand, the shift to higher wavenumbers of the P=N stretching band observed in the spectra of the organolithium compound clearly evidences the coordination of the iminophosphorane units to the metal centre through the nitrogen donor atom, and demonstrates that the reduced mass is responsible for this shift. The agreement between the theoretical and experimental values of the structural parameters and the calculated and observed vibrational modes indicates that the Lewis-basic imido nitrogen atom is involved in coordination both in the solid state, as well as in the gas phase.

In subsection 4.2. FT-Raman and infrared spectroscopy together with density functional theory calculations have been applied to the vibrational characterization of some new hexacoordinated silicon(IV) and germanium(IV) complexes with three symmetrical bidentate oxalato(2-) ligands. Kinetic investigations of the hydrolysis of two compounds, one with silicon and another one with germanium, have been performed, and it was found out that the hydrolysis reaction occurs only for the silicon compound. The hydrolysis rate constants at room temperature and at different pH values have also been determined, the fastest reaction taking place for acidic pH.

In section 4.3 infrared absorption and FT-Raman spectroscopy in conjunction with density functional theory calculations have been successfully applied to the vibrational characterization of the hexacoordinated silicon(IV) complexes with three unsymmetrical bidentate ligands of the hydroximato(2-) type and to the elucidation of the solid state conformational structures. A close analysis of the spectra of the geometrical isomers revealed that the *fac*-isomers display band shifting and a larger band splitting in their spectra compared to the *mer*-isomers.

Experimental (infrared and Raman spectroscopy) and theoretical (HF and DFT calculations) investigations have been performed on 10-isopropyl-10H-phenothiazine-5-oxide and were presented in section 5.1. SER spectra in activated silver colloids at different pH values were recorded and compared to the normal Raman spectrum. Having in view the shifts of the SERS bands ( $\Delta\nu \leq 5 \text{ cm}^{-1}$ ) in comparison to the corresponding Raman bands and the presence of the band given by the metal-molecule stretching vibration at all pH values the partial chemisorption of the molecules on the silver surface *via* the nonbonding electrons of the oxygen atom was assumed. The significant contribution of the electromagnetic mechanism to the overall SERS enhancement has been confirmed by the lack of a broad band in the long-wavelength region of the absorption spectrum of the colloid with added adsorbate. The changes observed in the SER spectra measured for different pH values were attributed to the reorientation of the adsorbed molecules with respect to the silver surface.

In section 5.2 infrared, FT-Raman and surface-enhanced Raman spectroscopy have been applied to the vibrational characterization of 5-(4-fluor-phenyl)-furan-2-carbaldehyde. Density functional theory calculations performed for both sample conformations revealed that the *anti*-form isomer is more stable than *syn*-form isomer by  $808.65 \text{ J mol}^{-1}$ . In solid state the *anti*-form isomer is the preponderant species, while in solution both rotamers exist approximately in the same proportion. The changes in peak positions and relative intensities found in the SER spectrum compared to the FT-Raman spectrum indicate the chemisorption of the 5-(4-fluor-phenyl)-furan-2-carbaldehyde molecules on the silver surface. The absence of the carbonyl band in the SER spectrum was explained by the hydration of the C=O bond in the surface adsorption state. The molecules are adsorbed on colloidal silver particles *via* the nonbonding electrons of the ring oxygen and are orientated perpendicular or at least tilted with respect to the silver surface.

In section 5.3 the quinoline derivatives, isoquinoline and lepidine have been investigated using FT-Raman spectroscopy together with DFT calculations. SER spectra at different pH values have been also recorded and their close analysis reveals the strong dependence of the adsorbed molecules with the pH conditions.

The isoquinoline molecules are adsorbed *via* the non-bonding electrons of the nitrogen as neutral molecules, the variation in the SER spectra measured for different pH values being attributed to a change in orientation of the adsorbed molecules. In contrast, the lepidine molecules at acidic pH values are preferentially adsorbed on the silver surface in the protonated form, *via* the  $\pi^*$  electrons of the ring. At alkaline pH values the adsorbed molecules are tilted orientated to the metal surface and bonded to it *via* the lone-pair of the nitrogen.

## 6.2. Zusammenfassung

In der vorliegenden Arbeit wurden strukturelle Untersuchungen einiger Koordinationsverbindungen mittels IR- und Raman-Spektroskopie in Kombination mit quantenchemischen Rechnungen basierend auf der Dichtefunktionaltheorie durchgeführt. Raman- und SERS-Spektroskopie in Kombination mit theoretischen Berechnungen wurden zur Schwingungscharakterisierung einiger biologisch aktiver Moleküle angewandt. Die experimentellen Ergebnisse wurden in den Kapiteln 4 und 5 dargestellt und sollen im folgenden kurz zusammengefasst werden.

In Kapitel 4.1 wurden Infrarot- und FT-Raman-spektroskopische Untersuchungen in Verbindung mit Dichtefunktionaltheorieberechnungen an den Edukten  $\text{Ph}_2\text{P-N(H)SiMe}_3$  (**1a**) und  $\text{Ph}_3\text{P=NSiMe}_3$  (**1b**) und ihren entsprechenden Metallkomplexen  $[(\text{Me}_3\text{Si})_2\text{NZnPh}_2\text{PNSiMe}_3]_2$  (**2a**) und  $[\text{Li}(o\text{-C}_6\text{H}_4\text{PPH}_2\text{NSiMe}_3)]_2\cdot\text{EtO}$  (**2b**) durchgeführt, um so den Einfluss der Koordination zu einem Metallzentrum auf die P-N-Bindungslänge festzustellen. Bei einer Koordination der Phosphanylamineinheiten zum Zinkatom tritt eine Verkürzung der P-N Bindung ein, während Ortho-Metallierung der Iminophosphoraneinheiten und *metal side-arm donation* der Imino-Gruppen eine Verlängerung der P-N-Bindung verursachen. In den Infrarot- und Raman-Spektren beider Komplexverbindungen wurden Verschiebungen der P-N-Valenzschwingungen zu höheren Wellenzahlen hin beobachtet. Die Verschiebung in Richtung höherer Wellenzahlen der P-N-Schwingung der Zinkverbindung steht in Einklang mit der Röntgenstrukturanalyse, die eine teilweise P=N Doppelbindung im Komplex zeigt. Andererseits beweist die Verschiebung der P=N Valenzschwingung von **2b** zu höheren Wellenzahlen, dass die Koordination der Iminophosphoraneinheiten zum Metallzentrum über das Stickstoffatom erfolgt und dass die Abnahme der reduzierten Masse ihre dominierende Ursache darstellt. Die Übereinstimmung zwischen den theoretischen und experimentellen Werten der strukturellen Parameter und der berechneten und beobach-

teten Schwingungsmoden zeigt, dass das Lewis-basische Imido-Stickstoffatom sowohl im Festkörper als auch in der Gasphase zur Koordination beiträgt.

FT-Raman- und Infrarot-Spektroskopie in Kombination mit Dichtefunktionaltheorieberechnungen wurden zur Schwingungscharakterisierung einiger neuer hexakoordinierten Silizium(IV)- und Germanium(IV)-Komplexe mit drei symmetrischen zweizähligen Oxalato(2-)-Liganden in Kapitel 4.2 herangezogen. Zudem wurden noch kinetische Untersuchungen der Hydrolyse zweier Silizium- bzw. Germanium-Komplexe durchgeführt und es konnte festgestellt werden, dass die Hydrolysereaktion nur im Fall des Siliziumkomplexes auftritt. Die Geschwindigkeitskonstanten wurden bei Raumtemperatur für unterschiedliche pH-Werte bestimmt. Somit konnte gezeigt werden, dass die Reaktion am schnellsten im Säuren abläuft.

In Kapitel 4.3 wurde die Infrarotabsorption- und FT-Raman-Spektroskopie in Verbindung mit DFT-Berechnungen zur Schwingungscharakterisierung hexakoordinierter Silizium(IV)-Komplexe mit drei antisymmetrischen zweizähligen Liganden vom Hydroximato(2-)-Typ angewandt, um die Konformation dieser Dianionen im Festkörper aufzuklären. Es konnte gezeigt werden, dass die *fac*-Isomere in ihren Spektren Bandverschiebungen und eine größere Bandenaufspaltung im Vergleich zu den Spektren der *mer*-Isomere aufweisen.

Kapitel 5.1 berichtet über experimentelle (IR- und Raman-Spektroskopie) und theoretische (HF- und DFT-Berechnungen) Untersuchungen an 10-Isopropyl-10H-Phenothiazin-5-Oxid. SER-Spektren dieses Moleküls wurden in aktivierten Silberkolloiden für unterschiedliche pH-Werte aufgenommen und mit herkömmlichen Raman-Spektren verglichen. Aufgrund von Verschiebungen der SERS-Banden im Vergleich zu den entsprechenden Raman-Banden (bis zu  $5\text{ cm}^{-1}$ ) und der Anwesenheit einer Metall-Molekülvalenzschwingung für alle pH-Werte lässt sich schließen, dass die untersuchten Moleküle auf der Silberoberfläche chemisorbiert sind. Die Bindung erfolgt über die freien Elektronen am Sauerstoffatom von 10-Isopropyl-10H-Phenothiazin-5-Oxid. Der bedeutende Beitrag der elektromagnetischen Mechanismus zur gesamten SERS-Verstärkung ist durch das Fehlen einer ausbreiten Bande in der langwelligen Re-



gion der Absorptionsspektren des Kolloids mit hinzugefügtem Adsorbat bestätigt worden. Die Änderungen, die in den SER-Spektren für unterschiedliche pH-Werte beobachtet wurden, lassen sich der Reorientierung der absorbierten Moleküle auf der Silberoberfläche zuordnen.

In Kapitel 5.3 wurden Infrarot-, FT-Raman- und Oberfläche-verstärkte Raman-Spektroskopie zur Schwingungscharakterisierung von 5-(4-Fluor-Phenyl)-Furan-2-Carbaldehyd angewandt. Die DFT-Berechnungen, die für beide Konformationen der Probe durchgeführt wurden, zeigten, dass das *anti*-Isomer um  $808,65 \text{ J mol}^{-1}$  stabiler als das *syn*-Isomer ist. Im Festkörper überwiegt das *anti*-Isomer, während in der Lösung beide Rotamere ungefähr zu gleichen Anteilen vorliegen. Die Änderungen der Wellenzahlpositionen und relativen Intensitäten der Banden, die im SER-Spektrum im Vergleich zum FT-Raman-Spektrum beobachtet werden, deuten auf die Chemisorption des 5-(4-Fluor-Phenyl)-Furan-2-Carbaldehyds auf der Silberoberfläche hin. Das Fehlen einer Carbonylbande im SER-Spektrum lässt sich durch die Hydratation der C=O-Bindung auf der Oberfläche erklären. Die Moleküle sind auf den kolloiden Silberpartikeln über die freien Elektronen des Ringsauerstoffs adsorbiert und sind senkrecht oder gekippt in Bezug auf die Silberoberfläche orientiert.

Experimentelle (FT-Raman und SER-Spektroskopie) und theoretische (DFT-Berechnungen) Untersuchungen von Isochinolin und Lepidin wurden in Kapitel 5.2 durchgeführt. Die SER-Spektren der absorbierten Moleküle sind stark vom pH-Wert abhängig. Die Isochinolinmoleküle sind über die freien Elektronen des Stickstoffatoms als neutrale Moleküle adsorbiert. Die Veränderung der SER-Spektren für verschiedene pH-Werte wird einer Änderung der Lage der absorbierten Moleküle zugeschrieben. Demgegenüber werden die Lepidinmoleküle für saure pH-Werte vorzugsweise auf der Silberoberfläche im protonierten Zustand über das  $\pi^*$ -Elektronenpaar des Ringes adsorbiert. Für basische pH-Werte sind die absorbierten Moleküle gekippt zur Metalloberfläche orientiert und über das freie Elektronenpaar des Stickstoffatoms gebunden.

## References

- [1] W. Herschel, *Phil. Trans. Roy. Soc.*, **90** (1800) 284.
- [2] P. W. Kruse, L. D. McGlauchlin, L. B. McQuistan, *Elements of Infrared Technology*, J. Wiley & Sons Inc. New York, 1962.
- [3] E. Lommel, *Wiedemanns Ann. d Phys.*, **3** (1878) 251.
- [4] A. G. Smekal, *Naturwissenschaften*, **11** (1923) 873.
- [5] H. A. Kramers, W. Heisenberg, *Z. Physik*, **31** (1925) 681.
- [6] E. Schrödinger, *Ann. Phys.*, **81** (1926) 109.
- [7] P. A. M. Dirac, *Proc. Roy. Soc. London*, **114 A** (1927) 710.
- [8] C. V. Raman, K. S. Krishnan, *Nature*, **121** (1928) 501.
- [9] G. Placzek, *Rygleigh Streuung und Ramaneffekt*, in: *Handbuch der Radiologie*, Vol. 6, G. Marx ed., Akad. Verlagsgesellschaft, Leipzig, 1934.
- [10] T. H. Maiman, *Nature*, **187** (1960) 433.
- [11] W. Kiefer, *Recent Techniques in Raman Spectroscopy*, in: *Advances in Infrared and Raman Spectroscopy*, Vol. 3, R. J. H. Clark, R. E. Hester eds., London, 1977.
- [12] K. Nakamoto *Infrared and Raman Spectra of Inorganic and Coordination Chemistry, Part A: Theory and Applications in Inorganic Chemistry*, Fifth Edition, John Wiley & Sons, Inc., New York, 1997.
- [13] L. A. Nafie, *Theory of Raman Scattering*, in *Handbook of Raman Spectroscopy*, I. R. Lewis, H. G. M. Edwards eds., Marcel Dekker Inc., New York, 2001.
- [14] R. G. Parr, W. Yang, *Density Functional Theory of Atoms and Molecules*, Oxford University Press, Oxford, 1989.
- [15] J. M. Seminario, P. Politzer, *Modern Density Functional Theory, a Tool of Chemistry*, Elsevier Science E. V. Amsterdam, 1995.
- [16] M. Moskovits, *Rev. Mod. Phys.*, **57** (1985) 783.
- [17] T. Vo-Dihn, *Trends in Analyt. Chem.*, **17** (1988) 557.
- [18] A. Champion, P. Kambhampati, *Chem. Soc. Rev.*, **27** (1998) 241.
- [19] T. M. Cotton, J.-H. Kim, G. D. Chumanov, *J. Raman Spectrosc.*, **22** (1991) 729.

## References

---

- [20] B. Schrader, *General Survey of Vibrational Spectroscopy*, in *Infrared and Raman Spectroscopy, Methods and Applications*, B. Schrader ed., VCH Weinheim, 1995.
- [21] T. Hirschfeld, B. Chase, *Appl. Spectrosc.*, **40** (1986) 133.
- [22] T. Hirschfeld, *Appl. Spectrosc.*, **30** (1976) 68.
- [23] T. Hirschfeld, E. R. Schildkraut, *Laser Raman Gas Diagnostics*, ed. M. Lapp, Academic Press, New York, 1974.
- [24] A. J. Barnes, *Fourier Transform Spectroscopy*, in *Vibrational Spectroscopy-Modern Trends*, A. J. Barnes and W. J. Orville-Thomas eds., Elsevier Scientific Publishing Company, Amsterdam, 1977.
- [25] R. J. Bell, *Introductory Fourier Transform Spectroscopy*, Academic Press, New York, 1972.
- [26] M. Fleischmann, P. J. Hendra, A. J. McQuillann, *Chem. Phys. Lett.*, **26** (1974) 163.
- [27] D. L. Jeanmaire, R. P. Van Duyne, *J. Electroanal. Chem.*, **84** (1977) 1.
- [28] M. G. Albrecht, J. A. Creighton, *J. Am. Chem. Soc.*, **99** (1977) 5215.
- [29] J. M. Sequaris, E. Koglin, *Anal. Chem.*, **321** (1985) 758.
- [30] M. Moskovits, *J. Chem. Phys.*, **79** (1982) 4408.
- [31] X. Gao, J. P. Davies, M. J. Weaver, *J. Phys. Chem.*, **94** (1990) 6858.
- [32] J. A. Creighton, *The Selection Rules for Surface Enhanced Raman Spectroscopy*, in *Spectroscopy of Surfaces*, R. H. Clark and R. Hester eds., John Wiley & Sons, 1988.
- [33] M. Moskovits, J. S. Suh, *J. Phys. Chem.*, **88** (1984) 5526.
- [34] D. A. Weitz, M. Moskovits, J. A. Creighton, *Chemistry and Structure at Interfaces, New Laser and Optical Techniques*, R. B. Hall and A. B. Ellis eds., VCH, Florida, 1986.
- [35] A. Otto, I. Mrozek, H. Grabhorn, W. Akermann, *J. Phys. Condens. Matter.*, **4** (1992) 1143.
- [36] A. Otto, *J. Raman Spectrosc.*, **22** (1991) 743.
- [37] D. A. Guzonas, D. E. Irish, G. F. Atkinson, *Langmuir*, **6** (1990) 1102.
- [38] A. Campion, J. E. Ivanecky, C. M. Child, M. Foster, *J. Am. Chem. Soc.*, **117** (1995) 11807.
- [39] P. Hildebrandt, M. Stockburger, *J. Phys. Chem.*, **88** (1984) 5935.
- [40] P. Hildebrandt, M. Stockburger, *J. Raman Spectrosc.*, **17** (1986) 55.

## References

---

- [41] T. Vo-Dinh, D. L. Stokes, G. D. Griffen, M. Volkan, U. J. Kim, M. I. Simon, *J. Raman Spectrosc.*, **30** (1999) 785.
- [42] J. A. Creighton, C. G. Blatchford, M. G. Albrecht, *Trans. Faraday Soc.*, **75** (1979) 790.
- [43] P. C. Lee, D. P. J. Meisel, *J. Phys. Chem.*, **86** (1982) 3391.
- [44] O. Siiman, H. Feilchenfeld, *J. Phys. Chem.*, **92** (1988) 453.
- [45] K. Suzan, A. Baiker, M. Meier, J. Wokaun, *J. Chem. Soc. Faraday Trans.*, **80** (1984) 1305.
- [46] G. Xue, J. Dong, M. Zhang, *Anal. Chem.*, **63** (1991) 2393.
- [47] A. Ruperez, J. J. Laserna, *Anal. Chim. Acta*, **291** (1994) 147.
- [48] J. J. Laserna, A. D. campiglia, J. D. Winefordner, *Anal. Chim. Acta*, **208** (1988) 21.
- [49] W. S. Sutherland, J. D. Winefordner, *J. Colloid Interface Sci.*, **148** (1988) 129.
- [50] S. E. Brandt, T. M. Cotton, *Physical Methods of Chem. Series*, 2-nd ed. J. Wiley, New York, 1993.
- [51] B. Foresman, *Ab initio Techniques in Chemistry: Interpretation and Visualization*, in *What Every Chemist Should Know About Computing*, Ed. M. L. Swift and T. J. Zielinski, ACS Books, Washington D. C., 1996.
- [52] A. Szabo, N. S. Ostlund, *Modern Quantum Chemistry*, Ed. McGraw-Hill, New York, 1982.
- [53] M. J. S. Dewar, C. H. Reynolds, *J. Comp. Chem.*, **2** (1986) 140.
- [54] J. J. P. Stewart, *J. Comp. Chem.*, **10** (1989) 221.
- [55] W. J. Hehre, L. Radom, P. v. R. Schleyer, J. A. Pople, *Ab initio Molecular Orbital Theory*, Wiley, New York, 1986.
- [56] M. J. Frisch, G. W. Trucks, H. B. Schlegel, G. E. Scuseria, M. A. Robb, J. R. Cheeseman, V. G. Zakrzewski, J. A. Jr. Montgomery, R. E. Stratmann, J. C. Burant, S. Dapprich, J. M. Millam, A. D. Daniels, K. N. Kudin, M. C. Strain, O. Farkas, J. Tomasi, V. Barone, M. Cossi, R. Cammi, B. Mennucci, C. Pomelli, C. Adamo, S. Clifford, J. Ochterski, G. A. Petersson, P. Y. Ayala, Q. Cui, K. Morokuma, D. K. Malick, A. D. Rabuck, K. Raghavachari, J. B. Foresman, J. Ciolowski, J. V. Ortiz, B. B. Stefanov, G. Liu, A. Liashenko, P. Piskorz, I. Komaromi, R. Gomperts, R. L. Martin, D. J. Fox, T. Keith, M. A. Al-Laham, C. Y. Peng, A.

## References

---

- Nanayakkara, C. Gonzales, M. Challacombe, P. M. W. Gill, B. Johnson, W. Chen, M. W. Wong, J. L. Andres, M. Head-Gordon, E. S. Repogle, J. A. Pople, *Gaussian 98, Revision A7*, Gaussian Inc.: Pittsburgh, PA 1998.
- [57] P. Hohenberg, W. Kohn, *Phys. Rev.*, **B 864** (1964) 136.
- [58] J. C. Slater, *Quantum Theory of Molecular and Solids. Vol 4: The Self-Consistent Field for Molecular and Solids*, Ed. McGraw-Hill, New York, 1974.
- [59] S. H. Vosko, L. Wilk, M. Nusair, *Canadian J. Phys.*, **58** (1980) 1200.
- [60] A. D. Becke, *Phys. Rev.*, **A 38** (1988) 3098.
- [61] C. Lee, W. Yang, R. G. Parr, *Phys. Rev.*, **B 37** (1988) 785.
- [62] A. D. Becke, *J. Chem. Phys.*, **98** (1993) 1372.
- [63] J. P. Perdew, Y. Wang, *Phys. Rev.*, **B 45** (1992) 13244.
- [64] J. B. Collins, P. v. R. Schleyer, J. S. Binkley, J. A. Pople, *J. Chem. Phys.*, **64** (1976) 5142.
- [65] J. S. Binkley, J. A. Pople, W. J. Hehre, *J. Amer. Chem. Soc.*, **102** (1980) 939.
- [66] M. S. Gordon, J. S. Binkley, J. A. Pople, W. J. Pietro, W. J. Hehre, *J. Amer. Chem. Soc.*, **104** (1982) 2797.
- [67] W. J. Pietro, M. M. Francl, W. J. Hehre, D. J. Defrees, J. A. Pople, J. S. Binkley, *J. Amer. Chem. Soc.*, **104** (1982) 5039.
- [68] A. D. McLean, G. S. Chandler, *J. Chem. Phys.*, **72** (1980) 5639.
- [69] R. Krishnan, J. S. Binkley, R. Seeger, J. A. Pople, *J. Chem. Phys.*, **72** (1980) 650.
- [70] G. A. Petersson, A. Bennett, T. G. Tensfeldt, M. A. Al-Laham, W. A. Shirley, J. Mantzaris, *J. Chem. Phys.*, **89** (1988) 2193.
- [71] G. A. Petersson, M. A. Al-Laham, *J. Chem. Phys.*, **94** (1991) 6081.
- [72] A. W. Johnson, *Ylides and imines of phosphorus*, Wiley Interscience, New York, 1993.
- [73] M. F. Lappert, P. P. Power, A. R. Sanger, R. C. Srivastava, *Metal and Metalloid Amides*, Ellis Horwood Ltd.; Chichester, U. K., 1980.
- [74] A. F. Cameroon, N. J. Hair, D. G. Morris, *Acta Crystallogr.*, **B30** (1974) 221.
- [75] V. J. Kaiser, H. Hartung, R. Richter, *Z. Anorg. Allg. Chem.*, **469** (1980) 188.
- [76] E. D. Jr. Morris, C. E. Nordman, *Inorg. Chem.*, **8** (1973) 1069.
- [77] R. Keat, L. Manoljovic-Muir, K. V. Muir, D. S. Rycroft, *J. Chem. Soc. Dalton Trans.*, (1981) 2192.

## References

---

- [78] S. Wingerter, M. Pfeiffer, F. Baier, T. Stey, D. Stalke, *Z. Anorg. Allg. Chem.*, **626**, (2000) 1121.
- [79] A. Steiner, D. Stalke, *Angew. Chem.*, **107** (1995) 1908; *Angew. Chem. Int. Ed. Engl.*, **34** (1995) 1752.
- [80] Reviews: (a) L. Mahalakshmi, D. Stalke, in: D. A. Atwood, H. W. Roesky (eds.), *Structure and Bonding-Group 13 Chemistry I*, **103** (2002) 85. (b) F. Baier, Z. Fei, H. Gornitzka, A. Murso, S. Neufeld, M. Pfeiffer, I. Rüdener, A. Steiner, T. Stey, D. Stalke, *J. Organomet. Chem.*, 2002, in press.
- [81] S. Wingerter, H. Gornitzka, R. Bertermann, S. K. Pandey, J. Rocha, D. Stalke, *Organometallics*, **19** (2000) 3890.
- [82] S. Wingerter, H. Gornitzka, G. Bertrand, D. Stalke, *Eur. J. Inorg. Chem.*, (1999) 173.
- [83] S. Wingerter, M. Pfeiffer, T. Stey, M. Bolboaca, W. Kiefer, V. Chandrasekhar, D. Stalke, *Organometallics*, **20** (2001) 2730.
- [84] H. Schmidbaur, A. Schier, S. Lautenschläger, J. Riede, G. Müller, *Organometallics*, **3** (1984) 1906.
- [85] M. T. Ashby, Z. Li, *Inorg. Chem.*, **31** (1992) 1321.
- [86] G. Trinquier, M. T. Ashby, *Inorg. Chem.*, **33** (1994) 1306.
- [87] R. G. Goel and W. O. Ogini, *Inorg. Chem.*, **16** (1977) 1968.
- [88] M. Bolboaca, A. Murso, T. Stey, D. Stalke, W. Kiefer, in preparation.
- [89] F. R. Dollish, W. G. Fateley, F. F. Bentley, *Characteristic Raman Frequencies of Organic Compounds*, John Wiley & Sons, Inc. New York, 1973.
- [90] Z. K. Ismail, R. H. Hauge, J. L. Margrave, *J. Chem. Phys.* **57** (1972) 5137.
- [91] R. Píkl, F. Duschek, C. Fickert, R. Finsterer, W. Kiefer, *Vib. Spectrosc.*, **14** (1997) 189.
- [92] N. B. Colthup, L. H. Daly, S. E. Wiberley, *Introduction to Infrared and Raman Spectroscopy*, Academic Press, New York and London, 1964.
- [93] O. Seiler, C. Burschka, M. Penka, R. Tacke, *Angew. Chem.*, in press.
- [94] R. Tacke, M. Penka, F. Popp, I. Richter, *Eur. J. Inorg. Chem.*, in press.
- [95] K. Krishnamurty, G. M. Harris, *Chem. Rev.*, **61** (1961) 213.
- [96] G. A. Jeffrey, G. S. Parry, *J. Chem. Soc.*, (1952) 4864.
- [97] R. E. Hester, R. A. Plane, *Inorg. Chem.*, **3(4)** (1964) 513.

## References

---

- [98] J. Fujita, A. Martell, K. Nakamoto, *J. Chem. Phys.*, **36**(2) (1962) 324.
- [99] P. A. W. Dean, D. F. Evans, R. F. Phillips, *J. Chem. Soc.*, **A** (1969) 363.
- [100] E. C. Gruen, R. A. Plane, *Inorg. Chem.*, **6**(6) (1967) 1123.
- [101] O. Svenson, M. Josefson, F. W. Langkilde, *Chemometrics and Intelligent Laboratory Systems*, **49** (1999) 49.
- [102] I. Artaki, M. Bradley, T. W. Zerda, J. Jonas, *J. Phys. Chem.*, **89** (1985) 4399.
- [103] R. B. Hagel, L. F. Druding, *Inorg. Chem.*, **9**(6) (1970) 1496.
- [104] H. H. Schmidtke, D. Garthoff, *Inorg. Chim. Acta*, **2**(4) (1968) 357.
- [105] I. Richter, A. Biller, C. Burschka, M. Penka, R. Tacke, 33-rd Organosilicon Symposium, Saginow USA 2001, Abstract PB18.
- [106] A. Biller, C. Burschka, M. Penka, R. Tacke, *Inorg. Chem.*, **41** (2002) 3901.
- [107] A. R. Gainsford, D. A. House, *Inorg. Chim. Acta*, **3**(3) (1969) 367.
- [108] G. P. Kushto, Y. Iizumi, J. Kido, Z. Yafali, *J. Phys. Chem.*, **A 104** (2000) 3670.
- [109] S. K. Brahma, S. Chattopadhyay, *J. Indian Chem. Soc.*, **75** (1998) 479.
- [110] M. Bolboaca, A. Biller, C. Burschka, M. Penka, R. Tacke, W. Kiefer, Proceedings of the XVIIIth International Conference on Raman Spectroscopy (ICORS), Budapest 2002, p. 599.
- [111] H. J. Shine, E. E. Mach, *J. Org. Chem.*, **30** (1965) 2130.
- [112] B. R. Henry, M. J. Kasha, *J. Chem. Phys.*, **47** (1967) 3319.
- [113] S. A. Alkalis, G. Beck, M. Grätzel, *J. Am. Chem. Soc.*, **97** (1975) 5723.
- [114] J. Delay, P. Deniker, J. M. Harl, *Am. Med. Psychol.*, **2** (1952) 111.
- [115] M. Tosa, Cs. Paizs, C. Majdik, L. Poppe, P. Kolonits, I. A. Silberg, L. Novak, F. D. Irimie, *Heterocyclic Commun.*, **7** (2001) 277.
- [116] M. Chetty, V. L. Pillay, S. V. Moodley, R. Miller, *Eur. Neuropsychopharmacol.*, **6** (1996) 85.
- [117] D. Pan, D. J. Phillips, *J. Phys. Chem.*, **A 103** (1999) 4737.
- [118] R. Hester, K. P. J. Williams, *J. Chem. Soc. Perkin Trans.*, **2** (1981) 852.
- [119] Q. X. Guo, Z. X. Liang, B. Liu, S. D. Yao, Y. C. Liu, *J. Photochem. Photobiol.*, **A 93** (1996) 27.
- [120] C. Garcia, G. A. Smith, W. M. McGimpsey, I. E. Kochevar, R. W. Redmond, *J. Am. Chem. Soc.*, **117** (1995) 10871.
- [121] S. Nath, H. Pal, D. K. Palit, A. V. Sapre, J. P. Mittal, *J. Phys. Chem.*, **A 102**

## References

---

- (1998) 5822.
- [122] J. R. Lombardi, R. L. Birke, T. Lu, J. Xu, *Chem. Phys.*, **84** (1986) 4174.
- [123] J. A. Creighton, *Surf. Sci.*, **124** (1983) 209.
- [124] J. J. H. McDowell, *Acta Crystallogr.*, **B 32** (1976) 5.
- [125] A. P. Scott, L. Radom, *J. Phys. Chem.*, **100** (1996) 16502.
- [126] M. W. Wong, *Chem. Phys. Lett.*, **256** (1996) 391.
- [127] G. Rauhut, P. Pulay, *J. Phys. Chem.*, **99** (1995) 3093.
- [128] P. Hildebrandt, S. Keller, A. Hoffmann, F. Vanhecke, B. Schrader, *J. Raman Spectrosc.*, **24** (1993) 791.
- [129] P. Gao, M. J. Weaver, *J. Phys. Chem.*, **89** (1985) 5040.
- [130] S. Sanchez-Cortes, J. V. Garcia-Ramos, *J. Raman Spectrosc.*, **23** (1992) 61.
- [131] J. Chowdhury, M. Ghosh, T. N. Misra, *J. Colloid Interface Sci.*, **228** (2000) 372.
- [132] M. Muniz-Miranda, *Vib. Spectrosc.*, **19** (1999) 227.
- [133] S. Fu, P. Zhang, *J. Raman Spectrosc.*, **23** (1992) 93.
- [134] E. J. Liang, C. Engert, W. Kiefer, *J. Raman Spectrosc.*, **24** (1993) 775.
- [135] S. Sanchez-Cortes, J. V. Garcia-Ramos, G. Morcillo, A. Tinti, *J. Colloid Interface Sci.*, **175** (1995) 358.
- [136] K. Takahashi, H. Furukawa, M. Fujita, M. Ito, *J. Phys. Chem.*, **91** (1987) 5940.
- [137] S. C. Sun, I. Bernard, R. L. Birke, J. R. Lombardi, *J. Electroanal. Chem.*, **196** (1985) 359.
- [138] M. R. Anderson, D. H. Evans, *J. Am. Chem. Soc.*, **110** (1988) 6612.
- [139] V. M. Hallmark, A. Champion, *J. Chem. Phys.*, **84** (1986) 2933.
- [140] M. Moskovits, D. P. DiLella, *J. Chem. Phys.*, **73** (1980) 6068.
- [141] M. Bolboaca, T. Iliescu, Cs. Paisz, F. D. Irimie, W. Kiefer, *J. Phys. Chem A*, submitted.
- [142] F. D. Irimie, Cs. Paisz, M. Tosa, C. Majdik, P. Moldovan, R. Misca, M. Caprioara, *Studia Universitates Babes-Bolyai, Chemia*, in press.
- [143] C. G. Dryhurst, *Electrochemistry of Biological Molecules*, Academic Press, New York, 1977.
- [144] A. R. Katritzky, *Physical Methods in Heterocyclic Chemistry, Vol. II*, Academic press, New York, 1963.



## References

---

- [145] R. Grigg, M.V. Sargent, *Tetrahedron Lett.*, **19** (1965) 1381.
- [146] F. A. Miller, W. G. Fateley, R. E. Witkovsky, *Spectrochim. Acta*, **23 A** (1967) 891.
- [147] K. Mukherjee, D. Bhattacharjee, T. N. Misra, *J. Colloid Interface Sci.*, **193** (1997) 286.
- [148] T. Iliescu, F. D. Irimie, M. Bolboaca, Cs. Paisz, W. Kiefer, *Vib. Spectrosc.*, **29** (2002) 235.
- [149] K. A. Bunding, M. L. Bell, *Surf. Sci.*, **118** (1996) 413.
- [150] T. Iliescu, F. D. Irimie, M. Bolboaca, Cs. Paisz, W. Kiefer, *Vib. Spectrosc.*, **29** (2002) 251.
- [151] G. Cavigilio, L. Benedetto, E. Boccaleri, D. Colangelo, I. Viano, D. Ossela, *Inorg. Chim. Acta*, **305** (2001) 61.
- [152] K. Taka-aki, H. Atsushi, M. Takaharu, S. Ken-ichi, *Mutation Research/ Genetic Toxicology and Environmental Mutagenesis*, **465** (2000) 137.
- [153] S. C. Wait, J. C. McNerney, *J. Mol. Spectrosc.*, **34** (1970) 56.
- [154] M. Fleischmann, I. R. Hill, G. Sundholm, *J. Electroanal. Chem. Interfacial Electrochem.*, **158** (1983) 153.
- [155] T. C. Stekas, P. S. Diamantopoulos, *J. Phys. Chem.*, **94** (1990) 1986.
- [156] S. M. Park, K. Kim, M. S. Kim, *J. Molec. Struct.*, **328** (1994) 169.
- [157] D. J. Rogers, S. D. Luck, D. E. Irish, D. A. Guzonas, G. F. Atkinson, *J. Electroanal. Chem.*, **16** (1984) 237.
- [158] M. Bolboaca, W. Kiefer, J. Popp, *J. Raman Spectrosc.*, **33** (2002) 207.

## Danksagung

An erster Stelle einen herzlichen Dank an Herrn Prof. Dr. Wolfgang Kiefer, der diese Arbeit ermöglichte und finanziell unterstützte. An dieser Stelle möchte ich mich auch für die Teilnahmemöglichkeit an mehreren internationalen Tagungen bedanken, erwähnt seien insbesondere die ICORS 2000 in Beijing und 2002 in Budapest sowie die ICAVS 2001 in Turku (Finnland) und ECSBM 2001 in Prag.

Für die gute Ratschläge und die Zusammenarbeit möchte ich mich bei Herrn Prof. Dr. Jürgen Popp herzlich bedanken. Herrn Prof. Dr. Dietmar Stalke und seinen Mitarbeitern gilt mein besonderer Dank für die sehr gute Zusammenarbeit im SFB. Bedanken möchte ich mich auch bei Prof. Dr. Reinhold Tacke und seinen Mitarbeitern für die gute Zusammenarbeit.

Bei meinen ehemaligen Professoren aus Rumänien, erwähnt seien insbesondere Herrn Prof. Dr. Traian Iliescu und Herrn Prof. Dr. Petru Stetiu, möchte ich mich herzlich bedanken. Ohne ihre Ermutigung und Ratschläge wäre ich nicht nach Deutschland gekommen, um weiter zu studieren.

Ein herzlichen Dankeschön möchte ich Herrn Dr. Michael Schmitt, der diese Arbeit korrigiert hat, aussprechen. Mein Dank geht auch an Adriana Szeghalmi und Joachim Koster für die Korrektur der deutschen Zusammenfassung.

Herrn Wolfgang Liebler von der Feinmechanik-Werkstatt und Herrn Rainer Eck von der Elektronik-Werkstatt bin ich sehr dankbar für die Erstellung der Raman-Meßzelle.

Ein besonderer Dank gilt meinen Kollegen und ehemaligen Arbeitskreismitgliedern Cristina Dem, Krisztina Babocsi, Claudiu Dem, Nicu Tarcea, Nicolae Leopold, Dr. Oliver Sbanski und Dr. Victor Roman für die immer interessanten Gesprächsabenden. Nicht vergessen sind alle, die mich während meiner Promotionszeit durch tatkräftige Hilfe oder gute Ratschläge unterstützt und so einen Beitrag zum Gelingen dieser Arbeit geleistet haben.

Zu guter Letzt danke ich Lucian, der mich auf seine Art ermutigte und mir während diesen drei Jahren als wertvoller Diskussionspartner zur Seite stand.

# Lebenslauf

## Persönliche Daten

Name	Monica-Maria Bolboaca
Geboren am	31.08.1974
in	Cluj-Napoca
Familienstand	ledig

## Ausbildung und Beruf

Schulbildung	1981 - 1985	Grundschule, Cluj-Napoca
	1985 – 1989	M. Eminescu Gymnasium, Cluj-Napoca
	1989 – 1993	Theoretisches Gymnasium Nr. 1 , Cluj-Napoca
Abitur	Juni 1993	
Studium	1993-1997	Physikstudium an der Babes-Bolyai Universität Cluj-Napoca
	Juni 1997	Lizenzprüfung
	1997 – 1998	Masterstudium Biophysik und Medizinische Physik an der Babes- Bolyai Universität Cluj-Napoca
	Juni 1998	Abschlussprüfung
	1998 – 1999	Masterstudium Atomphysik and der Babes-Bolyai Universität Cluj-Napoca
	Juni 1999	Abschlussprüfung

Promotion	Okt. 1999	Beginn der Promotion am Lehrstuhl für Physikalische Chemie II der Universität Würzburg bei Prof. Dr. Wolfgang Kiefer
Anstellungen	Okt. 1999 – Dez. 2001	Wissenschaftliche Mitarbeiterin im Sonderforschungsbereich 347 der Deutschen Forschungsgemeinschaft
	seit Jan. 2002	Wissenschaftliche Mitarbeiterin